A MULTI-CELLULAR APPROACH TO ENGINEER VASCULARIZED CARDIAC GRAFTS FOR MYOCARDIAL REGENERATION

by
Justin B.F. Morrissette-McAlmon

A dissertation submitted to Johns Hopkins University in conformity with the requirements for the degree of Doctor of Philosophy

Baltimore, Maryland
March, 2018

Abstract

Due to the limited endogenous regenerative potential of the myocardium, therapeutic interventions are necessary to restore function following the occurrence of myocardial infarction. Cardiac tissue engineering offers the promise of restoring lost functionality. With the highly complex make-up of the myocardium, a multi-component/multi-stage approach to regeneration is essential. Cardiomyocytes are highly metabolic and require continuous amounts of oxygen and nutrients following transplantation onto the native myocardium. To address this, several groups have attempted to create pre-vascularized grafts, in which the engineered vasculature would be able to anastomose with the host blood vessels to promote survival of transplanted cells. Hence, the culture of cardiomyocytes has been coupled with endothelial cell types. To stabilize endothelial cell-derived vascular networks, vascular mural cells are necessary. In an effort to improve vascular development, we investigate the use of an abundant clinically relevant cell source, the human adipose derived stem/stromal cells. The objective of this thesis is to identify the cell-cell interactions of human adipose derived stem/stromal cells (hASCs) when cultured with cardiomyocytes and endothelial cells and to also develop a biomaterial platform for engineering aligned, contractile, vascularized myocardium that can be used to regenerate a fibrotic heart.

This objective was achieved utilizing a multi-step approach which included first investigating the electrophysiological effects of co-culturing hASCs with

cardiomyocytes (CMs). After determining the concentration of hASCs that would not statistically impede the electrophysiological properties of CMs [NRVCM:hASC:HUVEC ~ 500:100:0 and 500:50:0 cells], we used these concentrations of hASCs with endothelial cells (ECs) to promote stabilized vasculature. After exploring the ratios of each co-culture, we combined the optimized ratios to develop tri-cultures for a vascularized cardiac system. The ultimate ratio of 250,000:25,000:12,500 cells/cm^2 resulted in dense vessel network development with electrophysiological properties with an average conduction velocity of 20 ± 2 cm/s, APD_{80} and APD_{30} of 122 ± 5 ms and 59 ± 4 ms, respectively, and maximum captured rate of 7.4 ± 0.6 Hz.

Following this, novel fibrin microfiber sheets were used in conjunction with these cell types to develop vascularized cardiac patches. Initially, the fibrin microfibers were characterized for mechanical properties. NRVCMs were seeded onto fibrin microfibers at a concentration of 1.5×10^6 cells/cm^2. NRVCMs were cultured for up until 56 days and achieved electrical conduction velocities of 22 ± 2.1 cm/s. Using a tri-culture system, we engineered contractile cardiac patches with vascular network structures that were capable of being implanted into the ischemic myocardium. Ultimately cardiomyocytes were seeded for 14 days prior to adding hASCs and HUVECs. Upon the addition of the supporting cell types, we found that the electrophysiological properties at the ratio of 1500:37.5:150 were conduction velocity of 14 ± 0.6 cm/s, APD_{80} and APD_{30} of 152 ± 11 ms and 71 ± 6 ms, respectively, and maximum capture rate of 3.9 ± 0.7 Hz. The values obtained at this ratio were not statistically significant different from the NRVCM only control

and appeared to match the closest compared to other tri-cultures. Lastly, we investigated the human interactions of development of a tri-culture system with completely translatable cell types which include human induced pluripotent stem cells differentiated towards the cardiomyocyte lineage and the endothelial cell lineage. This work will ultimately lead to the development of clinically translatable vascularized cardiac patches.

Advisor: Warren Grayson, Ph.D.

Thesis Readers: Warren Grayson, Ph.D. and Hai-Quan Mao, Ph.D.

Thesis Committee: Warren Grayson, Ph.D., Leslie Tung, Ph.D., Hai-Quan Mao, Ph.D., Sharon Gerecht, Ph.D.

Acknowledgments

First and foremost, I am thankful to my thesis advisor, Dr. Warren Grayson. He has truly let me explore my research interest and work toward the development of a project in which I am most passionate. Dr. Grayson was consistently there to answer any questions, take time out of his schedule to come to the lab and make observations with me, and help with anything. In addition, he has pushed me to increase my scientific curiosity, aided with any questions that I may have, and worked to become familiar with work that is not his primary expertise. For this, I am eternally grateful and appreciative.

I would like to thank my thesis committee members: Hai-Quan Mao, Ph.D., Leslie Tung, Ph.D., and Sharon Gerecht, Ph.D. I am eternally grateful for their mentorship, time, critiques, and open-door policies. Each of them has taken the time to make me feel as if I were one of their students and provided resources to undertake the completion of my Ph.D. I am forever grateful for these opportunities and support each of them has provided.

While in the Grayson Lab, my peers have aided in the completion of my Ph.D. I would like to thank Daphne Hutton-Hosmane, Ph.D. for all of her help with imparting all of her knowledge on vascular assembly. I would also like to thank Sarah Somers for her help with experimental design, experimental execution, and generally being an invaluable friend during all of the successes and stresses of my thesis work. My undergraduate research assistant Chanon

Thanitcul has been an amazing undergraduate research assistant and has been the driving force for many of the data analyses. I am forever grateful for his work ethic and your flexibility. In addition, Alexandria Rindone has been an amazing cheerleader and supporter during our tenure in lab together. Thank you to Kenny Tran and Makeda Stephenson for your friendship within the lab.

Finally, I would to thank my dear family and friends. I would like to thank my mother for all of her support and tireless efforts to provide a life for me that would foster my growth and development to reach any dream that I set for myself. She has been a listening ear anytime of the day, my confidant, my strength, and my biggest advocate throughout this process. I would also like to thank my friends from Hampton that have been encouragement as well as the friends I have met at Hopkins.

Table of Contents

vii

List of Tables

List of Figures

List of Abbreviations

ANOVA   Analysis of Variance

APD   Action Potential Duration

αSMA   Alpha Smooth Muscle Actin

αActinin   Sarcomeric Alpha-Actinin

Cx-43   Connexin 43

CV   Conduction Velocity

DAPI   4',6-diamidino-2-phenylindole

DMEM   Dulbecco's Modified Essential Media

DPBS   Dulbecco's Phosphate Buffer Saline

EBM-2   Endothelial Basal Medium-2

FBS/HI-FBS   Fetal Bovine Serum (Heat Inactivated)

FGF-2   Basic Fibroblast Growth Factor

H&E   Hematoxylin and Eosin Staining

hASCs   Human Adipose Derived Stem/Stromal Cells

hBM-MSC   Human Bone Marrow derived Mesenchymal Stem Cells

hDF   Human Dermal Fibroblasts (BJ Cell Line)

hECFC   Human Endothelial Colony Forming Cell

hESC-CM   Human Embryonic Stem Cell derived Cardiomyocytes

hiPSC-CM   Human Induced Pluripotent Stem Cell derived Cardiomyocytes

hiPSC-EC   Human Induced Pluripotent Stem Cell derived Endothelial Cells

hNCF-V   Human Normal Cardiac Fibroblasts, Ventricular

hNDF	Human Normal Dermal Fibroblasts
HUVECs	Human Umbilical Vein Endothelial Cells
MCR	Maximum Captured RateMedia
MI	Myocardial Infarction
NRVCM	Neonatal Rat Ventricular Cardiomyocytes
PTween	PBS with 0.1% (v/v) Tween-20
VEGF	Vascular Endothelial Growth Factor
vWF	von Willebrand Factor

Chapter 1: Introduction

1. Introduction:

Myocardial Infarction (MI) affects more than 1.3 million Americans each year[1]. MI, caused by thrombotic occlusion of coronary arteries, often results in heart failure, cardiac rupture, and death due to the limited regenerative capacity of human myocardium[2]. A lack of blood flow to the myocardium during MI results in necrosis of cardiac myocytes, which leads to the subsequent release of their intracellular contents, activating resident macrophages, and initiating an inflammatory cascade[3,4]. This inflammatory cascade further damages cardiac myocytes and leads to destruction of the extracellular matrix (ECM). Recent advances, which include stem cell transplantation, thrombolytic therapy, and stenting of coronary arteries, have improved myocardial salvage but therapies that directly induce regeneration of the ventricular wall and improvement in functionality are lacking.

Cardiovascular tissue engineering has the potential to ameliorate the damage resulting from the limited endogenous repair mechanisms of the heart following MI[5]. Currently, there are no methods that completely repair the damaged myocardium post injury. Tissue engineering approaches aim to regenerate the myocardium by mimicking the tissue structure and cell composition. The native make-up of the myocardium includes a host of cells that are critical for survival, maturation, and repair. These cell types include cardiomyocytes, fibroblasts, endothelial cells, vascular smooth muscle cells, and macrophages[7] (**Figure 1**). The

myocardium is a highly metabolic, vascularized tissue characterized as having three endothelial cells to every one cardiomyocyte[6] and an inter-capillary distance of 15 – 50 μm.[6] Tissue engineering of the myocardium requires the development of adequate interconnected capillary networks that have the ability to anastomose quickly with the host vasculature to maintain cell viability. Engineered pre-vasculature could expedite integration of the graft with host tissue and enhance regeneration. Vascular structures require perivascular cells for angiogenic growth factor release and stabilization. Thus, multiple cell types are required to form functional vasculature as well as a syncytium of cardiomyocytes.

Through tissue engineering, there have been several strategies developed to enhance cardiac regeneration. These strategies include the injection of cells within hydrogels or preassembly of epicardial patches with cells, natural and synthetic materials, and growth factors. Tissue engineering strategies aim to recapitulate key structural elements of the myocardium.

2. TISSUE ENGINEERED CARDIAC PATCHES:

Cardiac patches are designed to be placed epicardially where they integrate with the healthy tissue surrounding the infarcted region shunting the electrical signals over the scar tissue and contributing to the contractile function of the heart (**Figure 2**). *In vivo* studies of engineered cardiac patches primarily rely on two types of assessments: functional characterization and tissue-level analysis. Functional studies include measurements of cardiovascular output, such as ventricular ejection fraction, and end-systolic and -diastolic volumes, all of which can be measured in living specimens using echocardiography. Also included under

the functional umbrella is the organ-level electrophysiology of the heart which can be assessed by electrocardiogram in live specimens and by whole-heart optical mapping post-mortem[7]. Tissue-level investigations of *in vivo* experiments involve assessing cell survival and morphology as well as tissue organization. For example, a surgically implanted engineered cardiac patch might be assessed for anastomosis of host vasculature with engrafted vasculature or for migration of cells between graft and host. Histology and immunohistochemistry are crucial tools for these measurements as they can be used to differentiate cell types and sources and can help characterize the composition and organization of the extracellular matrix.

There are also several *in vitro* assessments performed on engineered cardiac tissues for which optimization is believed to correspond to improved clinical outcomes. Electrophysiological measurements are frequently treated as the gold standard for evaluating engineered cardiac tissues, with conduction velocities and action potential shapes seen in mature, adult tissues established as ideal. These measurements also allow engineers to evaluate the uniformity across the tissue and to gauge the maturity of stem cell-derived cardiomyocytes. However, full electrophysiological characterization of these tissues requires extensive facilities and expertise and as a result, much of the literature relies on stimulated contractile force measurements. Sometimes referred to in the literature as "twitch force", this assessment is frequently used as a measure of tissue development and increased force is believed to correlate with improved tissue maturity and clinical outcomes. Cell and tissue-level analysis are also frequently performed on engineered tissue

in vitro as cellular morphology and tissue organization are important determinants of tissue function.

3. CELL SOURCES:

Approaches to engineer cardiac grafts employ the combination of multiple cell types, typically including cardiomyocytes (electrically excitable cells), endothelial cells (vessel development), and fibroblasts/mural cells (vasculature stabilization). Each of these phenotypes may be derived from various sources (see **Table 1**).

3.1 Cardiomyocytes:

Typically, cardiac tissue engineering strategies have been studied using neonatal rat ventricular myocytes (NRVCMs). NRVCMs are isolated from newborn (day 0 – 3) rat hearts that have been minced and digested with trypsin and collagenase. To enrich the cardiomyocyte population, cells are usually plated into flasks and incubated for short periods to allow for the selective adherence of fibroblasts in order to purify the NRVCM population. NRVCMs retain the ability to contract *ex vivo,* undergo a rapid dedifferentiaition-redifferentiation cycle, and can be easily plated into monolayers. NRVCMs are widely used to study morphological, electrophysiological, and biochemical characteristics of cardiomyocytes. Despite their advantages, NRVCMs have the main disadvantage of being rodent-derived. Electrophysiologically, NRVCMs have little to no plateau phase when cultured *in vitro*. In addition, NRVCMs differ in their excitation-coupling with a lack of T-tubule systems relative to adult myocytes and their ability to maintain cytosolic Ca^{2+} signaling independent of the sarcoplasmic reticulum

calcium release[8]. And while the adult rat myocardium has conduction velocities of 69 ± 6 cm/s in the longitudinal direction and 19 ± 5 cm/s in the transverse direction, there is yet to be a report of tissue engineered grafts achieving these values[9]. These cells are also not able to be cultured for extended periods of time especially in monolayers[10].

While healthy human cardiomyocytes isolated from adult hearts cannot be obtained ethically, the use of pluripotent stem cells has provided an avenue to obtain viable human cardiomyocytes. Human embryonic stem cells have been used to differentiate stem cells into functional human cardiomyocytes. hESC-CM have well documented electrophysiological properties, contract rhythmically, and are responsive to cardiac compounds. Similar to NRVCMs, hESC-CMs can be genetically manipulated but have the advantage of being maintained *in vitro* for longer periods. These cells can also be engrafted into the human myocardium[11]. While these cells are advantageous for studying human cardiomyocytes, there are ethical and regulatory concerns related to the accessibility to embryos as well the immune response that arises with transplantation[12]. Additionally, hESCs have been shown to have genetic instability and specifically, cardiomyocytes are immature in their development. In addition, due to the pluripotent state of the stem cells, they have the potential to form teratomas when transplanted *in vivo*. Recent work has established that purifying the culture and removing undifferentiated stem cells, should reduce the probability of uncontrolled cell proliferation.

Human induced pluripotent stem cells (hiPSCs) have similar characteristics to hESCs and have the advantage that they can be used autologously. The hiPSC-

derived cardiomyocytes (hiPSC-CMs) circumvent the ethical concerns associated with hESCs, but there is variability among cell lines derived from different patients. While these cell types are capable of spontaneously contracting, their functional and structural immaturity needs to be addressed. For example, hiPSC-CMs are polygonal in shape and mononucleated (while the adult myocytes are larger, rod-like and binucleated) and they exhibit fetal-like sarcomeric organization, ion-channel expression, force generation, and action potential shape. The sarcomeres in hiPSC-CMs are also shorter and more disorganized than in the adult myocyte[13]. The hiPSC-CMs also have reduced contractile machinery as compared to the adult myocyte and have not undergone isotype switch to a stiffer form of titin. Similar to neonatal rat cardiomyocytes, these cells exhibit immature calcium handling properties and no T-tubule formation[14]. Finally, gap junction proteins are located around the cardiomyocytes rather than located at the intercalated disk space in pluripotent stem cells, which yields slower conduction velocities compared to the native human adult heart[13]. In spite of these limitations, hiPSC-derived cardiomyocytes (hiPSC-CMs) are a suitable cell source for drug screens and disease modeling based on their electrophysiological characteristics.

3.2 Endothelial Cells:

Several sources of endothelial cells have been used for vessel development. These include human umbilical vein endothelial cells (HUVECs), endothelial colony forming cells (ECFCs) also termed blood outgrowth endothelial cells (BOECs) or endothelial progenitor cells (EPCs), human embryonic stem cell-derived and human induced pluripotent stem cell-derived endothelial cells (hESC-

ECs & hiPSC-ECs). HUVECs display a mature phenotype and have been shown to develop cord-like structures in monolayers and vascularized lumens in 3D microenvironments that can anastomose with host vasculature *in vivo.*

ECFCs are critical in wound healing/ischemic environments and are found circulating in peripheral blood. These endothelial progenitor cells are advantageous for patient-specific therapies and have the ability to mature and anastomose with host vasculature. While these cells can be patient-specific, there is a limited supply circulating in the peripheral blood, they are initially slow growing, and take many passages to acquire enough cells to perform experiments or use for therapies.

More recently, hESC-EC, and hiPSC-EC have been used to make to vascular structures *in vitro* and can anastomose with host vasculature *in vivo.* hESC-ECs and hiPSC-ECs have the ability to make lumens in 3D (i.e. hydrogels) and are responsive to vascular endothelial growth factor (VEGF) and basic fibroblast growth factor (bFGF) signaling[15,16]. While phenotypically similar to both mature and immature endothelial cells, some studies indicate that the hESC-ECs and hiPSC-ECs may be less responsive to shear stress[17] but retain the ability to be differentiated into arterial and venous endothelial cells[18].

3.3 Fibroblast (-like) cells:

Developing stable, perfusable vascular networks that can anastomose with host vasculature to deliver nutrients provides the capacity to enhance the viability of engineered grafts. Vascular stabilization occurs through the activity of mural cells i.e. pericytes or smooth muscle cells and several mesenchymal phenotypes

(characterized as being positive for surface markers CD73, CD90, and CD105) have been used to perform this function[19]. In particular, fibroblasts from the skin, lung, and bladder have been widely used though their perivascular characteristics vary with the anatomical site of isolation. Dermal fibroblast are the most translatable due to the ability to be easily obtained from the skin and their potential to rapidly proliferate, and express limited perivascular potential. Chen et al. have demonstrated vessel development using normal human lung fibroblasts in co-culture with HUVECs or EPCs. Vessel development was monitored over 7 days in the presence of low (0.2 million cells/mL) or high (2 million cells/mL) concentrations of fibroblasts. The higher concentration of normal lung fibroblasts co-cultured with HUVECs or EPCs resulted in longer vessels compared to the lower concentration of fibroblasts[20]. Costa-Almeida *et al* compared the vessel development of human dermal fibroblasts coupled with HUVECs or blood outgrowth endothelial cells (BOECs). Studies were completed at 2:1 ratio of EC:FB. Cells were co-cultured for up to 21 days. By day 21, the co-culture of BOECs and NHDF resulted in ~32 capillary like structures/mm^2, while HUVEC and NHDF co-cultures developed ~30 capillary like structures/mm^2. Average length of the capillary like structures decreased from day 14 to day 21 in both groups[21].

Cardiac fibroblasts are specifically derived from the myocardium through biopsy. This, however, causes damage to the myocardium. Cardiac fibroblasts contribute to the myocardial structure and can potentially aid in signal transduction between cardiomyocytes. They can be found in the wound healing environment post injury and provide paracrine signaling[22,23]. Cardiac fibroblasts have

perivascular potential and serve as a suitable source for cardiomyocyte co-culture. Twardowski *et al* focused on the role of vascular development with cardiac fibroblasts coupled with endothelial cells. The study specifically looked at using rat aortic endothelial cells (rAEC) coupled with neonatal cardiac fibroblasts (nCF) in fibrin hydrogels. As a positive control for pericyte-like cells, rat bone marrow-derived mesenchymal stem cells (BM-MSCs) were used to compare vessel assembly. Seeding support cells and endothelial cells at 1:1 ratio, this study demonstrated that nCF:rAEC developed longer sprouting networks compared to when endothelial cells were co-cultured with BM-MSCs [24].

As indicated above, BM-MSCs have the potential to serve as pericyte-like cells/mural cells and stabilize vascular structures. While these cells have many potential benefits, there is high morbidity associated with their extraction and the cell yields are relatively low. In contrast, adipose-derived stem/stromal cells (ASCs) can be procured in high numbers from a minimally invasive liposuction procedure. In addition to acting as mural cells, ASCs secrete an abundance of pro-angiogenic growth factors. ASCs are also capable of modulating inflammatory responses, reducing apoptosis, preventing fibrosis, stimulating endogenous repair and neovascularization, and can withstand temporary ischemia[25–27]. ASCs have also been shown to electrically couple with neonatal rat cardiomyocytes by forming gap junctions, which would indicate that these cells have the potential to behave as cardiac fibroblasts.[28] There has not been a study to date that demonstrates the potential of hASCs to behave as both cardiac fibroblasts and perivascular cells within the same cultures.

Merfeld-Clauss *et al* have monitored vessel assembly of hASCs coupled with cord blood endothelial colony-forming cells (cbECFCs). In the monolayer culture, there was dense vessel network assembly which appeared to regress over time. When cbECFCs were cultured with coronary artery smooth muscle cells (SMCs), aortic SMCs, normal human dermal fibroblasts, or human ASCs, the hASCs had statistically higher tube lengths[29]. In a 2015 report, this group reported that Activin A expression directed hASC differentiation down the smooth muscle lineage when in direct contact with cbECFCs [30]. Hutton *et al* found that heterogeneous hASCs contained a small amount of endothelial cells that have the ability to expand and form vessel networks. These cells cultured in high density (20,000 cells/cm^2) monolayer resulted in the development of CD31+ vessel structures[31]. This study was followed up with 3D vascular development in fibrin hydrogels[32]. Freiman *et al* developed vessel networks with co-cultures of hASCs or normal human dermal fibroblasts and human adipose derived microvascular endothelial cells (HAMECs) or HUVECs. It was found that the co-culture of hASCs and HAMECs resulted in the greatest increase in vessel length by day 7 and maintained the vessel length up until day 14[33].

4. MULTICELLULAR STRATEGIES:

Several strategies have been used to develop vascularized contractile grafts that recapitulate key characteristics of the native myocardium. A common feature of these approaches is the culture of the three essential cell types: (i) contractile, electrically excitable cardiomyocytes, (ii) endothelial cells to self-assemble into vascular networks, and (iii) fibroblasts-like cells to stabilize cardiac

and vascular function (see **Table 2**). The first such reported tri-culture system utilized hESC-CMs, hESC-ECs or HUVECs, and mouse embryonic fibroblasts (mFBs) combined in a cell ratio of 1:1:1 (hCM:mFB:hEC) and seeded into 1:1 mixed poly L-lactic acid (PLLA) / polylactic glycolic acid (PLGA) scaffolds via Matrigel[34,35] (**Figure 3**). Within this study, it was demonstrated that vascular structures were stabilized in the presence of fibroblasts and developed increased lumens and vessel density. Without the presence of fibroblasts, vessel structures were limited in development. In this tri-culture system, cardiomyocytes displayed chronotropic responses to compounds like isoproterenol and carbamylcholine[34,35]. While this approach was a landmark in the development of vascularized cardiac tissues, there was limited quantitative characterization of cardiomyocyte interconnectivity or electrophysiology.

Fibrin hydrogels have also been used extensively as a scaffold for cardiac grafts[36–38]. Ye et al. co-cultured cardiomyocytes, smooth muscle cells, and endothelial cells all derived from hiPSCs at a ratio of 1:1:1. These cells were directly injected into the infarct or directly injected into a fibrin hydrogel loaded with insulin-like growth factor (IGF). Groups that were tested included direct cell injection, fibrin patch only, and hEC plus hSMC encapsulated within the fibrin hydrogel. After 4 weeks *in vivo*, the cardiac patch resulted in ejection fraction increase near sham and the lowest infarct size compared to sham, MI with no treatment, patch only, and cells with patch. In this study, cells were not cultivated before injection and subsequent characterization of the cardiomyocyte contractility or vessel development were not characterized. Schaefer *et al* co-cultured hiPSC-

CMs, human pericytes, and human blood outgrowth endothelial cells (BOEC). Within this study, presence of vasculature structures improved the force of contraction over time. Increased presence of the mature form of troponin (cTnI) compared to the immature form (ssTnI). There was near 1 mN of force generated in these constructs by day 14. When the patch was implanted *in vivo*, the vasculature anastomosed with the host vasculature and also integrated with cardiomyocytes. There were nearly 150 vessels/mm^2 in the tri-culture system. One limitation of these approaches is that hydrogel systems are isotropic with cells growing in several directions. The native myocardium is anisotropic. In addition, hydrogels do not allow for the highest level of homotypic cell-cell connections among cardiomyocytes when multiple cell types are encapsulated.

Scaffold and hydrogel studies typically require all cells to be seeded simultaneously. Subsequent studies have demonstrated advantages associated with a sequential seeding strategy whereby cardiomyocytes were cultured for a period of time before supporting cells were added (**Figure 3**). In one such study, cells were seeded onto micropatterned polyethylene glycol (PEG) hydrogels that were coated with Matrigel™ to enhance cell attachment and the development of cardiac organoids[39]. NRVCMs were seeded with D4T endothelial cells and neonatal cardiac fibroblasts at three different CM:FB:EC ratios (40:13:47; 60:9:31; and 80:4:16). Cells were seeded simultaneously or sequentially. In sequential seeding, the cell ratios were maintained and D4T ECs and nCFs were seeded 2 days prior to the addition of cardiomyocytes and evaluated for electrophysiological and contractile changes relative to NRVCM-only cultures. Simultaneously seeded

tri-cultures resulted in increased excitation threshold to 6 V/cm, compared to ~3V/cm in NRVCM-only controls, and decreased maximum captured rates from ~4.2 to 3 Hz. Upon sequential seeding however, the conditions containing the highest percentage of cardiomyocytes coupled with supporting cells types resulted in an excitation threshold closest to the NRVCM-only control of about 3 – 4 V/cm with statistically unchanged maximum captured rates. The data demonstrated that the greatest presence of CD31/PECAM-1 positively stained cells was found in the simultaneously-seeded cultures but electrophysiological and functional parameters were sacrificed relative to the sequentially-seeded cultures. Although the cells were positive for CD31, the development of cord-like structures was not uniformly seen throughout the constructs. Recent studies have also investigated the impact of using hASCs in lieu of human dermal fibroblasts together with NRVCMs and HUVECs. ASCs have been found to be beneficial in ischemic settings like myocardial infarction. Studies that have injected hASCs into rats and pigs have found paracrine secretion of multiple growth factors. From the echocardiogram, there was decrease in infarct size, increase in wall thickness, decrease in end systolic and diastolic volumes, and an increase in left ventricle ejection fraction and left ventricle fractional shortening[40]. Therefore, within a monolayer *in vitro* system, NRVCM:hASC and hASC:HUVEC co-cultures were first used to determine the appropriate tri-culture ratios. In the tri-culture system, an NRVCM:hASC:HUVEC ratio of 10:2:1 resulted in vessel development of 70 mm per 3,240 mm^2 with an average of 454 junctions. The electrophysiological properties were reported as 20 ± 2 cm/s, APD_{80} and APD_{30} of 122 ± 5 ms and 59

± 4 ms, respectively, and maximum capture rate of 7.4 ± 0.6 Hz[41]. From these studies it could be seen that sequential seeding allowed for cardiomyocytes to develop cell-cell connections allow for improved electrophysiological outcomes for cardiomyocytes. Although this allowed for the development of close cell-cell connections, the cultures were 2D in nature.

Zhang *et al* developed the AngioChip that enabled the formation of 3D tissues with spatial and temporal control while seeding different cell populations (**Figure 3**). AngioChip was made from the micropatterned biodegradable elastomer poly(octamethylene maleate (anhydride) citrate) POMaC and cells were encapsulated into collagen hydrogels. The tri-culture system was developed from NRVCMs or hESC-CMs, hMSCs, and HUVECs. Uniquely these devices allowed for the development of channels to accommodate medium perfusion to provide adequate nutrient transfer to cardiomyocytes. After optical mapping the resulting conduction velocity was 4.8 cm/s. In this system the channels were coated with vascular cells to develop a channel for nutrient perfusion and ideal integration when implanted *in vivo*. The AngioChip was surgically implanted and demonstrated 'artery to artery' anastomosis with host vasculature[42]. Employing similar principles for spatial control, Gershlak *et al* developed a decellularized spinach leaf system, which served as an attractive biomaterial for cardiac tissue engineering. The native venous architecture of the leaves provided intrinsic vasculature networks. The spinach leaf was reseeded with a tri-culture system consisting of hESC-CMs, hMSCs, and HUVECs. After 10 days of culture, the tri-culture system resulted in 10% contractile strain. Contractile strength peaked at

day 7 and was maintained until day 17. After day 17, there was a decrease in contractile strength. The endothelial cells (HUVECs) were reseeded through the cannula and appeared to line the spinach leaf to form vessel like structures within the inherent plant structure[43].

Another promising strategy used cell clusters rather than individual cell suspensions (**Figure 3**). Stevens *et al* developed spheroid/cell cluster tri-culture systems which were seeded with hESC-CMs, hDF, and HUVECs. In this system, there was increased force of contraction over time as well as increased force-length relationships in the presence of all three cell types. In addition, these clusters developed a similar percentage of contraction in the patches as the control group up to 3 Hz pacing. The vessel characterization showed increased CD31 staining compared to cardiomyocyte only control and anastomosis with host vasculature when implanted *in vivo*[44]. Ong *et al* developed a 3D printed tri-culture system, in which cells are the matrix. This tri-culture consisted of hiPSC-CMs, hCFs, and HUVECs. The electrophysiological properties consisted of ventricular-like action potentials and conduction velocity near 4.6 cm/s which appeared to decrease with increased fibroblast percentage. CD31 staining was found in the histology inside the cell cluster but vessel density was not calculated. When the scaffold was implanted *in vivo,* there was nascent vasculature development[45].

5. BIOMATERIALS:

Biomaterials are designed to provide structural support, alignment cues, and bioactive signaling to enhance cardiomyocyte function and maximize contractile and electrophysiological properties. In addition, incorporation of proangiogenic cues facilitates the development of dense vasculature[46]. Biomaterial choices for the development of vascularized cardiac grafts range from natural to synthetic biopolymers. For example, PLLA/PLGA (in a 1:1 ratio) has been used to create a sponge-like, biocompatible scaffold. PLGA has a high degradation rate while PLLA provides mechanical support to the 3D structure[47]. Alternatively, PEG and Poly (octamethylene maleate (anhydride) citrate) (POMaC) which degrades easily through hydrolysis are the materials to which hydrogels containing cells will be cultured[39,48,49]. These polymers were coated with Matrigel™ or the combination of Matrigel™ and collagen.

Hydrogels are an attractive material because they are generally made from the natural materials and can be modified to tune their properties, encapsulate cells, and serve as an adhesive to maintain cells in desired location. While hydrogels are attractive sources for providing a scaffold for development, there are drawbacks. These include limited mechanical integrity, reduced flexibility in seeding procedures, and isotropy[50]. The native myocardium is composed of mostly collagen and collagen gels would facilitate a similar extracellular matrix composition.

Despite collagen being one of the major extracellular matrix proteins of the native myocardium, many multi-cellular approaches utilize fibrin as a scaffold.

Fibrin is composed of fibrinogen and cross-linked with thrombin. Fibrin has the ability to recruit vasculature because it is proangiogenic [20]. Fibrin is often used in cardiac patch systems because it has many attractive features and naturally occurs at wound sites[51,52]. Among the benefits of fibrin are its ability to promote angiogenesis, cell survival, and extracellular matrix secretion[36]. This matrix secretion in combination with the natural strain stiffening of fibrin mimic the mechanics of the cardiac microenvironment[53,54].

To provide mechanical integrity and facilitate the development of alignment and tension for cardiomyocyte contractility, researchers have developed casting methods like posts for fibrin hydrogels[55–57]. Recently, fibrin has been electrospun into microfibers. Electrospun microfibers offer the added advantage of tunable mechanical properties and alignment cues, which is critical for myocardial tissue[58]. Also groups have initiated a bilayer scaffold approach which includes culturing cardiomyocyte gels and vascular gels both independently and in combination for therapy[38].

Decellularized matrices are also attractive for the development of tissues because they utilize nature's platform. Most recently, there has been the development of vascularized cardiac tissue on a decellularized spinach leaf by the Gaudette group. The spinach leaf was specifically used because of the intrinsic network that it possesses that could be used for the development of dense vessel networks alongside contractile cardiomyocytes[43]. Other groups have decellularized rat, porcine, and human myocardium and reseeded with cardiomyocytes and endothelial cells[59]. The drawbacks currently to decellularized

matrix are the reseeding efficiency and the detergents used to decellularize can alter the stiffness of the matrix.

6. BIOPHYSICAL CUES:

Cellular behavior is strongly influenced by the properties of the cells' microenvironment. Hence, tissue engineering strategies aim to tightly regulate the biochemical, mechanical and electrical cues experienced by cells to influence cell- and tissue-level behaviors. However, the ideal microenvironment for cardiac development is not necessarily conducive to angiogenesis and vice-versa. This discord presents a challenge in the engineering of tissues with both mature cardiac function and functional vasculature and necessitates a firm understanding of how environmental factors contribute to each process.

6.1 Biochemical Cues:

Embryological studies have proven that cardiac development relies heavily on the biochemical makeup of its surroundings, as small variations in localization, timing or concentration of certain signaling molecules can result in hugely consequential cardiac defects. The earliest stage of cardiogenesis, the formation of cardiac progenitor cells, relies on Nodal, a cytokine in the TGF-β family[60]. Wnt/β-catenin and bone morphogenic protein (BMP) signaling also play critical roles in early differentiation and facilitate the proliferation of those progenitors, although evidence suggests that both factors can exert an inhibitory effect on terminal cardiac differentiation[61–64]. These embryological revelations have yielded a variety of approaches to promote myocardial differentiation in pluripotent cells, the most efficient of which rely on modulating Wnt, BMP, and Fibroblast growth factor (FGF)

signaling with small molecule regimens[65]. In a widely cited report, Burridge and colleagues found that L-ascorbic acid 2-phosphate and recombinant human albumin along with transient exposure to CHIR99021, a glycogen synthase kinase 3 inhibitor, and IWR-1, an inhibitor of Wnt/β-catenin signaling, are sufficient to induce cardiac differentiation in 11 hiPSC lines[66].

Dozens of factors have been identified as promoting angiogenesis, enacting their effects via a variety of mechanisms. Among the most relevant and researched in the context of vascularized cardiac tissues are vascular endothelial growth factor (VEGF), platelet-derived growth factor subunit B (PDGF-B), and angiopoietin-1 (Ang-1). In tri-culture experiments combining hESC-derived cardiomyocytes with endothelial cells and fibroblasts, Caspi *et al* showed that the tri-cultures developed much more significant vasculature and also showed increased expression of VEGF, PDGF-B and Ang-1[34]. The importance of these factors was further confirmed when Hao and colleagues reported increased vascular development in the infarcted myocardium of mice in response to hydrogel-delivered VEGF-A and PDGF-BB[67]. In addition to traditionally recognized proangiogenic factors, some hormones and cytokines with unrelated primary functions have been shown to improve vasculature in engineered cardiac tissues; specifically, insulin-like growth factor 1 (IGF-1) and stromal cell-derived factor 1 (SDF-1) along with VEGF increased the vascular development in an engineered cardiac patch[68]. This effect was at least partially mediated by SDF-1's ability to attract CD34-positive hematopoietic progenitor cells.

The functional mechanisms of cytokines and hormones are often complex and influenced by the method of delivery. Alberti and colleagues concluded that these effects can drastically alter stem cell fate by showing that immobilizing Leukemia Inhibitory Factor in a gelatin matrix significantly improved its ability to maintain pluripotency in hESCs[69]. Similarly striking effects have been observed in studies of biochemical control of vascularization. Early experiments revealed that heparin-mediated binding of VEGF to a collagen matrix promoted endothelial cell proliferation [70] and that immobilizing VEGF promoted penetration of endothelial cells into collagen matrices[71]. Chiu and Radisic subsequently demonstrated that endothelial cells formed significantly more vasculature on scaffolds with covalently immobilized VEGF and Ang-1 than scaffolds treated with soluble factor[72]. In that experiment the authors utilized 1-ethyl-3-[3-dimethylaminopropyl]carbodiimide hydrochloride (EDC) and N-hydroxysulfosuccinimide (sulfo-NHS) to covalently bind VEGF and Ang-1 to the collagen substrate. Factor immobilization using sulfonated alginate matrices has proven a very effective tool for promoting vasculature in complex tissue environments with many cell types, including cardiac tissue. FGF presented in this matter produced twice the blood vessel density as soluble FGF when implanted subcutaneously in mice and matrix-bound hepatocyte growth factor (HGF) similarly increased vascular density by nearly two-fold over all controls in mouse hindlimb ischemia model[73,74]. Despite these advances, the utility of presenting pro-cardiac molecules in this manner has not been rigorously evaluated as, for the most part, experiments using multiple cell

types have administered these molecules either before they are used in the patch or by including them as soluble factors in the media.

6.2 Effect of Substrate Stiffness, Guidance, & Alignment Cues:

Of the many characteristics of the extracellular matrix, the mechanical stiffness has been identified as particularly important to cellular differentiation and behavior. The role of matrix stiffness in supporting cardiomyocytes is poorly understood and a wide range of elasticities has been reported as optimal for their culture. In one of the earliest studies on this topic, Jacot *et al* reported that NRVCMs grown on 10 kPa polyacrylamide (PA) displayed improved markers of functional maturity, such as contractile force generation and sarcoplasmic calcium stores[75]. Similarly, Engler and colleagues found that embryonic cardiomyocytes isolated from rats displayed much greater functional maturity on collagen-coated polyacrylamide matrices with elastic moduli in the range of normal rat myocardium (~11kPa) as opposed to stiffer matrices falling in the range of infarcted myocardium (~34kPa)[76]. However, shortly thereafter it was reported that NRVCMs cultured on very soft, 3 kPa PA scaffolds developed more electrophysiologically mature phenotypes but that other measures of functional maturity such as cellular elongation and contractile force generation were optimized on stiffer 50 kPa scaffolds[77]. The question of optimal substrate stiffness is further complicated by evidence that cardiomyocytes require different levels of substrate stiffness at different stages of differentiation. In 2010 Young and Engler found that a hyaluronic acid matrix engineered to stiffen over time increased expression of maturity markers in NRVCMs nearly threefold over standard scaffolds [78] and a recent report

suggested that CMs derived from iPSCs display improved initial differentiation on protein-coated tissue culture plastic (elastic modulus ~2GPa) but that they developed more mature beating behavior and contractile function on 20kPa PA scaffolds[79].

Stiffness is also an important consideration in vascularization as evidenced by experiments showing that angiogenesis in hydrogels seeded with HUVECs is strongly affected by the elastic modulus of the hydrogel. In a key report, Sieminski and colleagues showed that the softer collagen gels (Young's Modulus = 6 kPa) developed much more robust vascular networks than the stiffer gels (10 kPa) they tested[80]. This report also suggested that the relative magnitudes of the matrix stiffness and the force of endothelial cell traction regulate angiogenesis. They found that human blood outgrowth endothelial cells (HBOEC), which exert more traction force than HUVECs, formed thin, branched vasculature with thick walls in floating 10kPa gels while HUVECs formed vasculature with thin walls and larger lumens. However, if the stiffness was decreased to 6kPa, both cell types formed narrow, thick-walled structures while if the apparent stiffness was increased by mechanically restraining the gel, both cell types formed thin-walled vasculature with large lumens.

Determining the ideal elasticity for vascularization of cardiac tissues is further complicated by inconsistencies in the literature. Wide varieties of matrix materials have been utilized but it is very possible that optimal stiffness is different for each material. Also, stiffness is measured and reported differently throughout the literature with some authors reporting elastic modulus and others choosing to

measure storage or complex moduli; these are related but they can be substantively different in the context of viscoelastic materials. Despite these irregularities, it is likely that substrates optimized for endothelial proliferation and angiogenesis are much softer than those optimized for cardiomyocyte maturation as the reported stiffnesses of angiogenic substrates have ranged from under 100 Pa to about 6 kPa[80–82] while cardiomyocyte differentiation and maturation has been reported to thrive in matrices with elastic moduli in the range of 10-50kPa and has been shown to be actively suppressed on very soft (1-3 kPa) substrates[79,83].

6.3 Alignment:

Anisotropy and cellular alignment is a prominent characteristic of cardiac physiology and the alignment of cardiomyocytes is critical to normal electrophysiological and contractile behavior. In comparing cultures of NRVCMs grown on a flat surface with random orientation to cultures grown on a grooved substrate with increased alignment, Chung *et al* found that the aligned cultures exhibited increased conduction velocities[84]. Alignment of 3D NRVCM cultures was also shown to increase the stimulated force of contraction[53]. Reproducing this organization has been a major goal of the tissue engineering field and cardiomyocyte alignment is frequently used as a measurement of tissue maturity and predictor of functional capacity.

This anisotropy is not limited to cardiomyocytes as it is also present in the vasculature of native myocardium, where blood vessels are highly aligned in near-parallel organization[85,86]. There have been efforts to recapitulate this vessel-level alignment to maximize biosimilarity and because, in theory, microvascular

alignment could improve nutrient delivery and promote the survival of cardiomyocytes in the construct. An experiment in which pre-vascularized cardiac patches, formed with either randomly oriented or uniaxially aligned vasculature, were grafted onto infarcted myocardium in mice showed improved lumenal density and network length among the aligned samples in vitro but also showed that their in vivo effects were indistinguishable as they displayed similar total and perfused luminal densities as well as similar improvements in scar tissue formation and functional outcomes[56]. These results have raised questions regarding the importance of vascular alignment to the function of engineered cardiac tissues. In another set of experiments, researchers combined separately generated layers of aligned microvessels and aligned cardiomyocytes. They found that the combined patch exhibited much greater force of contraction in vivo and that it significantly reduced scar formation in mouse myocardial infarction models, while patches just containing CMs did not [38], but without controlling for a patch with randomly oriented vasculature, the importance of the alignment is impossible to assess.

6.4 Electrical and Mechanical Stimulation:

Electrical and mechanical stimulation applied in culture can have a significant impact on the maturation of CMs and the development of vasculature in tissue engineered constructs. In the development of engineered cardiac tissues that recapitulate the behavior of native myocardium, the ability to control the cellular environment and apply external stimuli is very important. Therefore, significant investment has been made in developing devices capable of reliably

applying electrical and mechanical stimulation to these tissues and investigating optimal stimulation for cardiac development and angiogenesis.

6.5 Electrical Stimulation:

Electrical forces play a key role in cardiac development as spontaneous electrical activity begins in what will become the sinoatrial node as early as 20 days after fertilization[87]. Electrical stimulation has proven a useful tool in cardiac tissue engineering since Radisic and colleagues showed that applying electrical pulses at 1 Hz to cardiomyocyte-laden hydrogels resulted in improved CM alignment, a 50% increase in maximum capture rate, a 3-fold increase in gap junctions, and a 4-fold increase in the fractional change in the surface area of the construct induced by each beat, suggesting increases in electrical coupling, electromechanical coupling and force of contraction[88]. It has since been demonstrated that a ±2.5 V biphasic pulse applied at 1 Hz can drive progenitor cells toward cardiomyocyte lineages, evidenced by increases in cell length and alignment along with increased expression of GATA-4, Cx43, and troponin T apparent after only 1 day of stimulation[89]. It has also been suggested that "electrical conditioning" can help establish automaticity in CMs, since the cultures electrically paced for 7 days displayed autonomous beating at the stimulated rate even after the stimulus has been removed[90].

Electrical activity certainly has some effect on vasculature as sympathetic nervous signaling is an important regulator of vascular tone and sub-millisecond, 250 V electrical pulses applied at 10 Hz has been shown to cause vascular contraction in less than 10 seconds and reduce blood loss in models of acute

traumatic injury[91]. However, the effects of electrical stimulation on endothelial cells and angiogenesis are much more poorly understood. Various kinds of electrical stimulation have been shown to increase angiogenesis in a wide array of settings including diabetic ischemia and neural progenitor cell treatment for ischemic stroke[92,93]. These effects are believed to be primarily mediated by upregulation of VEGF in other cell types as opposed to by directly acting on endothelial cells[94], though there is some evidence that direct current electrical stimulation can upregulate VEGF receptors on endothelial cells, essentially priming them for biochemical stimulation[95,96].

Experiments using electrical stimulation to promote angiogenesis generally utilize constant electrical fields as opposed to experiments focusing on cardiomyocyte development which usually use regular electrical pulses. Thus far, investigations of cardiomyocyte-endothelial cell co-cultures have opted to either forego electrical stimulation or have used periodic electrical stimulation regimens created for CMs, even though the effects of periodic electrical stimulation on endothelial cells and angiogenesis is largely unknown. More directed investigation would be critical to understanding how electrical stimulation of engineered tissues can be optimized for both CM maturation and for vascular development.

In the design of bioreactors with electrical stimulation capabilities, the application of field pulses to a 3D culture is relatively easily adapted from 2D systems. A common configuration for such devices involves using two parallel electrodes to generate an electric field across a substrate[89,97–99]. Tandon and colleagues, for example, developed a system that uses carbon rods to induce an

electric field across a chamber that can support monolayers, 3-dimensional cardiac tissue constructs and micropatterned cellular substrates[97]. In subsequent studies, 1 Hz stimulation applied using this setup was shown to improve CM elongation and alignment, increase conduction velocity and strengthen the tissue-level force of contraction[100]. This strategy has proven successful even with more complicated systems like the Biowire platform, a cell culture system that utilizes both architectural and electrical signaling to generate more mature cardiomyocyte[98]. The system consists of a collagen matrix embedded with cardiomyocytes and supporting cell types surrounding a single surgical suture, all within a template PDMS channel. This platform has since been expanded to also allow for perfusion of the Biowire systems during culture, facilitating an array of pharmacologic experiments.

6.6 Mechanical Stimulation:

Myocardial development depends on a complex series of mechanical forces acting in concert to promote cardiomyocyte maturation, organization and electrophysiological function. Animal studies provided strong evidence for the importance of mechanical stimulation as they showed that altering hemodynamic pressure and contractility in the fetal heart had dramatic effects on myocardial function[101–103]. It has since been established that imposing static or cyclic strain onto an engineered tissue has the ability to induce cardiomyocyte hypertrophy, promote maturity in stem cell-derived CMs, and improve myocardial organization[104,105]. Cyclic strain has come to be understood as particularly important to CM development. Gwak and colleagues showed that applying 10%

strain at 1 Hz to rat ESC-CMs upregulated cardiomyocyte-specific genes and resulted in a more mature microstructure with Z-line formation and more organized myofibrillar bundles[106]. Another study found that the frequency of strain applications could have important differential effects on gene expression. Using ESC-CMs, they found that 10% strain applied at 3 Hz for 3 days resulted in a two-fold increase in α-cardiac actin expression compared to unstretched controls while 1 Hz and 2 Hz stimulation did not produce statistically significant changes[107].

Mechanical forces also play a powerful role in regulating endothelial cell behavior and vascularization. *In vitro* and *in vivo* studies have confirmed that the shear stress caused by blood flow strongly affects the phenotype of vascular endothelial cells[108]. However, in engineered cardiac tissues, where there is generally no blood flow during *in vitro* culture, the field has relied on tissue-level strain instead. Like cardiomyocytes, endothelial cells in engineered scaffolds have been shown to respond positively to uniaxial static strain, displaying improved angiogenesis and vascular alignment[109,110]. However, the effect of cyclic strain on angiogenesis is more controversial. Some early reports suggested that cyclic uniaxial strain can actually disrupt endothelial networks and result in more random vascular organization[111]. Other studies have presented evidence that cyclic strain promotes endothelial cell and vascular alignment parallel to the strain[110,112–114], and some have suggested that the strain induced by surrounding cell contraction is sufficient to induce that effect[115]. Again, the frequency of this strain is an important factor as experiments using human coronary artery endothelial cells showed that a minimum threshold frequency of 0.1 Hz was required to elicit an

alignment effect and that the alignment developed more robustly and on a shorter time scale when the strain was applied at 1 Hz[113].

Experiments culturing endothelial cells and cardiomyocytes together along with a variety of vascular support cell types (detailed above) have thus far been conducted used either cyclic strain conditions or no induced strain at all. These co-culture and tri-culture experiments have produced significant advancements in generating vascularized cardiac tissue, but very little work has been done to evaluate whether using these conditions are optimal for promoting both cardiomyocyte development as well as endothelial cell survival and vascular network formation. It is very possible that conditions chosen to promote cardiomyocyte maturation are impeding angiogenesis in the tissues. Careful optimization of mechanical stimulation will be important in the continued development of these systems.

6.7 Combined Electrical and Mechanical Stimulation:

Applying strain conditions and electrical stimulation together has proven a particular engineering challenge and several bioreactors have been designed with the aim of incorporating these stimuli into hydrogel cultures[116–120]. These devices take advantage of the full diversity of mechanical strain modalities detailed above an have been configured to apply uniaxial and circumferential strain[116,118–121]. Across these devices, though, the vast majority generates electrical stimulation using the parallel electrode setup. A notable exception is the bioreactor reported by Cook and colleagues which applies electrical impulses via the integration of a direct contact in the clamping mechanism that secures the tissue in place[120]. There

are several characteristics that vary widely between these devices including substrate material compatibility, sterility requirements, incubator compatibility, and the integration of sensors, all of which must be considered in selecting the appropriate system for a particular application.

7.CONCLUSIONS:

Multi-cellular systems have been developed to mimic the native myocardium and prolong survival of cardiac grafts when implanted *in vivo.* Several strategies utilizing simultaneous seeding, sequential seeding, and the combination of vascularized and cardiac constructs have been explored to achieve fully vascularized, contractile grafts. While a complete human system will be critical to the clinical translation of this technology, there are important questions surrounding the maturation of pluripotent stem cell derived cardiomyocytes that must be addressed. Several techniques are under investigation to improve the maturation of those cells and the overall organization and functionality of engineering cardiac grafts including electrical stimulation, mechanical stimulation, and a combination of electromechanical stimulation. Recent developments have greatly improved the physiological relevance and translational potential of engineered cardiac patches, but further applications will hinge on the incorporation of dense, functional vasculature and co-alignment of cardiomyocytes.
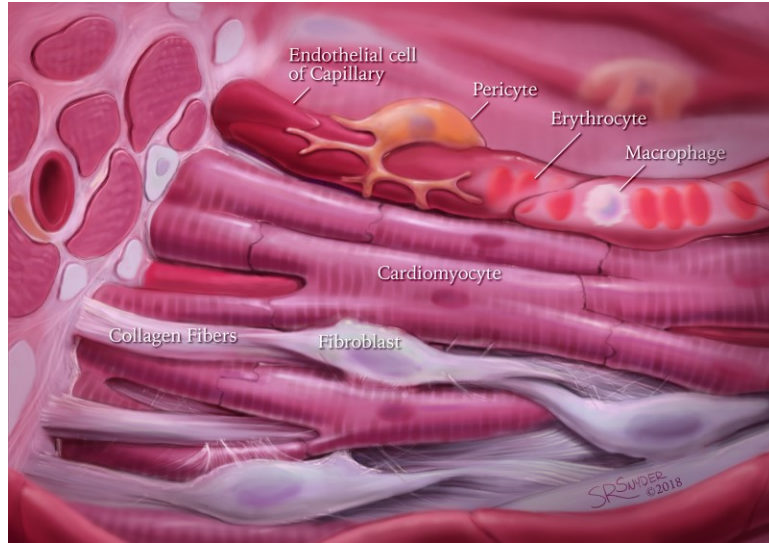
Figure 1: Schematic illustrating structure and composition of the native myocardium.
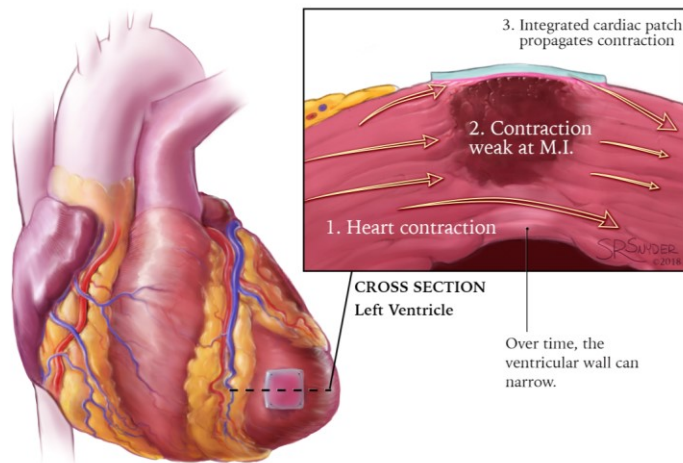
Figure 2: Schematic demonstrating the theoretical application of a myocardial patch placed over an infarct to aid in restoration of lost contractility.
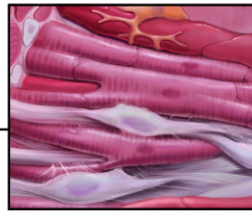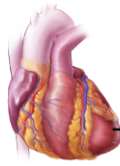
Native Heart Properties

Structured collagen network that guides cardiomyocyte alignment.

Highly vascularized with supporting cell types such as pericytes.
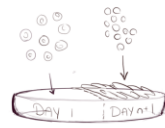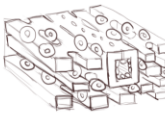
Scaffold Materials		Culture Procedures	
Type	Description	Type	Description
PLLA/PLGA	Cells seeded onto 3D printed bioscaffold	Sequential Seeding	Cells of tri-culture seeded in separate groups over a period of time.
Hydrogels	Cells suspended in tunable microscaffold	Spatial Separation	Cells of tri-culture seeded on different areas of bioscaffold.
Aggregation Spheroids	Cell clusters of tri-culture cell types		

Figure 3: Strategies for the development of vascularized cardiac tissue grafts for infarct repair.

Table 1: Summary of Cell Types used for Tri-Culture Systems

		Advantages	Limitations	Ref.
Cardiomyocytes	**NRVCMs**	• Contract *ex vivo* • Relatively easy to form in monolayers • Well documented electrophysiological properties • Reproducibility of phenotype • Easily accessible	• Rodent specific • No direct clinical translatability • Little to no plateau phase • Immature calcium handling • Limited t-tubule formation • Isolation techniques vary	10,8
	hESC-CMs	• Contractile • Well documented electrophysiological properties • Derived from human embryos • Mimics human cell characteristics • Can be sorted by markers like VCAM-1	• Ethics • Teratoma Formation • Accessibility • Immunogenicity • Genetic Instability • Fetal like in morphology and electrophysiology	122,106
	hiPSC-CMs	• Contractile upon differentiation • Obtained from reprogrammed somatic cells with factors (Oct 4, Sox 2, Klf4, and c-Myc1 or Oct4, Nanog, Sox2, and Lin28) • Have the potential to provide unlimited numbers of cardiomyocytes • Mimics human cell characteristic • Model monogenic diseases • Can be sorted to increase purity • Autologous/Patient Specific with less immunogenicity	• Reprogramming techniques vary • Scale Up • Inter line variability • Cell purity • Relatively immature • Fetal Like Sarcomere Organization • Fetal Like Force Generation • Fetal Like Ion Channel Expression • Mononucleated • Polygonal in cell shape • Mixed Phenotypes • Epigenetic memory	123,13,7

Endothelial Cells	**Primary Endothelial Cells (HUVECs)**	• Mature like endothelial cells from large vessels • Easily expanded • Positive for markers CD31, CD54, CD62e, vWF, and AcLDL • Responsive to exogenous growth factors (i.e. VEGF, FGF2) • Ability to anastomose with host vasculature *in vivo*	• Allogenic • Typically are pooled from multiple donors • Sensitive to cell density during expansion • Sensitive to hypoxia	124– 126,27,127
	hECFCs/ BOECs/EPCs	• Progenitor Cells • Found in circulation • CD31, CD34, CD105, CD144, CD146, vWF, eNOS, VEGFR2 positive • Autologous/Patient Specific • Ability to anastomose with host vasculature • Found in sites of ischemia and wound healing • Paracrine support for myocytes • Express Connexin 43 (Cx-43) and Cx-45 • Integrate with resident vasculature • Can be used for many passages *in vitro*	• Low in number in peripheral blood • Require many expansions • Slow growing initially	27,128,129
	hESC-ECs	• Can form tubes like structures *in vitro* with sorted pure population • Can anastomose with host vasculature *in vivo* • CD31 positive	• Ethics • Immunogenicity • Teratocarcinoma Formation • Differentiation protocol varies causing potential instability in passages post differentiation • Requires selection for EC specific cells	130–132
	hiPSC-ECs	• Autologous/ Patient Specific • Can be disease specific • Can form tubes like structures *in vitro* with sorted pure population • Can anastomose with host vasculature *in vivo* • Have the ability to develop large numbers of endothelial cells quickly	• Various differentiation protocols • Interline variability due to reprogramming methods. • Differentiation protocol varies causing high heterogeneity in the derived ECs. • Requires flow sorting/magnetic sorting for EC specific cells	16,133,15, 134,135

		Advantages	Disadvantages	References
Fibroblast-Like Cells	**Fibroblast**	• Patient Specific • Easily Accessible • Multipotent • Perivascular potential • Can act as pericyte-like cell when coupled with endothelial cells	• Limited Perivascular Potential • Characteristics vary based off of site of isolation • May alter electrophysiological properties of CMs	20,136,19, 137
	Cardiac Fibroblasts	• Cardiac specific • Major cellular component of the native myocardium • Maintain cardiac structure and function • Found in wound healing post infarction • Promoted sprouting of endothelial cells in co-culture.	• Causes damage to myocardium upon isolation • Has experimentally slowed conduction in co-culture with cardiomyoctes *in vitro* •	138,139,22 ,49,140,24
	BM-MSC	• Immunomodulatory • CD73, CD90, and CD105 positive • Pericyte-like cell • Multipotent • Autologous/Patient Specific • Stabilize vasculature • Secrete VEGF, bFGF, Ang-1 and EGF when co-cultured with ECs	• Painful Isolation • Limited Cell Numbers • Can potentially differentiate down the osteogenic lineage in the myocardium • May alter electrophysiological properties of CMs	27,26,25
	hASC	• Pro-angiogenic • High perivascular potential • Differentiate down the smooth muscle lineage when co-cultured with ECs • Relatively easy isolation • Immunomodulatory • May develop gap junctions when coupled cardiomyocytes	• Limited mechanistic information on effects when coupled with cardiomyocytes •	31,32,29,3 0,33

	Pericytes	• Promote vascular stabilization • Secrete pro-angiogenic growth factors • When coupled with cardiomyocytes *in vivo* have shown improvement post MI in ejection fraction and fractional shortening	• Difficult to isolate • Not an abundant cell source • Limited data on the CM electrophysiology when coupled	141,57

Table 2: Tri-Culture studies used for engineering vascularized cardiac grafts

	Cells	Culture Conditions	Cardiac Characterization	Vascular Characterization	Ref
NRVCM	**NRVCM** • 80,000 – 160,000 cells/disk • Percentage: 40 – 80% **D4T Endothelial Cells** • 8,000 – 24,000 cells/disk Percentage: 4 – 13% **Cardiac Fibroblasts** • 28,000 – 48,000 cells/disk • Percentage: 16 – 47%	• Matrigel-coated PEG disks Size: $0.32cm^2$ • Microchannels: $100 – 200 \mu m$ diam × 3 – 4 mm • PEG Disk were coated with Matrigel • Supporting cells cultured for 2 days before addition of NRVCMs • Cell Tracking: Day 1 and Day 4	<u>Advantages</u> • Excitation Threshold: statistically similar in the 65:17:18 group (4 V/cm) and NRVCM control (3.2V/cm) • Maximum Captured Rate: Statistically similar in tri-culture groups and NRVCM only control (value) <u>Limitations:</u> • Cardiomyocytes were clustered into cell aggregates	<u>Advantages</u> • Positive staining for CD31/PECAM-1 • 31% EC yielded statistically higher percentage of positive staining for CD31 compared to 47% and 16% <u>Limitations:</u> • Network development cannot be	39,49
	NRVCM • 1,140,000 cells • Percentage: 57% **Neonatal Cardiac Fibroblasts** • 580,000 cells • Percentage: 29% **Rat Aortic Endothelial Cells** • 280,000 cells • Percentage: 14%	• Microtemplated PMMA with PC molds for fibrin hydrogels • Fibrin hydrogels were rehydrated through sterile PBS • 2mm diameter biopsy punch was used to establish scaffold • 200mg/ml Fibrinogen • Tri-culture cellular mixture was pipetted into fibrin hydrogel • Constructs were cultured for 8 days	<u>Advantages:</u> • Cardiomyocytes survived in the scaffolds over time • Positive staining for Desmin for cardiomyocytes • Revealed maintenance of stiffness of fibrin hydrogels in the presence of Factor XIII and Aprotinin <u>Limitations:</u> • No functional characterization of the cardiomyocytes	<u>Advantages</u> • Vessel formation occurred in pore channels of the scaffold • RECA-1 positive staining colocalized within pore channels • Vessels appeared to form lumens <u>Limitations:</u> • Vessels density not robust • Vessel quantity not characterized	36

			Advantages:	Advantages:	
	NRVCM • 500,000 cells • Percentage: 77 -90 % **hASCs** • 50,000 – 100,000 cells • Percentage: 9 – 16% **HUVECs** • 5,000- 50,000 cells • Percentage: 1 – 8%	• Monolayer Culture on Plastic Coverslips: 2cm^2 • Coated with Fibronectin • NRVCM cells cultured 2 days before addition of supporting cell types. • Cells were optically mapped on days 5-8	• Electrophysiological properties are similar to NRVCM only group (Max Captured rate ~ 7 Hz) • Assessed the Limitations: • Cultured on monolayer • Cardiomyocyte source is not clinically translatable to humans. • Maturation of cardiomyocytes in the presence of supporting cell types not evaluated	• Dense vessel networks were created in the presence of all three cell types at 500:50:25 ratio Limitations: • Cord-like structures • No 3D vessels with lumens • Vasculature is not organized relative to cardiomyocytes	41
hESC-CM	**hESC-CM** • 400,000 cells • Percentage: 33 -40% **Embryonic Mouse Fibroblasts** • 200,000-400,000 cells • Percentage: 20-33% **hESC-EC or HUVECs** • 400,000 cells • Percentage: 33-40%	• 50% PLLA: 50% PLGA Size: 9mm^3 (3mm x 3mm x 1mm) • Pore Size: 212 - 600μm 93% Porosity • Cultured for 2 weeks • 8-10 μL Culture Media:Growth Factor Reduced Matrigel Mix (1:1) • Simultaneously seeded	Advantages: • Spontaneous beating occurred at day 4 • Ca^{2+} impulse propagation in line with contraction • Contractility is responsive to cardiac drugs like isoproterenol and carbamylcholine • Increased proliferation of cardiomyocytes in the presence of endothelial cells Limitations: • Alignment of cardiomyocytes were not characterized • Electrophysiological properties not characterized (i.e. conduction velocity and maximum captured rate)	Advantages • No significant difference with between 1:1 and 1:2 (FB:EC) • Tri-culture resulted in 5.12 lumen density while endothelial was 1.57 • Implanted *in vivo* and becomes functional with host vasculature Limitations: • Did not organize into blood vessels without fibroblasts • Mainly compact clusters	142, 143

hESC-CM	Spheroid/ Cell Clusters	Advantages:	Advantages:	
• 2,000,000 cells • Percentage: 40% **Mouse Embryonic Fibroblasts (MEF) or NHDF** • 2,000,000 cells • Percentage: 40% **hESC-EC or HUVECs** • 1,000,000 cells • Percentage: 20%	• Cultured in Low Attachment Plates • Cultured for 3 days and 8 days • Placed *in vivo* in a skeletal muscle defect and nude rat hearts	• Human cardiac tissues patches contracted and could be paced up to 2-3 Hz. • Increased collagen content in the tri-culture • Increased force of contraction ~8 mN/mm^2 compared to 2 mN/mm^2 • Increased normalized force in the presence of all three cell types • Increased force in tri-culture with increased differential strain Limitations: • Unorganized structure • Lack of mechanical integrity	• Vessel structures increased in HuEB Media as compared to RPMI B27 • Increased CD31 staining compared to cardiomyocyte only control • Anastomosis with host vasculature *in vivo*. Limitations: • Vessel length not assessed *in vitro* before implantation	44

hESC-CM					
hESC-CM /NRVCM • 32 million cells • Percentage: 80% **hMSC** • 4 million cells • Percentage: 10% **HUVECs** • 4 million cells • Percentage: 10%	• POMaC base of scaffold • 5 mm length • 3.1mm width • 150-300μm thickness • Fibrin hydrogel for seeding cells (33mg/mL fibrinogen and 25 U/mL thrombin)	<u>Advantages:</u> • Synchronous contractions occurred as early as day 4 • Conduction velocity was near 4.8 cm/s in vascularized samples without conduction block • Responsive to epinephrine • Cultured with perfusion in bioreactor • Tunable mechanical properties based off of design • Lactate dehydrogenase decreased with perfusion <u>Limitations:</u> • Not uniformly aligned although anisotropic design • Electromechanical stimulation needed to improve electrophysiology	<u>Advantages:</u> • Endothelial cells coated the lumen structure in the parenchymal space. • Connection of vasculature throughout scaffold • 3D microvasculature observed • Connected to the femoral vessels *in vivo* <u>Limitations:</u> • Vasculature is not interspersed through cardiomyocytes which is not similar to the native myocardium	42
hESC-CM • Not Provided **hMSC** • Not Provided **HUVECs** • 375,000 cells	• Decellularized Spinach Leaf • Coated with 10µg/mL fibronectin for cell attachment • Grown for 14 days	<u>Advantages:</u> • Cardiomyocytes have the ability to attach to the surface of the leaf with ECM protein coating • Spontaneous beating at day 5 • Calcium activity was maintained for 21 days on spinach leaf <u>Limitations:</u> • Cardiomyocytes clustered across the spinach leaf rather than making a syncytium • Decreased contractility over time • Contractility strain on TCPS was higher than spinach substrates • Structural integrity for *in vivo* implantation	<u>Advantages:</u> • HUVECs perfused into decellularized plant vasculature to obtain develop vasculature <u>Limitations:</u> • Vasculature is not interspersed through leaf while cardiomyocytes which is not similar to the native myocardium	43

hiPSC-CM	Cells	Method	Advantages/Limitations	Advantages/Limitations	Ref
	hiPSC-CM • 2 million cells • Percentage: 33% **hiPSC-SMC** • 2 million cells • Percentage: 33% **hiPSC-EC** • 2 million cells • Percentage: 33%	• Fibrin Hydrogel loaded with IGF-1 for cell survival • Directly injected cells into hydrogel on the myocardium • Cells are differentiated into three lineages (CM, SMC, and EC) and injected directly into hydrogel without *in vitro* culture	Advantages: • Improved functionality *in vivo* with tri-culture and patch present and reduced CM apoptosis of myocytes • Increased ejection fraction • Decreased infarct size • Cell survival was greatest in tri-culture cells + patch group Limitations: • Cardiac electrophysiology not characterized prior to *in vivo* implantation	Advantages: • Tri-culture promoted survival and proliferation of cardiomyocytes • Engineered Vasculature promotes host vasculature angiogenic response Limitations: • Vasculature was not characterized before implantation into the infarcted myocardium	37
	hiPSC-ECM • 1 million cells • Percentage: 76% **hMSC** • 400,000 cells (w/hiPSC-ECM) • 300,000 cells (w/hCMVECs) • Percentage: 23% / 38% **hCMVECs** • 500,000 cells • Percentage: 63%	• 3D Collagen Cell Carrier • hMSC/hCMVECs culture for 7 days under vascular conditions • hMSC/hiPSC-ECMs cultured for 7 -14 days on top pre-vascularized cultures	Advantages: • Positive staining for Cardiac MHC across the construct • Rhythmic contractions • Calcium flux monitored across system Limitations: • Cardiomyocyte orientation not controlled • Electrophysiological parameters not examined	Advantages: • CD31 Positive cord-like structures established • Pericyte-like cell stained positive for SMA • Sequential seeding of vasculature cells • Positive staining for AcLDL and vWF in the tri-culture system Limitations: • Vasculature is reduced in the presence of all three cell types	144
	hiPSC-CM • 14,850 – 23,100 cells • Percentage: 45-70 % **hCF** • 0 to 13,200 cells • Percentage: 0-40% **HUVECs** • 4,950 – 9,900 cells • Percentage: 15-30 %	• 3D Bioprinting (0.32cm^3) • Single layer of cell aggregates (cardiospheres) that were 450 to 550 μm in diameter • Printed on Needle Array • Cardiac patch was matured for 72 hours with needle array in place	Advantages: • Electrophysiological parameters quantified • Ventricular-like action potentials • Developed gap junctions (Cx-43) to propagate signal as a syncytium • Low levels of cell death from TUNEL assay • Conduction velocity near 4.6 cm/s	Advantages: • CD31 staining throughout the cardiosphere • Nascent vasculature development *in vivo* Limitations: • Vasculature not quantified • Presence of 3D lumens not investigate or represented	45

		• Cardiospheres beat after 2 days and fused after removal of needle array • Cardiospheres were implanted onto myocardium and secured with tissue glue *in vivo*	Limitations: • Conduction velocity decreased with increased fibroblast percentage	
	hiPSC-CM • 4 M/mL • Percentage: 65% **hPC** • 0.36 M/mL • Percentage: 6% **BOEC** • 1.82 M/mL cells • Percentage: 29%	• Fibrin Hydrogel • 8.4mm x 5 mm • 4 mg/mL fibrinogen • 120µL total volume • Bilayer patch was created by coating with fibrinogen and 10U/mL thrombin • Grown for 14 days	Advantages: • Bilayer patch resulted in increased CM density compared to control (237 vs 35 CM/mm^2) • CM only patches underwent more apoptosis than bilayer (75.4% vs 37.5%) • Bilayer patch output was 2.17nN/input CM vs 0.3 nN/input CM Limitations: • Electrophysiological properties not analyzed • Alignment of cardiomyocyte	Advantages: • ~34 lumens/mm^2 • ~65 vessels/mm^2 *in vivo* • ~67% perfused fraction of vasculature Limitations: • Vasculature developed independently of cardiomyocyte culture which is not similar to the native myocardium	145

2

Modular Approach to Vascularized Cardiac Tissue: Exploring Cell-Cell Interactions in a Tri-Culture System

1. INTRODUCTION:

Cardiac tissue engineering is a promising approach to regenerate the damaged myocardium. The native myocardium is composed of many different cell types which all play a specific role in the functionality and survival of the organ. These cell types include cardiomyocytes, endothelial cells, and fibroblasts [5,6,146]. Although cardiomyocytes account for the largest volume of cells at 80-90% [147], supporting cell types account for the largest number of cells [123,146,148]. Endothelial cells, which are primarily responsible for blood vessel development, provide the heart with nutrient and oxygen supply through the coronary vasculature [149]. In addition to dense vessel networks, the heart has a large population of fibroblasts. Fibroblasts have been shown to make up greater than 50% by number of the cellular population in the adult mammalian heart [23,146]. Fibroblasts maintain the mechanical properties of the heart, provide the structure of the extracellular matrix, and produce growth factors [138,140,148,150].

Previous studies have shown that utilizing the native cellular makeup for cardiac muscle improves cardiomyocyte survival, force of contraction, and

maximum capture rate of engineered grafts and promotes vascular development for possible anastomosis with host vasculature to provide prolonged survival [6,142]. A delicate balance of cellular ratios is necessary to develop vascularized cardiac tissue that is able to maintain normal electrophysiological function while developing robust vascular structures[149,151–153].

Fibroblasts have traditionally been excluded from cultures of NRVMs as they can impede and/or alter the electrophysiological function (e.g. action potential conduction) of cardiomyocytes [154]. However, fibroblasts also provide mechanical and biochemical support and have at times been intentionally included in co-cultures with cardiomyocytes [155]. Previous tri-cultures have utilized fibroblasts from lung or foreskin as a means to stabilize the nascent vasculature formed by endothelial cells [39,49]. The source of the fibroblast impacts the levels of pro-angiogenic factor secretion [20]. In several studies mesenchymal stem cells have served as fibroblast replacements [33]. Bone marrow-derived mesenchymal stem cells (BM-MSCs) can be an attractive cell source, but isolations are painful and result in low cell yields. BM-MSCs have been shown to aid in the stabilization of vasculature in the presence of endothelial cells, but when co-cultured with cardiomyocytes have been shown to fuse and reduce the electrophysiological properties of cardiomyocytes [156,157]. Consequently, there is a need for a cell population that has the potential to act as vascular mural cells [158] and does not significantly inhibit the electrical functioning of cardiomyocytes.

Human adipose derived stem/stromal cells (hASCs) are a clinically relevant stem cell source that is of mesodermal origin and are available in large quantities

upon isolation. They have the ability to differentiate into vascular mural cells [29,31], and form gap junctions with electrically excitable cells allowing the electrical signal to propagate across and trigger calcium transients [28]. The hASCs in co-culture with endothelial cells display a pericyte-like phenotype, ultimately stabilizing newly-formed vascular networks (Merfeld-Clauss et al., 2014, 2010). Crisan et al. has shown that cells derived from white adipose tissue can display perivascular markers such as CD146, α-SMA, NG2 and showed negative expression of endothelial markers CD31 and CD144 [160–162]. They also have the ability to withstand temporary ischemia, release trophic and paracrine factors, and prevent inflammation [136,163]. These properties of hASCs suggested that it might be beneficial to assess their role as fibroblast replacements in co-culture with NRVCMs and HUVECs.

In this study, we aimed to determine the potential benefits of using hASCs relative to dermal fibroblasts to provide vascular stabilization while maintaining the electrophysiological properties of cardiomyocytes in a tri-culture system. In the development of a vascularized cardiac tissue, prior studies have demonstrated that tri-cultures (cardiomyocytes, endothelial cells, and fibroblasts) exhibit significantly better outcomes with the development of stabilized vasculature structures, decreased excitation threshold, and maintenance of maximum capture rate relative to enriched cardiomyocyte populations and co-culture systems in which cardiomyocytes and endothelial cells alone were utilized [39,49]. We assessed the functional outcomes of co-cultures of varying ratios of NRVCM:hASC (and NRVCM:hDF) in a well-established monolayer model utilizing optical recordings of

transmembrane voltage. We also evaluated the effect of the ratio of hASC:HUVEC (and hDF:HUVEC) on vessel length and interconnectivity. This information was used to develop a tri-culture system with a ratio of NRVCM:hASC:HUVEC that incorporated the benefits of hASCs for vascularized cardiac regeneration while maintaining the electrophysiology of enriched cardiomyocyte cultures.

2. MATERIALS & METHODS:

2.1 Isolation of Adipose Derived Stem Cells:

Isolation of human adipose derived stem/stromal cells (hASCs) was performed at the Stem Cell Biology Laboratory, Pennington Biomedical Research Center, under an Institutional Review Board approved protocol according to published methods [164]. Briefly, fresh human subcutaneous adipose lipoaspirates were obtained under informed consent from healthy Caucasian female donors with a mean age of 47.6 ± 1.9 years and mean body mass index of 27.1 ± 0.6 and undergoing elective liposuction surgery. The lipoaspirate tissue was extensively washed with warm Dulbecco's phosphate-buffered saline solution (DPBS) to remove erythrocytes and then digested in DPBS supplemented with 0.1% Collagenase Type I (Worthington), 1% BSA, and 2 mM $CaCl_2$ for one hour at 37°C. Following room temperature centrifugation at 300 g and suspension in Stromal Medium (DMEM/F-12 (Life Technologies) supplemented with 10% FBS (Atlanta Biologicals) and 1% penicillin/streptomycin), the stromal vascular pellet obtained from 35 mL of digested lipoaspirate was plated in a T175 flask (0.2 mL per cm^2). After 24 hours of incubation at 37 °C, 5% CO_2, the adherent cells were washed with warm DPBS and maintained in Stromal Medium until reaching 80-90%

confluency. The adherent population ("passage 0") was harvested by digestion with trypsin with 0.05% EDTA (1 mM) at 37 °C for five minutes, washed with Stromal Medium, and cryopreserved for shipment to Johns Hopkins University. Prior studies have shown that there are no deleterious effects on hASCs due to cryopreservation, such as loss of viability or multipotency [164]. For expansion, hASCs were thawed and cultured in expansion medium, which consists of DMEM high glucose (Life Technologies), 10% FBS (Atlanta Biologicals), 0.5% penicillin/streptomycin (Cellgro), 0.5% antibiotic/antimycotic, 1ng/mL Fibroblast Growth Factor-2 (bFGF/FGF-2) (PeproTech). Cells were utilized at passage 4 (P4) to minimize contamination of heterogenic cell types.

2.2 Isolation of Neonatal Rat Ventricular Cardiomyocytes:

All procedures with animals were completed in accordance with the regulations set forth by the Johns Hopkins Committee on Animal Care and Use along with all state and federal regulations. In brief, Neonatal Rat Ventricular Cardiomyocytes (NRVCMs) were enzymatically dissociated from the hearts of 1-3 day old Sprague Dawley rats (Charles River Laboratories, Frederick, MD) as previously described [165,166]. Freshly isolated cells were suspended in NRVCM culture media (Medium 199 (Life Technologies), 1% HEPES buffer solution (Life Technologies), 1% MEM non-essential amino acids (Life Technologies), 2mM L-glutamine (Life Technologies), 20µM glucose (Sigma Aldrich), 4μg/mL Vitamin B$_{12}$ (Sigma Aldrich), 1% Penicillin (Cellgro), and 10% or 2% Heat Inactivated (HI)-FBS (Sigma Aldrich)) and pre-plated in flasks twice, for one hour each time in order to reduce the proportion of fibroblasts.

2.3 Human Umbilical Vein Endothelial Cell Culture:

A vial of pooled Human Umbilical Vein Endothelial Cells (HUVECs) (Lonza) were expanded in tissue culture flasks up to passage 4-5 using Endothelial Basal Medium 2 (EBM-2) culture medium (Lonza, USA) supplemented with the Endothelial Growth Medium-2 (EGM-2) Bullet Kit (Hydrocortisone, human fibroblast growth factor (hFGF)-2, vascular endothelial growth factor (VEGF), R3-insulin-lke growth factor (IGF)-1, ascorbic acid, human epidermal growth factor (hEGF), Gentamicin & Amphotericin (GA-1000), and Heparin) and 2% FBS. HUVECs were used for experimentation at Passage 5-6.

2.4 Fibroblast Expansion and Characterization:

The human Dermal Fibroblast-BJ Cell Line (hDF) (ATCC) was expanded in tissue culture flasks up to passage 5 (P5) using DMEM (Life Technologies), 10% FBS (Atlanta Biologicals), and 0.5% penicillin/streptomycin (Cellgro), 0.5% antibiotic/antimycotic (Life Technologies). The cells were examined for CD73, CD90, and CD105 as mesenchymal markers, CD31, CD34, and CD309 as vascular markers.

2.5 Flow Cytometric Analysis of hASCs and hDFs:

Cells were detached with 0.05% Trypsin/EDTA and washed with phosphate buffer saline (DPBS) containing 2% FBS. They were then incubated with monoclonal antibodies conjugated with fluorescein isothiocyanate (FITC) or phycoerythrin (PE) to detect mesenchymal markers (CD73, CD90, and CD105) or vascular markers (CD31, CD34, and CD309 (VEGFR2)) for 30 minutes at 4 °C. Similarly conjugated isotype controls (BD Biosciences) were used as negative

controls. After incubation with the antibodies, cells were washed three times for 5 minutes each with DBPS containing 2% FBS, then analyzed with the BD Accuri C6 flow cytometer.

2.6 Co-Culture and Tri-Culture Experiments:

Cells were plated onto bovine fibronectin (5mg/mL diluted in cold distilled water) (Sigma Aldrich)-coated 14 mm-diameter plastic coverslips that were placed in 24 well plates. All studies were performed on 2cm^2 surfaces. We will utilize the consistent nomenclature – thousands of NRVCM:hASC:HUVEC (or NRVCM:hDF:HUVEC) per cell culture well – to describe co-culture and tri-culture cell plating densities throughout the manuscript. Therefore, for NRVCM:hASC co-cultures, the HUVEC concentration is reported as zero. Likewise, in hASC:HUVEC experiments, the NRVCM numbers are reported as zero. The design of the protocol was based on keeping the total number of NRVCMs constant. The results of the co-culture studies were used to obtain the input cell ratios for the tri-culture studies (**Fig 1**).

2.7 NRVCM-hASC/hDF Co-Culture:

NRVCMs were plated at a concentration of 500,000 cells in NRVCM medium containing 10% FBS. This number of NRVCMs was determined to form a confluent monolayer and was kept constant in all experiments. On the next day, different amounts of hASCs were plated on top of the NRVCMs resulting in ratios of 500:500:0, 500:250:0, 500:100:0, 500:50:0, and 500:0:0. An hASC-only well (0:500:0) was utilized as a negative control. Medium was switched to 2% FBS-containing medium, to reduce fibroblast proliferation, on the following day and

refreshed every other day. Upon day 5-8, cells were assessed using optical mapping and were fixed with 4% paraformaldehyde for immunocytochemistry analysis. These studies were used to assess the maximum number of hASCs that could be added without causing significant changes in electrophysiology. To compare hASCs and hDFs, the studies were repeated for hDFs with cell ratios of 500:100:0 and 500:50:0.

2.8 hASC/hDF-HUVEC Co-Culture:

hASCs and HUVECs were mixed together in ratios of 0:100:100, 0:100:50, 0:100:20, 0:100:10, 0:50:50, 0:50:25, 0:50:10, and 0:50:5, and plated on coated cover slips. A HUVEC-only control 0:0:100 or 0:0:50 was included. The constructs were cultured *in vitro* for 7 days and fed every other day with EGM-2 (Lonza).

2.9 NRVCM /hASC/HUVEC Tri-Culture:

NRVCMs were plated at a concentration of 500,000 cells in NRVCM media containing 10% FBS. On the following day, the media was removed, and coverslips were washed with DPBS prior to simultaneously plating hASCs and HUVECs to give final ratios of 500:100:50, 500:100:20, 500:100:10, 500:50:25, 500:50:10, 500:50:5. Two additional controls were included: no hASCs (500:0:50) and NRVCM only (500:0:0). Tri-cultures were fed EGM-2 (Lonza) media containing 2% HI-FBS (Sigma Aldrich), 20µM glucose (Sigma Aldrich), 0.5% penicillin/streptomycin (Cellgro), and 0.5% antibiotic/antimycotic (Life Technologies). Culture media was refreshed every other day.

2.10 Optical Mapping:

Co-cultures and tri-cultures containing NRVCMs were optically mapped using voltage-sensitive dye in order to record changes in their transmembrane voltage and visualize their excitation and repolarization (Tritthart, 2005). Optical mapping was performed on days 5-8. Coverslips containing cell monolayers were stained with 10 µM of the voltage-sensitive dye di-4-ANEPPS (Invitrogen), in Tyrode's solution for 10 minutes at 37 °C while being protected from light.

After staining, the dye solution was removed, cells were washed with Tyrode's solution, and placed on a heated stage in Tyrode's solution with 5 µM blebbistatin to prevent motion artifacts due to contraction. Optical mapping was performed using a CMOS camera (MiCAM Ultima, Scimedia, Costa Mesa, CA). Cells were electrically stimulated by placing a bipolar point electrode near the edge of the coverslip, out of the field of view of the camera, and paced starting at 0.5 Hz and incrementally increased by 0.5 Hz. At each new pacing rate, the cell monolayers were stimulated for 1 minute to achieve steady state before an optical recording was taken. Pacing rate was increased until the ability of the sample to be captured at the pacing rate (i.e., action potential response with each pacing pulse) was lost or reentrant spiral waves were formed.

2.11 Immunocytochemistry:

On day 7, or after mapping, if applicable, co-cultures and tri-cultures were fixed in 4% paraformaldehyde for 20 minutes at room temperature. After removing formaldehyde, cells were washed three times with DPBS for 30 minutes each time. Samples were permeabilized with 0.2% Triton X-100 (Sigma Aldrich) for 10

minutes and then blocked with 10% normal goat serum (Sigma Aldrich) in DPBS for 30 minutes. Coverslips were then incubated overnight at 4 °C with 1) mouse (Ms) anti-Sarcomeric α-Actinin [1:200] (Sigma Aldrich), rabbit (Rb) anti-Connexin-43 [1:100] (Sigma Aldrich), or 2) mouse anti-Vimentin [1:200] (Dako) and TRITC conjugated Phalloidin [1:50] (Sigma Aldrich), or 3) mouse anti-CD31 [1:250] (Sigma Aldrich). Primary antibodies were diluted in DPBS with 5% normal goat serum. Coverslips were washed three times with DPBS, then incubated overnight at 4°C with secondary antibodies DyLight 488-conjugated goat anti-mouse [1:200] and DyLight 649-conjugated goat anti-rabbit [1:200] (Jackson ImmunoResearch) that were diluted in 5% normal goat serum in DBPS. Samples were washed three times with DPBS and then incubated for 10 minutes at room temperature with DAPI [1:2000] (Sigma Aldrich) diluted in DPBS. Following the initial round of immunostaining, the samples stained with mouse anti-Sarcomeric α-Actinin and rabbit anti-Connexin-43 were further blocked in 5% normal mouse serum in DPBS. Following blocking, samples were incubated with Cy3 conjugated mouse anti-α Smooth Muscle Actin [1:400] (Sigma Aldrich) diluted in 5% normal mouse serum in DPBS incubated overnight at 4 °C. Coverslips were subsequently washed three times with DPBS. Samples were mounted with mounting medium and imaged under a Zeiss Axio Observer inverted fluorescence microscope or a Zeiss LSM 510 confocal microscope with 5x, 20x, and 40x objectives.

2.12 Image Analysis:

5x z-stacks were taken with 15 μm spacing, while 20x z-stacks had 3 μm spacing. Immunostained images were z-projected and thresholded in order to calculate

vessel parameters including network length and junctions in the 3,240 mm^2 imaged region. Thresholded images were subsequently analyzed with AngioQuant software to determine the total vessel length, area, and interconnectivity. Using a custom Image J macro, connexin 43 (Cx-43) stained images were thresholded, and the number of stained foci were calculated. Cx-43 foci counts were divided by the area to report as Cx-43 $foci/mm^2$.

2.13 Statistical Analysis:

Quantitative data is reported as the mean +/- the standard deviation. One-way ANOVA with Dunnett's post-hoc test or Tukey's post-hoc test was performed to determine statistical difference between testing groups. Differences were considered statistically significant at $*p < 0.05$; $**p < 0.01$; $***p < 0.001$.

3. RESULTS:

3.1 Effect of hDFs and hASCs on electrophysiological parameters of cardiomyocytes.

NRVCMs and hASCs were plated on sequential days, as described in the Methods, at varying ratios in order to determine the maximum number of hASCs that did not induce a statistically significant decrease in the conduction velocity or change in action potential duration when compared with NRVCM-only cultures. During testing, the action potential durations at 80% repolarization (APD_{80}) during 1 Hz pacing were significantly longer in the 500:500:0 (325 ± 42 ms) and 500:250:0 groups (268 ± 64 ms) relative to the 500:0:0 (cardiomyocyte only) group (168 ± 17 ms). APD_{80} of the other co-culture ratios, 500:100:0 (201 ± 30 ms) and 500:50:0 (188 ± 13 ms) was not significantly different from that of the cardiomyocyte-only

group (**Fig. 2A**). Similar trends occurred with APD_{30} with values of 137 ± 26 ms (500:500:0), 83 ± 29 ms (500:250:0), 56 ± 9 ms (500:100:0), 50 ± 9 ms (500:50:0), and 48 ± 10 ms (500:0:0) (**Fig. 2A**) (*n=2-6*) . These trends held at other pacing rates as seen in **Fig. S1A.** Maximum capture rate (MCR) decreased from roughly 4 ± 0.4 Hz (500:0:0) to 1.5 ± 0.03 Hz (500:500:0) with the addition of 500,000 hASCs. MCRs were statistically indistinguishable in the 500:250:0, 500:100:0, 500:50:0, and 500:0:0 groups but exhibited a statistically significant decrease in the 500:500:0 group (**Fig. S1C**).

Based on these results, we compared the effects of co-culturing NRVCMs with hDFs or hASCs using a subset of these cell ratios – 500:100:0 and 500:50:0 – as these groups did not exhibit significant increases in APD_{80} or APD_{30} compared to the cardiomyocyte-only cultures. Flow cytometry was performed to characterize the two cell populations. P5 hDFs and P4 hASCs were primarily positive for mesenchymal markers, CD73 (99.4%/ 99.8%), CD90 (99.9%/ 99.9%), and CD105 (99.9%/ 92.8%), respectively and mostly negative for vascular markers CD31 (0.39%/0.02%), CD34 (0.01%/ 1.6%), and CD309/VEGFR2 (0.23%/ 0.08%) (**Fig. 2B**) (*n=3*). Immunocytochemistry revealed the presence of hDFs and hASCs in the co-cultures via positive staining for vimentin, a marker of fibroblast-like cells (**Fig. S2A**). APD_{80} and APD_{30} values were significantly shorter in the hASC co-cultures compared to the hDF co-cultures at both cell ratios. At 1.5 Hz, APD_{80} was 173 ± 12 ms (500:100:0) and 169 ± 15 ms (500:50:0) for NRVCM:hDF co-cultures, compared to 126.5 ± 27 ms and 125.6 ± 27 ms for NRVCM:hASC cultures at 500:100:0 and 500:50:0 ratios, respectively (**Fig. 2C, D**). The NRVCM only control

resulted in an APD$_{80}$ of 112 ± 20 ms. APD$_{30}$ ranged from 57 ± 5 ms in the 500:100:0

mixture containing hDFs to 40 ± 7 ms 500:50:0 containing hASCs, while APD$_{30}$ was

consistently near 47 ± 11 ms in the NRVCM only control group (500:0:0) (**Fig. 2E**).

The conduction velocity (CV) at all pacing rates was maintained between 15 ± 2

and 19 ± 2 cm/s in both NRVCM:hDF and NRVCM:hASC co-cultures with no

significant differences between groups (**Fig. 2F,G**). The NRVCM-only group

(500:0:0) had CVs ranging from 15.7 ± 6 to 20.6 ± 7 cm/s at pacing rates from 0.5

Hz to 2.0 Hz (**Fig. 2F,G**) *(n=4-6).*

We were able to pace co-cultures with hASCs at faster rates (MCR=5 ± 1.5

Hz for 500:100:0 and 6 ± 1.3 Hz for 500:50:0 ratio) than co-cultures containing

hDFs (2.08 ± 0.7 Hz and 3 ± 1.6 Hz, respectively, **Fig. 2H**). We also noted

NRVCM:hASC co-cultures exhibited increased expression of Cx-43, (500:100:0

and 500:50:0) as compared to NRVCM:hDF co-cultures (**Fig. S2B, C**). Although

there was increased expression of Cx-43 in the NRVCM:hASC co-culture relative

to pure NRVCM cultures, there were no significant differences in conduction

velocity compared to NRVCM:hDF co-cultures. Other pacing rates exhibited

similar trends (**Fig. S3**).

3.2 Effect of hASC and HUVEC concentration on vessel formation.

To determine the effects of cellular concentration on vessel assembly, we

co-cultured hASCs and HUVECs. Two hASC seeding densities were used –

100,000 cells/well or 50,000 cells/well – as these were the numbers of hASCs that

did not significantly increase the APD$_{80}$ of the cardiomyocytes in the

NRVCM:hASC co-cultures (**Fig. 2A**). Various numbers of HUVECs were tested

with these hASC concentrations. At a HUVEC density of 10,000 cells per well, vessel length increased when more hASCs were seeded (**Fig 3B**). For hASC:HUVEC co-cultures containing 100,000 hASCs/well, vessel lengths and number of junctions both increased with decreasing amounts of HUVECs (**Fig 3B,C**). No vessels were formed in HUVEC-only controls. Staining in Fig. 3A shows that the endothelial cells have not yet formed vasculature structures. For hASC:HUVEC co-cultures with only 50,000 hASCs/well, the opposite results were observed, and vessel lengths and number of junctions both decreased with decreasing amounts of HUVECS (**Fig 3B**,**C**). hASCs in co-culture with HUVECs appeared to take on a pericyte-like cell phenotype and stained positively for α-smooth muscle actin (**Fig S4**). Similar ratios were tested with dermal fibroblasts and resulted in vessels structures that did not develop like those in groups with hASCs (**Fig S5**).

3.3 Effect of tri-culture on cardiomyocyte electrophysiology.

Based on the results of our initial studies, tri-cultures were established using only hASCs and not hDFs. The NRVCM:hASC:HUVEC ratios were determined by the previous co-culture studies and included (i) the amount of hASCs that did not significantly increase the APD_{80} (50,000 and 100,000) and (ii) the ratios of hASCs:HUVECs that allowed for formation of robust vasculature. The study employed six ratios of NRVCM:hASC:HUVEC in addition to no hASC controls (500:0:50) and NRVCM only controls (500:0:0). Samples were stained with CD31/PECAM-1 to indicate endothelial cell elongation and connectivity of endothelial cells. Groups which formed vessel networks included 500:100:50,

500:100:20, 500:100:10, 500:50:25, and 500:50:10 ratios (**Fig 4A**). Samples were also stained for Cx-43 and CD31, revealing that Cx-43 positive loci were present near CD31-positive cells, and thus, that gap junctions, sites of the electrical connections of the cardiomyocytes, formed in close proximity to nascent vasculature (**Fig. 4A**). Generally, vessel lengths decreased when the ratio of hASCs:HUVECs increased. There were no vessels detected in the ratios of 500:50:5, 500:0:50, and 500:0:0 (**Fig 4B**). Vessel interconnectivity was determined by the number of junctions, which also tended to decrease when the ratio of hASCs:HUVECs increased (**Fig 4C**). We found that the 500:50:25 ratio ultimately provided the best vessel assembly with the longest vessel length and supporting one of the higher amounts of interconnectivity extrapolated through number of junctions. In this group, average total vessel length was 70 mm per 3,240 mm^2, and vessel networks had an average of 454 junctions (*n=3)*.

Following tri-culture vessel characterization, electrophysiological properties of the tri-cultures were evaluated. There was no statistical difference in APD_{80} of any of the tested tri-culture groups as compared to the cardiomyocyte-only control (120 ± 9 ms at 1.5 Hz pacing rate) (*n=4-6)* (**Fig. 5A,B**). Although no level of significance was reached, there appeared to be a trend of increasing APD_{80} with more hASCs present in cultures. The APD_{30} values were measured and calculated similarly. All tri-culture groups' APD_{30} values were not significantly different from the NRVCM only control (51 ± 5 ms at 1.5 Hz pacing rate) (*n=4-6)* (**Fig. 5C**). Similar trends were noted at the 2 Hz pacing rate for both APD_{80} and APD_{30} (**Fig S6A,B,**).

CVs of the ratios 500:50:25 and 500:0:50 were not statistically different when compared to the NRVCM control (500:0:0), while all other groups had significantly lower CVs (25 ± 1 ms at 1.5 Hz pacing rate for control) (**Fig 5D,E**). MCR was not significantly different between groups and fell between 6.7 ± 0.8 Hz (500:100:50) and 7.2 ± 0.2 Hz (500:0:0) (*n=4-6)* (**Fig 5F**). Similar trends were noted at the 2 Hz pacing rate for CV (**Fig S6C**).

4. DISCUSSION:

Previous tri-cultures have utilized either embryonic stem cell-derived cardiomyocytes (ESC-CM) or NRVCMs with endothelial cells that were either embryonic stem cell-derived (ESC-EC) [6,142], or mature, such as HUVECs [142]. For example, Caspi et al. (2007) developed a tri-culture system with ESC-CMs, ESC-ECs, and mouse embryonic fibroblasts (MEFs) cultured on poly(l-lactic-acid)/poly(lactide-co-glycolide) PLLA/PLGA scaffolds. MEFs provided vascular stabilization, increased proliferation, and reduced apoptosis of ESC-ECs, and the presence of stabilized vasculature correlated with increased cardiomyocyte proliferation. Additionally, Iyer et al. (2009a; 2009b; 2012) investigated simultaneous seeding and sequential seeding of tri-culture systems. Simultaneous seeding of all three cell types impeded the development of gap junctions between cardiomyocytes and resulted in the presence of rounded cardiomyocytes with no ability to contract. Just as importantly, simultaneous seeding of cardiomyocytes with endothelial cells and fibroblasts resulted in endothelial cells that did not elongate to form vessel-like structures. However, when cardiomyocytes were seeded first and allowed to attach and form electrical connections with each other

prior to adding other cell types, they elongated and expressed the gap junction protein Cx-43, and cardiac troponin. Thus, we utilized a sequential seeding approach, where a high density of NRVCMs was plated into each well one day prior to the addition of co-culture or tri-culture cells. In hASC-HUVEC co-cultures, cells were seeded simultaneously. The main objectives of this study were to assess the potential for using hASCs as a suitable cell source for vascular stabilization in tri-cultures with HUVECs and NRVCMs and to determine the appropriate cell ratios required for the development of vascularized cardiac tissues. The key success criteria were that the tri-cultures should be capable of maintaining similar electrophysiological function (maintenance of repolarization rates and maximum capture rates) compared to NRVCM-only controls and simultaneously demonstrate the presence of well-developed vascular structures.

Previous studies have also used hDFs with endothelial cells to establish in vitro models of vasculogenesis [172,173] though, more recently, studies of vascular co-culture have shown that hASCs outperform hDFs and SMCs as vascular support cells [29]. Previously published studies of tri-culture systems with NRVCM and endothelial cells used primary cardiac fibroblasts [49] and embryonic fibroblasts [142] as vascular support cells. Therefore, in our studies, we compared hASCs to the hDF cells to incorporate the functionality of the previous tri-culture systems with the improved vascular support of hASCs. Previous studies have also demonstrated the potential of hASCs to act as cardiomyocyte support cells [28] as well as perivascular cells to maintain the stability of nascent vascular structures formed by endothelial cells [30–32]. To determine an upper limit of their role as support

cells, we probed the maximum concentration of hASCs that could be added to pure cultures of NRVCMs before the electrophysiological properties of the NRVCMs would be significantly compromised. Typically, co-cultures of cardiomyocytes with fibroblasts or fibroblast-like cells in culture have increased action potential durations and reduced conduction velocities [174]. Similarly, we found that NRVCMs co-cultured with either hASCs or hDFs at concentrations above a threshold level had similar CVs but shorter action potential durations than NRVCM-only control groups. hASC concentrations that exceeded 20% of the cardiomyocytes reduced the maximum capture rates, increased the duration of action potentials, and reduced the rates of conduction (**Fig S1**). This led us to conduct further studies with NRVCM:hASC co-cultures at ratios of 20% or less (500:100:0 and 500:50:0). When hASCs were directly compared with hDFs, we found that hDFs had significantly lower maximum capture rates and significantly longer repolarization times at equivalent concentrations. hASCs thus proved to be a more attractive cell source than hDFs for tri-culture systems. It is interesting to note that co-cultures of NRVCMs with hASCs exhibited increased Cx-43 expression, relative to NRVCM:hDF co-cultures (**Fig. S2**). However, further experiments are needed to identify the exact underlying mechanisms for improved outcomes with hASCs as opposed to hDFs.

To assess the effect of hASCs on the development of vascular structures, we co-cultured them with HUVECs. Prior studies have reported that EPCs or HUVECs co-cultured with hASCs developed robust vascular structures in cell monolayers [29,30]. These findings indicated that hASCs can act as a vascular mural

cell which contributes to the development and stabilization of cord-like vessel structures. Mechanistically, hASCs promote vascular development by paracrine signaling [25,160], including growth factor secretion [175], and direct cell-cell contact (for stabilization) with the endothelial cells [29–31,175]. Vessel development occurred at all tested ratios of hASC:HUVEC co-cultures. In these studies, we kept the initial numbers of hASCs constant at 100,000 cells/well and 50,000 cells/well to be consistent with the hASC numbers that did not significantly alter APD, CV and MCR in the NRVCM:hASC studies. There were measurable differences in the total vessel length and interconnectivity among the various ratios. However, no general trends emerged: when 100,000 hASCs were used per well, lower numbers of endothelial cells resulted in longer vascular structures, while the opposite was true when 50,000 hASCs/well were used. However, HUVECs were unable to form network structures in the absence of hASCs. When hDFs were used in lieu of hASCs, the ability of HUVECs to form vascular structures was significantly lower (**Fig. S3**). Our study did not assess the mechanistic reason for this difference in pro-angiogenic potential of hASCs and hDFs. However, prior studies suggest that hASCs may secrete higher concentrations of VEGF than hDFs [136]. Another study compared co-cultures of EPCs and hASCs to co-cultures of EPCs and hDFs, and found that total tube length and branch points were significantly decreased in the dermal fibroblast group [29]. We note that the vascular structures developed in our cultures are two-dimensional and may not contain lumens. However, the data gleaned from this study provides fundamental insights for subsequent studies in 3D scaffolds and hydrogel systems.

These two co-culture studies of NRVCM:hASC and hASC:HUVEC, were used to provide starting cell ratios for the tri-culture system. Based on the superior performance of hASCs relative to hDFs in both NRVCM and HUVEC co-culture systems, we did not assess the efficacy of hDFs in our tri-culture studies. The concentrations of NRVCMs were maintained constant at 500,000 cells/well and plated a day prior to the addition of hASCs and HUVECs. Based on NRVCM:hASC co-culture studies, we tested only two concentrations of hASCs (50,000 cells/well and 100,000 cells/well). We assessed three hASC:HUVEC ratios (0:100:50/0:50:25; 0:100:20/0:50:10, and 0:100:10/0:50:5), and consequently, HUVEC seeding densities varied from 5,000 cells/well up to 50,000 cells per well. The six resulting ratios for the tri-culture were compared to cultures of pure NRVCMs. Interestingly, the relative cell numbers in the tri-cultures do not reflect the reported cell ratio for the native myocardium. The total number of NRVCMs found in our monolayer cultures is necessary for high levels of connectivity possibly due to the limited proliferative potential of NRVCMs compared to hASCs and HUVECs [176]. We found that vessels developed in all tri-culture groups except for 500:50:5, where the number of endothelial cells may have been too low. Likewise, the absence of hASCs from the cultures (500:0:50) resulted in no vascular structures forming indicating that the hASCs were essential for vascular morphogenesis in these cultures. Vessel development was highest at the ratio of 500:50:25. While previous studies suggest that VEGF-VEGFR2 signaling correlates with increased Cx-43 expression and maintenance of electrophysiological function (i.e. excitation threshold and maintenance of

maximum capture rate) [171], our tri-cultures maintained relatively similar conduction velocities and maximum capture rates, however, increased concentrations of non-cardiomyocytes resulted in increased repolarization times.

5. CONCLUSION:

The high metabolic demands of the myocardium require robust vascularization to maintain survival/viability, maintain force of contraction, and prevent necrosis due to ischemia in deeper layers of the engineered tissue. Therefore, a tissue engineered cardiac tri-culture must include a ratio of cells that maximizes formation of nascent vasculature without compromising electrophysiological function of the graft. Multiple cell types are essential for complex tissue assembly, but they should not interrupt the formation of functional cardiac syncytium. In this study, we demonstrated that a 500:50:25 ratio of NRVCM:hASC:HUVEC facilitated the development of a graft with unaltered electrophysiological parameters with dense capillary-like vessel structures. The success of this tri-culture system was supported by the use of hASCs, which played a critical role as a vascular mural cell that did not impede the electrical activity of cardiomyocytes, as fibroblasts do. Additionally, hASCs performed significantly better than dermal fibroblasts in forming vascular networks and maintaining electrophysiological properties that were similar to cardiomyocyte only controls. These findings suggest that ASCs may be a highly suitable cell source for use in future tri-culture studies for engineering functional, vascularized myocardium.

FIGURE LEGENDS:
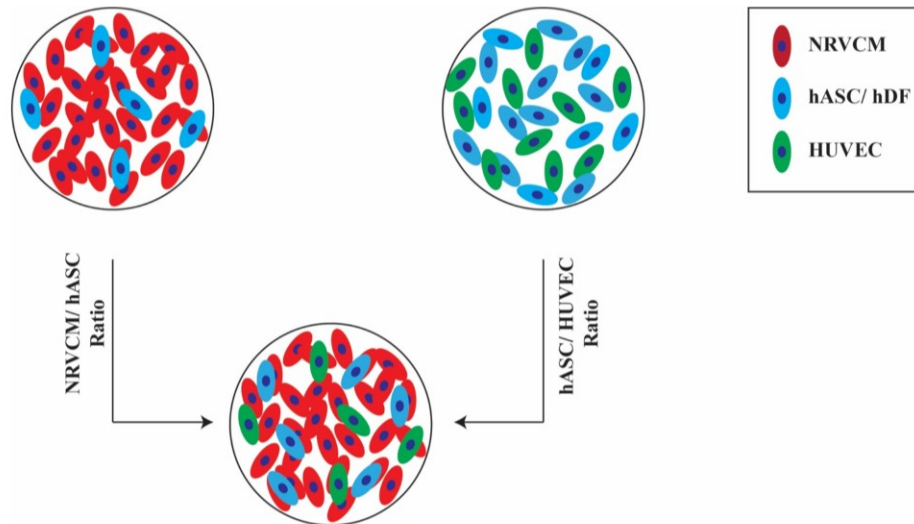
Figure 1

Figure 1: Schematic of Experimental Design: Co-culture experiments were used to compare the effects of hASCs and hDFs on NRVCM electrophysiology and on vessel formation. The cell ratios obtained from co-culture studies were used to inform the inputs for the NRVCM:hASC:HUVEC tri-culture system.
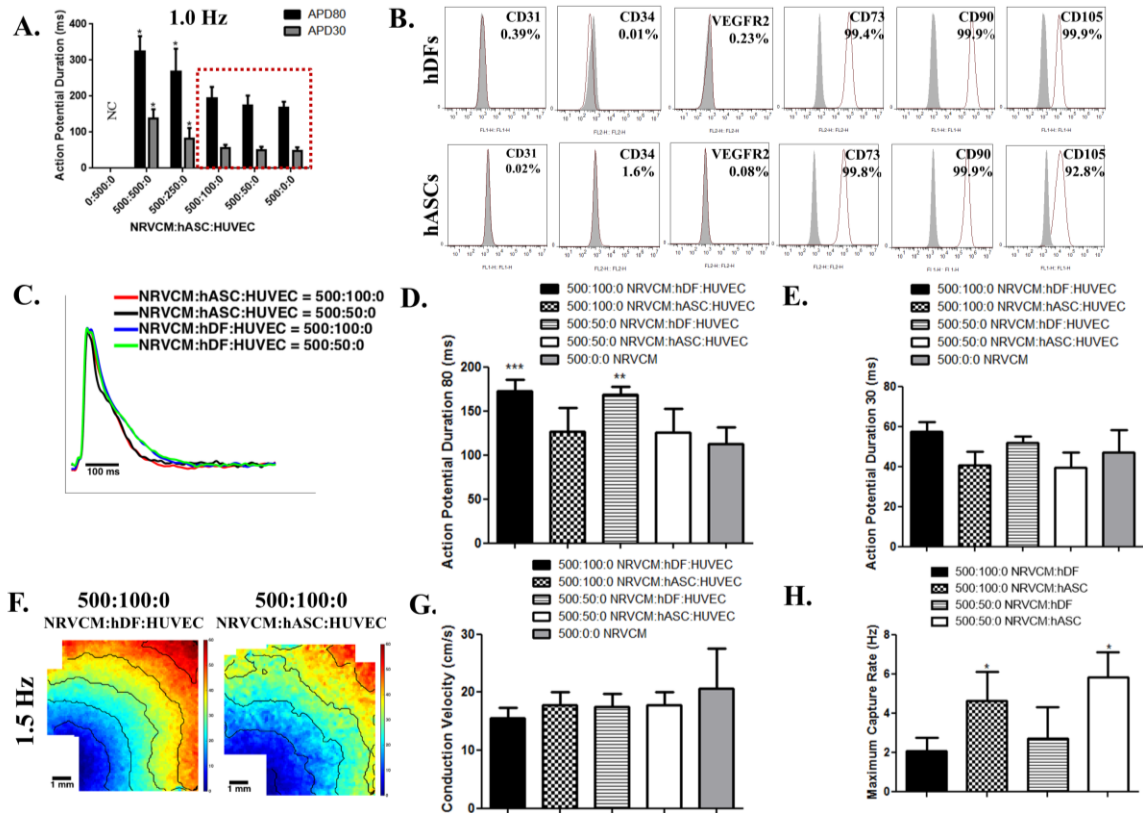
Figure 2: Effects of NRVCM:hASC and NRVCM:hDF ratios on electrophysiological function. (**A**) APD_{80} and APD_{30} values for different NRVCM:hASC:HUVEC ratios at a pacing rate of 1 Hz (*n=3-5).* NC = not captured. *= $p < 0.05$ compared to 500:0:0. The red box indicates the groups that were used in subsequent studies as the electrophysiological parameters were not statistically different from NRVMs only. (**B**) Phenotypic profile of P5 hDFs and P4 hASCs. Mesenchymal markers are CD73, CD90, and CD105, while vascular markers are CD31, CD34, and VEGFR2. (**C**) Action potential traces showing shorter durations in hASCs co-cultures relative to hDF co-cultures. (**D**) Comparison of APD_{80} among different experimental groups (*n=5-6),* *= $p < 0.05$; **$p < 0.01$; ***$p < 0.001$. (**E**) Comparison of APD_{30} among different experimental groups (*n=5-6*) (**F**) Representative activation maps of selected cell ratios with isochrones 5 ms apart.

(**G**) Comparison of conduction velocities among different experimental groups *= $p < 0.05$; **$p < 0.01$; ***$p < 0.001$. (**H**) Maximum captured rates at identical ratios of NRVCM:hASC:HUVEC and NRVCM:hDF:HUVEC. *= $p < 0.05$ compared to identical ratio of NRVCM:hDF:HUVEC.
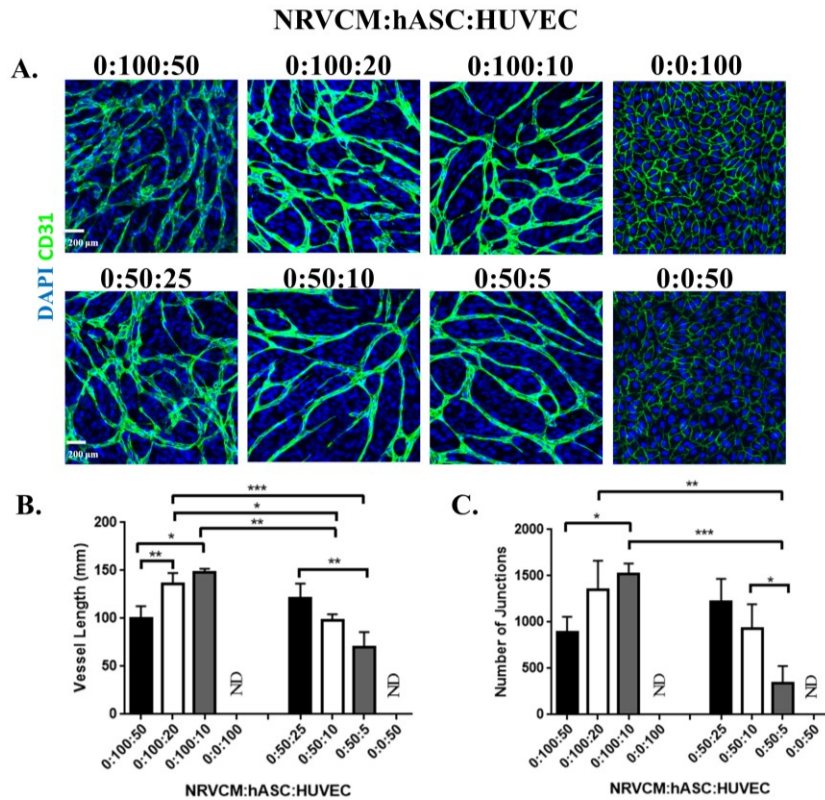
Figure 3: Effect of hASC:HUVEC ratios on vessel formation: A) Immunofluorescent staining of CD31 positive vascular structures (green) and cell nuclei (DAPI; blue). Scale Bar is 200 μm. **B**, **C**) Quantification of vessel structure based on length (*n=3)* (**B**) and interconnectivity (*n=3)* (**C**). ND designates not detected. *$p < 0.05$; **$p < 0.01$; ***$p < 0.001$.
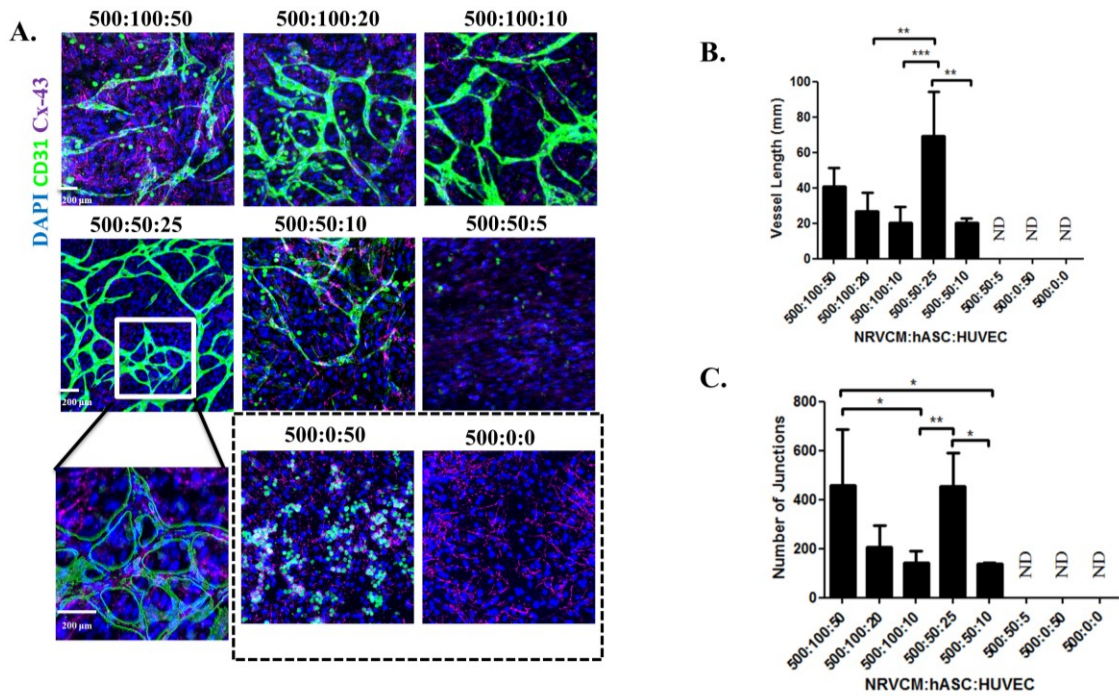
Figure 4

Figure 4: Vessel formation in Tri-Culture System: A) Immunofluorescent staining of CD31 positive vascular structures (green), connexin-43 (Cx-43; purple), and cell nuclei (DAPI; blue). Scale Bar is 200 μm. --- surrounds groups with no hASCs present that were cultured as controls. **B**, **C**) Quantification of vessel structure based on length (*n=4-6*) (**C**) and interconnectivity (*n=4-6*) (**D**). ND designates not detected. *$p < 0.05$; **$p < 0.01$; ***$p < 0.001$.
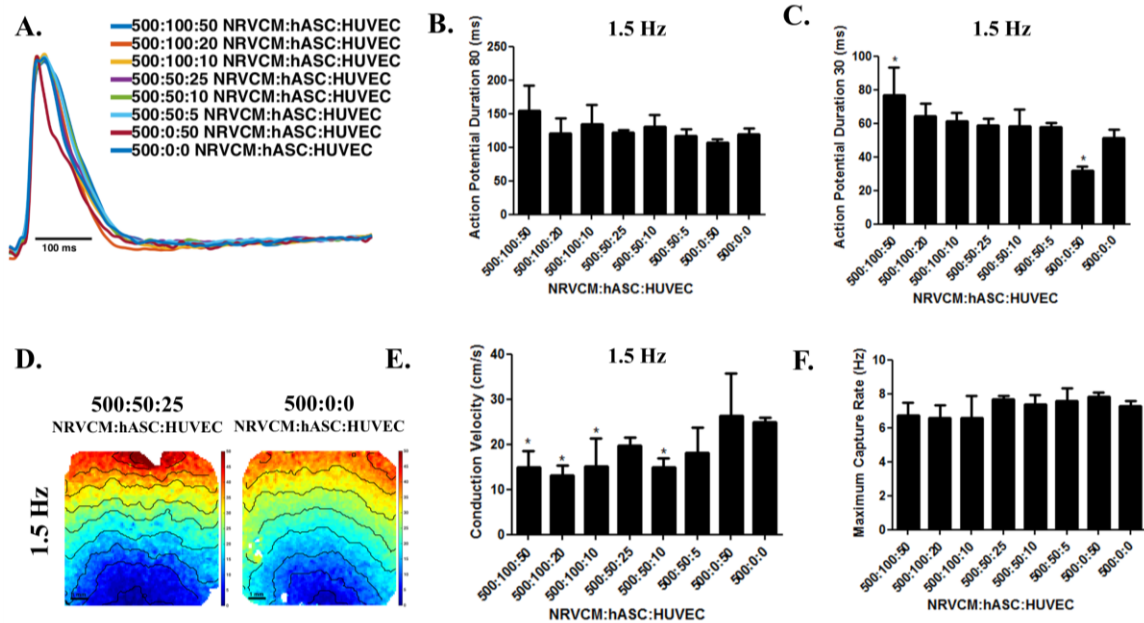
Figure 5: Effects of tri-culture ratios on electrophysiological function: Effects of tri-culture ratios on **A).** Representative action potential traces of all selected ratios. **B**). APD$_{80}$ (*n=4-6)*, **C**) APD$_{30}$ (*n=4-6)*, **D**). Activation maps of selected ratios with isochromes 5 ms apart **E).** conduction velocity at 1.5 pacing rates (*n=4-6)*. **F).** Assessment of maximum capture rate for various tri-culture ratios. *p < 0.05 compared to the cardiomyocyte only group (500:0:0).
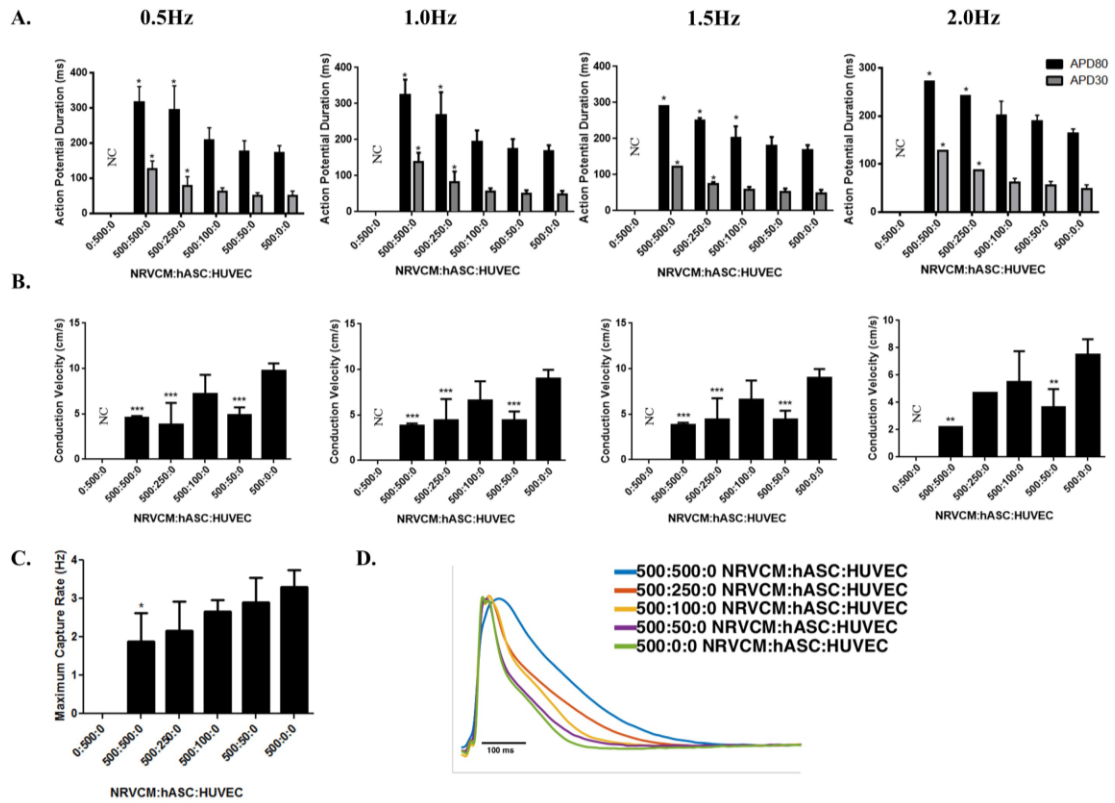
Supplementary Figure 1: Effect of NRVCM:hASC ratios on electrophysiological function at different pacing frequencies. A). APD_{80} and APD_{30} values (*n=3-5*). **B).** Conduction velocities (*n=3-5)*. **C).** Maximum capture rates. * $p < 0.05$; **$p < 0.01$; ***$p < 0.001$ compared to the cardiomyocyte only group (500:0:0) **D).** Representative action potential traces of all selected ratios.
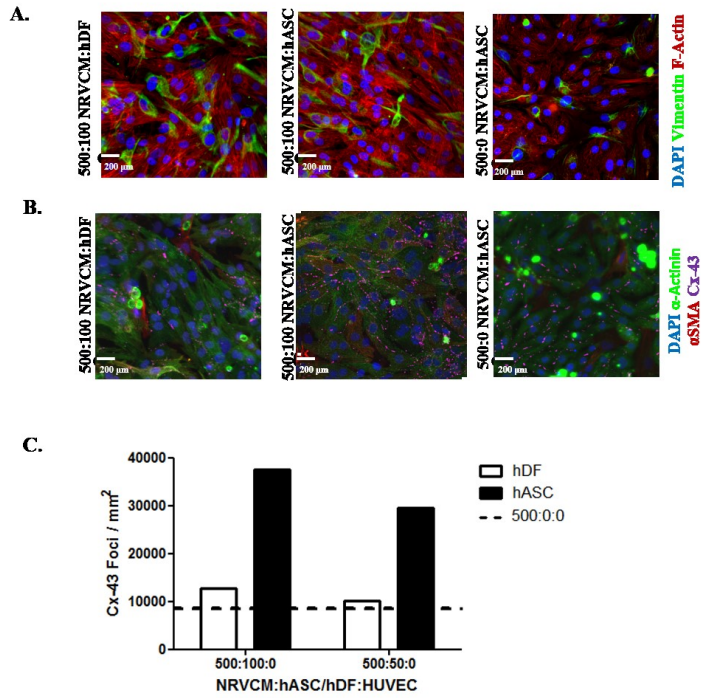
Supplementary Figure 2

Supplementary Figure 2: Immunofluorescent staining of NRVCM:hASC and NRVCM:hDF co-cultures. A) Immunofluorescent staining of vimentin (green), F-actin (red), and DAPI (blue) in co-cultures. **B**) Immunofluorescent staining of αSMA (red), connexin 43 (purple), α-actinin (green) and DAPI (blue) in co-cultures. Scale Bar is 200 μm. **C).** Quantification of connexin43 (Cx-43) expression.
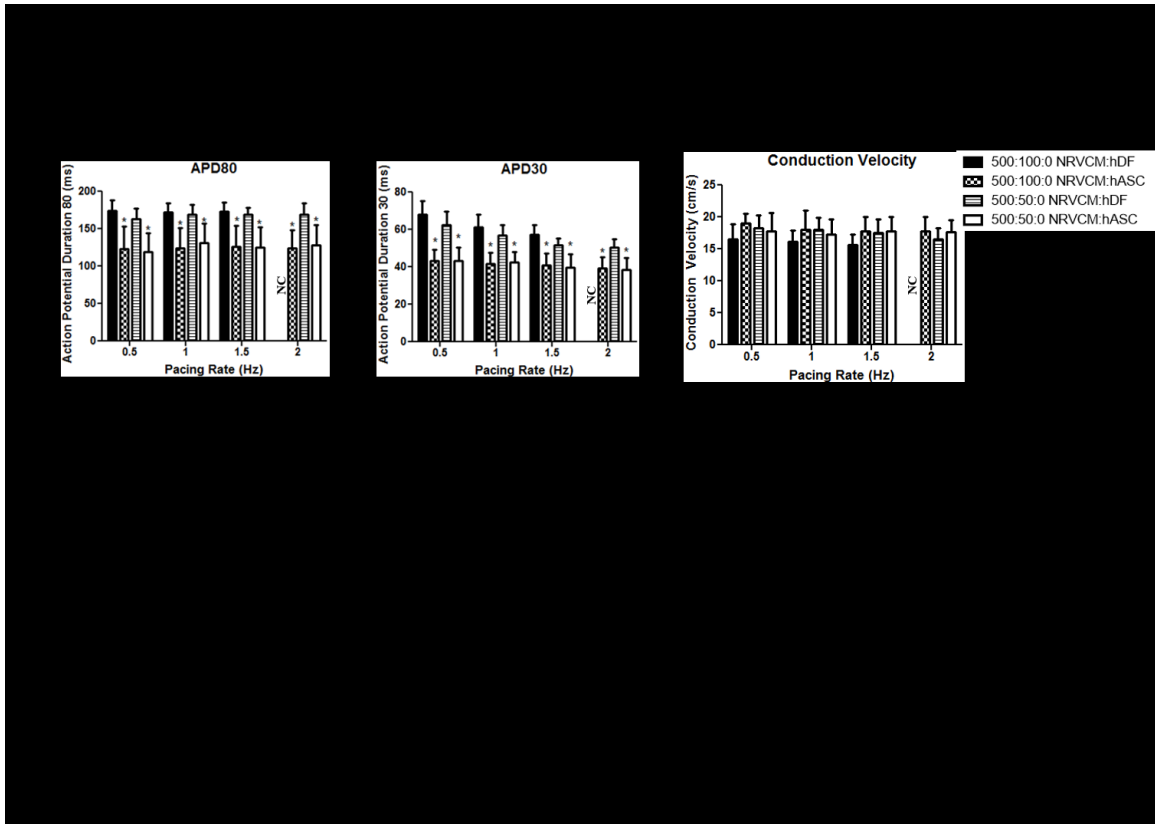
Supplementary Figure 3: Comparison of the electrophysiological impact of hASCs and hDFs co-cultured with NRVCMs. A). APD_{80} values of NRVCM:hDF and NRVCM:hASC co-cultures at various pacing rates. **B).** APD_{30} values of NRVCM:hDF and NRVCM:hASC co-cultures at various pacing rates. **C).** Conduction velocity values of NRVCM:hDF and NRVCM:hASC co-cultures at various pacing rates. NC = not captured. *= $p < 0.05$ compared to identical ratio of NRVCM:hDF:HUVEC (*n=5-6*).
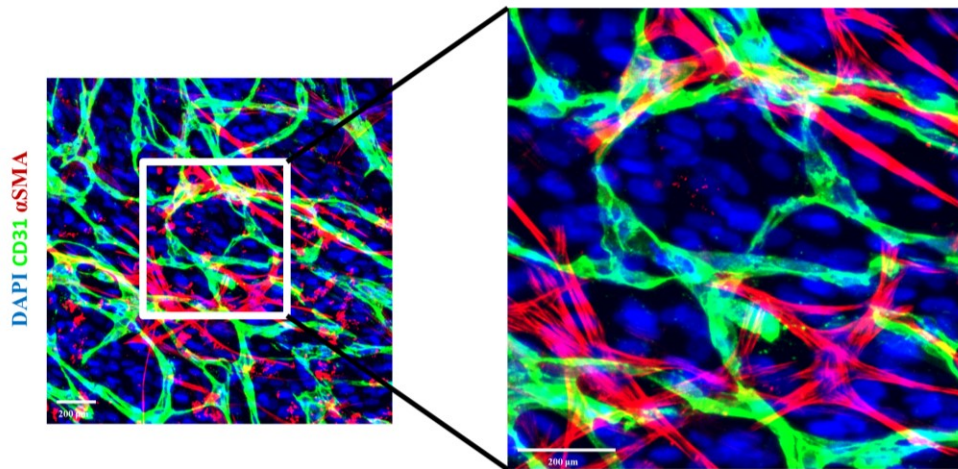
Supplementary Figure 4

Supplementary Figure 4: hASC:HUVEC co-culture results in pericyte-like cell phenotype in hASC. Immunofluorescent staining of CD31 (green), αSMA (red), and DAPI (blue) showing pericyte-like differentiation of hASCs in close proximity to CD31 cells. Scale Bar is 200 μm.

0:100:20   0:100:10   0:50:10   0:50:5

hDF:HUVEC

200 µm
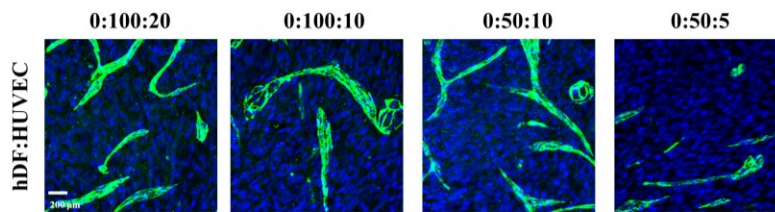
Supplementary Figure 5

Supplementary Figure 5: Effect of hDF:HUVEC ratios on vessel formation.

Immunofluorescent staining of CD31 positive vascular structures (green) and cell

nuclei (DAPI; blue). Scale Bar is 200 µm.
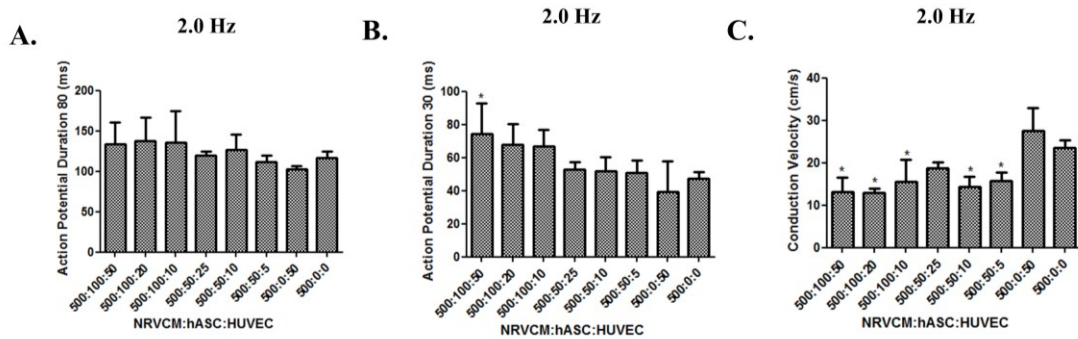
Supplementary Figure 6: Electrophysiological properties of various tri-culture ratios paced at 2 Hz. A). APD$_{80}$ values of NRVCM:hASC:HUVEC tri-cultures at 2 Hz. **B).** APD$_{30}$ values of NRVCM:hASC:HUVEC tri-cultures at 2 Hz. **C).** Conduction velocity values of NRVCM:hASC:HUVEC tri-cultures at 2 Hz. *= p < 0.05 compared to 500:0:0 control (n=4-6)

3

Biomimetic Approach to Vascularized Cardiac Patch for Myocardial Regeneration

1. Introduction:

Myocardial Infarction (MI) is one of the leading causes of death in the Western world.[1] According to the Center for Disease Control (CDC), there are nearly 790,000 infarcts that occur annually, with approximately 500,000 of those being first time MI. During MI, occlusion of the coronary arteries causes apoptosis and necrosis of cardiomyocytes which, due to the limited endogenous regenerative potential of the myocardium, ultimately results in a fibrotic response and ventricular wall thinning. [177] Cardiac tissue engineering is a promising approach to repair the infarcted area and attempts to restore lost functionality. Several strategies have been used to regenerate the damaged myocardium and these range from direct injections of cells suspended in saline to biomaterial-based strategies. [2,50,178] The use of biomaterials is generally considered to be more promising. However, due to the complex architecture of the native myocardium, it may be necessary to employ multifaceted scaffold designs to guide regeneration of fully functional tissues. Key features of cardiac scaffolds that may be controlled to maximize the regenerative response include alignment topography, compliance,

biodegradability, flexibility, and the ability to integrate with the native myocardium [46].

Fibrin is an attractive biomaterial substrate for engineering vascularized cardiac grafts due to its mechanics, degradation and remodeling properties, and its ability to promote both cell survival and angiogenesis [137,141,179]. Fibrin based scaffolds exhibit strain stiffening behavior similar to that displayed by the myocardium [155] and have the ability to undergo remodeling and degradation as the cells secrete their own extracellular matrix (ECM) over time. Fibrin has been shown to stimulate the secretion of extracellular matrix [141]. Recently, fibrin has been electrospun into microfibers, which are extruded on the range of $\sim 10 \mu m$. The electrospun microfibers offer tunable mechanical properties in the range of the native myocardium (10-20 kPa in the short myofiber direction and 40-50kPa in the long microfiber direction [48,180,181]). Substrate mechanics influences cell maturation, action potential duration, contractility [75,182,183], gene expression and twitch force [184,185]. Electrospun microfibers can also mimic alignment cues, flexible geometry, and the structure of the native ECM [58].

Contraction of the myocardium is mediated by tightly packed interconnected cardiomyocytes. [186] The high metabolic demands of the cardiomyocytes are supported by densely packed vasculature (endothelial cells supported by vascular mural cells) [187]. Likewise, the survival of tissue engineered grafts relies on the development of interconnected capillary networks that can anastomose quickly with the host vasculature upon implantation [35,152]. Therefore, the objective of these studies is to engineer contractile myocardial grafts with dense vascular network

assembly capable of integrating with the native myocardium and enhancing tissue function following MI. To accomplish this goal, we work with electrospun fibrin microfiber sheets of two varying stiffness that correlate with physiologic and pathophysiologic myocardial tissues. We used these to test the effect of elastic modulus on tissue assembly. We hypothesized that the softer substrate would provide increased electrophysiological parameters and increased functionality compared to the stiffer substrate. [57,145,185] To establish the vascular network, we incorporated human adipose-derived stem cells (hASCs) and human umbilical vein endothelial cells (HUVECs) with neonatal rat ventricular cardiomyocytes (NRVCMs). We assessed the contractile and histologic properties of the resulting grafts and implanted them in vivo to evaluate their potential for regenerating functional myocardial tissues.

2. MATERIALS & METHODS:

2.1 Fibrin Microfiber Sheet Production:

Fibrin microfiber sheets were formed using two different fibrinogen concentrations. The 0.75% fibrin microfiber sheets were spun using a solution of 0.75 wt% fibrinogen in 0.2% PEO while the 2.0% fibrin microfiber sheets were generated using 2.0 wt% fibrinogen. PEO is prepared as a 1.0 wt% stock in DI water that is dissolved over several days at 37°C. To prepare at 0.75 wt% fibrinogen precursor solution, ~9 mg of fibrinogen is added to an empty 2 ml round bottom Eppendorf tube (~24 mg added for 2.0 wt% fibrinogen). Once added, the fibrinogen was dissolved by adding 1.2 ml of 0.2 wt% PEO to the 2 ml Eppendorf tube, which was

then placed in a 37°C water bath for at minimum least 15 minutes to ensure dissolving into solution.

Following dissolution of the fibrinogen, the precursor solutions were sterile filtered into autoclaved round bottom Eppendorf 2 ml tubes using a 0.22 μm filter. The filtered fibrinogen was loaded into a 1 cc syringe and large air bubbles were dislodged by gently moving the syringe plunger back and forth while the syringe is facing upwards. The syringe was then loaded onto a syringe pump set to dispense at a rate of 5.0 ml/hr for 0.75 wt% fibrinogen or 3.25 ml/hr for 2.0 wt% fibrinogen. A collection solution of 20 U/ml thrombin in 50 mM $CaCl_2$ was prepared by dissolving 1 ml of a 1000 U/ml thrombin stock solution into 50 ml of sterile filtered 50 mM $CaCl_2$. The DC motor controller was turned on and the power to the collection wheel motor was increased until the wheel was rotating at ~45 RPM, at which point the 50 ml collection solution was added. The linear stage upon which the syringe pump sits was powered on and begins rastering at a rate of ~ 3 cm/min over a distance of 1.5 cm. The syringe pump was set to run and begins dispensing the fibrinogen solution at which point the power supply was turned on and set to 4.5 kV to initiate jet formation.

Fibrin microfibers were developed by extruding fibrinogen from a syringe onto a rotating stage containing thrombin and calcium chloride for crosslinking (**Figure 1A,D**). The solutions were electrospun onto the collector for 17 minutes when using 2.0 wt% fibrinogen or 20 minutes total using 0.75 wt% fibrinogen with a pause in spinning after 10 minutes to refill the syringe. Upon completion of the spin time, the fibrin sheets are allowed, at minimum, two additional minutes in the

crosslinking solution to ensure fibrinogen deposited later in the spin has had sufficient time to stabilize with the power supply off. A 1 cm x 1 cm plastic frame was then placed onto the resulting fibrin sheet and a cut was made along one side of the fibrin sheet (typically the side of the frame distal to the operator). The frame was flipped end over end towards the operator a total of six times, being careful to ensure entrapped air bubbles did not significantly disrupt alignment. A single spin will normally yield six frames with six fibrin layers. Once collected with the frames, fibrin sheets were placed in DI water to dilute residual thrombin for a minimum of 30 minutes before use. Sheets can be stored in DI at 4°C indefinitely should there be no contamination if sheets were not needed on the day they were spun.

Prior to cell seeding, excess water was wicked away from the fibrin sheets by touching the frame edge against autoclaved KimWipes and then briefly touching the fiber sheet face against the same KimWipes. This has been found to enhance the adhesion of cardiomyocytes. Once partially dried, sheets were placed vertically in a 24 well plate and stored at 4°C until use to prevent sheets from drying out. Partially dried fibrin sheets were used within a couple days to prevent damage to fibrin sheets due to dehydration.

2.2 Scanning Electron Microscopy (SEM):

SEM images for the native tissue samples and hydrogel microfibers sheets (with or without cells) were acquired using an SEI Quanta 200 Environmental SEM. All samples were fixed with cold methanol and then thoroughly washed with Dulbecco's Phosphate Buffer Saline (5x wash, 30 minutes each at room temperature). Then, the samples underwent gradual ethanol dehydration (25%,

50%, 75% 100%), after which they were critical point dried using a Tousimis Samdri-795 and sputtered with 4 nm of Pd layer using an Anatech USA Hummer 6.2. Samples were then imaged.

2.3 Mechanical Testing:

Fiber stiffness experiments were performed using a custom bioreactor developed in our lab.[1] Bulk cylindrical fibers (3 cm × 1 mm) were clamped between the actuator and the force sensor in the bioreactor system allowing for an active region of approximately 18 mm between the clamped regions. The use of the custom bioreactor system allowed for the sample to stay hydrated throughout the duration of the testing period. The elastic modulus was determined through extension of the fiber to a 20 percent strain at 1 percent strain/ second. The sample length was increased through the movement of the linear actuator to which the sample is clamped. This motion is controlled by a linear stepper motor and motor controller (Haydon Kerk). The force associated with extending the fiber was recorded as voltage changes through the force sensor (Cooper Instruments 50 gram max load cell) attached to a strain gauge amplifier unit (Industrologic SGAU). The voltage output from this system was read through the Lab Jack U3-HV and was recorded in real time through Lab Jack's custom software. Following the tensile test, the data was converted to stress by measuring the diameter of the fiber through bright-field imaging.

2.4 NRVCM Culture on Fibrin Microfiber Sheets:

NRVCMs were seeded at a concentration of 1.5×10^6 cells/cm^2 in 80μL of NRVCM media containing 10% FBS onto fibrin microfibers with the dimensions of 1cm × 1 cm. Fibrin microfiber sheets were placed on to agarose coated culture plates to prevent cells from attached to tissue culture plastic. After 1.5 hour of incubation at 37°C allowing the cells to attach to the fibrin microfibers, cells were fed 3mLs of 10% containing NRVCM media with 33μg/mL Aprotinin (USB Affymetrix). On the next day microfiber sheets were washed with DPBS and fed with 10% containing NRVCM media with 33μg/mL Aprotinin (USB Affymetrix). On day 3 of culture, microfibers were washed with DPBS and feed 6% containing NRVCM media with 33μg/mL Aprotinin (USB Affymetrix). Media was changed every other day until and electrophysiological and functional testing occurred.

2.5 Tri-Culture of NRVCM:hASC:HUVEC Fibrin Microfiber Sheets:

We will utilize the consistent nomenclature – thousands of NRVCM:hASC:HUVEC per fibrin microfiber – to describe co-culture and tri-culture cell plating densities throughout the manuscript. Therefore, for NRVCM:hASC co-cultures, the HUVEC concentration is reported as zero. Likewise, in hASC:HUVEC experiments, the NRVCM numbers are reported as zero.

NRVCs were seeded at a concentration of 1.5×10^6 cells/cm^2 in NRVCM media containing 10% FBS in 80μL onto fibrin microfiber sheets (1cm^2) were seeded onto agarose coated culture plates to prevent cells from attached to tissue culture plastic. After one hour of incubation and allowing the cells to attach to the fibrin μfibers, cells were fed 3mLs of 10% containing NRVCM media with 33μg/mL

Aprotinin (USB Affymetrix). On the next day microfibers were washed with DPBS and fed with 10% containing NRVCM media with 33μg/mL Aprotinin (USB Affymetrix). On day 3 of culture, microfibers were washed with DPBS and feed 6% containing NRVCM medium with 33μg/mL Aprotinin (USB Affymetrix). Media was changed every other day until day 14. On day 14, media was removed and hASCs and HUVECs were added at specific concentration (i.e. 3.7 × 10^4 hASC/cm^2 and 1.5 × 10^5 HUVEC/cm^2) in 20μL of tri-culture media. After one hour of incubation, cells were fed 3mL tri-culture media containing 33μg/mL Aprotinin. Media was refreshed every other day until 21 days of culture. At 21 days, microfiber sheets underwent functional testing, which consisted of optical mapping and force of contraction. Upon harvest, cells were assessed using optical mapping and were fixed with ice-cold methanol overnight at -20C for immunocytochemistry analysis.

2.6 Optical Mapping & Analysis:

Optical mapping measures changes in transmembrane voltage of electrically conductive cells and has the overall objective of providing a method to visualize patterns of excitations and repolarization.[168] Fibrin fibers were stained with 10 μM di-4-ANEPPS (Invitrogen), which is a voltage sensitive dye, in Tyrode's solution for 10 minutes at 37 °C while being protected from light. Di-4-ANEPPS works by incorporating into the plasma membrane of cells by binding to the outer layer of cell bilayer membranes. The dye is then excited by a light source and responds to an increase in membrane potential with a decrease in fluorescence (440nm to 530nm). Electronic structure changes with transmembrane potential/voltage. There is an excitation from a shorter wavelength to a longer wavelength. [167–170]

After staining, the dye solution was removed and cells were then washed with Tyrode's solution. After being washed with Tyrode's solution, the cells were then placed on a heated stage in Tyrode's solution with 5 µM blebbistatin, which stops contraction to remove motion artifacts. Cells were electrically stimulated by placing an electrode near the edge of the coverslip, out of the field of view of the lens, and paced starting at 0.5 Hz and incrementally increased by 0.5 Hz until the sample is unable to capture the paced cycle length or has reentrant spiral waves. Between each new cycle length, fibrin fibers were allowed to be stimulated for 1 minute to achieve steady state before losing the ability to maintain signal propagation at set pacing rate. Optically mapping occurred using a CMOS camera (MiCAM Ultima).

2.7 Force of Contraction:

Force of contraction experiments were performed using a custom bioreactor developed in our lab [188] and modified for the cardiac patch system. Following the indicated culture period and conditions, longer microfiber sheets (3 cm x 1 cm) were clamped between the actuator and the force sensor in the bioreactor system allowing for an active region of approximately 18 mm between the clamped regions. The bioreactor allows the sample to be maintained in media and in the incubator for the duration of the testing period. Following the loading of the sample between the clamps, the bioreactor was allowed to sit in the incubator for 15 min to ensure that the sample had time to resume contraction following the change in environment. The force of contraction measurements was recorded as voltage changes through the force sensor (cooper instruments 50 gram max load cell) attached to a strain gauge amplifier unit (Industrologic SGAU). The voltage output

from this system was read through the Lab Jack U3-HV and was recorded in real time through Lab Jack's custom software. The spontaneous force of contraction was recorded for 10 min following the 15 min equilibration period. Following these recordings, a custom built stainless steel and platinum point electrode was attached to the bioreactor and placed such that it contacted the sample along the outer edge half way along the length of the sample. The sample was stimulated with 10 volts of direct current with a 20 ms pulse width at a variety of frequencies until it was no longer able to keep up with the stimulus. This testing was performed at 1 Hz intervals starting at 1 Hz and increasing up to 4 Hz. The force length relationship data was measured at a frequency of 1 Hz as this was the frequency that most samples were able to be paced. The sample length was increased through the movement of the linear actuator to which the sample is clamped. This motion is controlled by a linear stepper motor and motor controller (Haydon Kerk). The sample was extended in intervals of 2% of the initial length and the stimulated (1 Hz, 10V) contractions were recorded at each length up to 20% strain.

2.8 Immunocytochemistry:

Samples were permeabilized with 0.2% triton X-100 in DPBS with 5mM HEPES for 10 minutes and then blocked with 10% normal goat serum (Sigma Aldrich) or normal donkey serum (Sigma Aldrich) for 3 hours at room temperature. The samples were incubated overnight with mouse anti-Sarcomeric α-Actinin [1:200] (Sigma Aldrich), rabbit anti-Connexin-43 [1:100] (Sigma Aldrich), and Cy3 conjugated mouse anti- α Smooth Muscle Actin [1:400] (Sigma Aldrich) or mouse anti-Vimentin [1:200] (Dako)), or mouse anti-CD31 [1:250] (Sigma Aldrich) primary

antibodies diluted in DPBS with 5mM HEPES with 10% normal goat serum or normal mouse serum at 4 °C. Primary antibody was washed three times with deionized water. Samples were incubated with secondary antibodies DyLight 488-conjugated goat anti-mouse [1:200] and DyLight 649-conjugated goat anti-rabbit [1:200] (Jackson ImmunoResearch) or corresponding donkey secondary antibodies. Samples were washed three times with deionized water. Samples were incubated with DAPI (1:2000) (Sigma Aldrich) diluted in deionized water. Coverslips were mounted with mounting medium and imaged under Zeiss Axio Observer inverted fluorescence microscope or Zeiss LSM 510 confocal microscope with a 5x, 20x, 40x, and 63x objective. Immunostained images were z-projected and thresholded in order to calculate vessel parameters including network length and junctions. Thresholded images were subsequently analyzed with AngioQuant software to determine the total vessel length, area, and interconnectivity.

2.9 In Vivo Implantation:

Immunodeficient female 9-12 week old athymic nude rats (Charles River Laboratories) were used as patch candidates for the *in vivo* implantation. Rats were intubated and induced with anesthesia by using 4% isoflurane inhalation and maintained with 2% inhalation during procedures. Hearts were exposed through a left lateral thoracotomy. Visceral pericardium was removed by using 2.5% trypsin (Invitrogen/GIbco). After removal of the pericardium, 20μL fibrin hydrogels 20mg/mL fibrinogen (Sigma-Aldrich) diluted DPBS and 10U/mL (Sigma Aldrich) diluted in calcium containing DPBS) were placed on the myocardium.

Subsequently, fibrin microfibers were sided cell side down onto the fibrin gel. Co-culture vasculature patches were placed on the right ventricle. Myocardial infarction was induced by ligation of the left anterior descending coronary artery. Subsequently, steps are the same as the vascular co-culture implantation.

2.10 Echocardiogram:

Echocardiography (Vevo2100, Visualsonics) was performed prior to myocardial infarction (MI), the day following MI, 7 days post MI, 14 days post MI, and 28 days post MI. Rats were imagined in the supine position at the fourth and fifth intercostal space with a 710B transducer. The transducer was moved around to avoid the lung and rib obstruction while obtaining a clear heart image. Both 2D and M-mode images were used for experimental measurements, and images were later analyzed. From the 2D guided M-mode images, measurements of the left ventricle anterior wall thickness, posterior wall thickness, ejection fraction, and fractional shortening were measured.

2.11 Histology:

Following euthanasia, hearts were either placed into OCT solution and flash frozen in cold 2-methylbutane (Sigma-Aldrich) or fixed in 60% methanol, 10% Glacial Acetic Acid, and 30% water. Tissue sections were section in the cryostat or paraffin embedded and sectioned on the microtome. Slides were stained with hematoxylin and eosin (H&E) or Masson's Trichrome.

For immunostaining, slides obtained from cryosectioning were fixed in ice cold acetone and washed with DPBS 3x for 5 minutes. Subsequent steps are the same as immunocytochemistry.

2.12 Statistical Analyses:

All experiments were conducted with a minimum of three biological replicates. Quantitative data are expressed as the mean $\pm$ standard deviation. Statistical analysis was performed using GraphPad Prism 5/6 software. Statistical significance was determined by two-way ANOVA with Bonferroni post-hoc test or t-test and is denoted as * $p< 0.05$, **$p<0.01$, ***$p<0.001$.

3. RESULTS:

The overall flow of data in these experiments is depicted in **Fig. S1**. We characterized the physical properties of the fibrin microfiber sheets used for these studies and then evaluated the growth of NRVCM only, hASC and HUVEC co-cultures, and tri-cultures on these scaffolds. Through the process, we determined the appropriate cell seeding densities, medium compositions, and growth periods required to enable the formation of robust, contractile, vascularized cardiac patches that could be sutured onto rat myocardium following induction of MI.

3.1 Fibrin Microfiber Sheets Development and Characterization:

SEM images were used to compare the structure of the fibrin microfiber sheets to the native myocardium. The acellular fibrin microfiber sheets exhibited similar alignment topography to the decellularized myocardium, while regions of the NRVCM-seeded microfiber sheets showed a similar architecture compared to the native myocardium (**Fig. 1B**). Tensile testing demonstrated the elasticity of 0.75% and 2.0% fibrin microfiber sheets and the resulting stress-strain curves were

used to determine their tensile moduli of 50.0 ± 11.2 (*n*=3) and 90.0 ± 16.4 kPa (*n*=3), respectively (**Fig. 1C**).

3.2 NRVCM Cultures on Fibrin Microfiber Sheets:

NRVCMs cultured on both 0.75% and 2.0% fibrin microfiber sheets appeared to elongate and align on the substrate (**Fig. 2A, Fig. S2**). Data from the PicoGreen DNA assay demonstrated similar DNA content in both groups at 1, 7, and 14 days following seeding of freshly isolated NRVCMs on both 0.75% and 2.0% fibrin microfiber sheets. Both groups exhibited similar cell viability at Day 14 with calcein AM (LIVE) and ethidium bromide (DEAD) stain (**Fig. S2**).

The optical mapping data for the NRVCMs exhibited smooth propagations when point paced across the field of view in both groups. Cells grown on both the 0.75% and 2.0% fibrin microfibers were optically mapped at 7, 14, 28, and 56 days. We noted that the cardiomyocytes cultured on the 0.75% fibrin sheets exhibited slightly higher conduction velocities than those on 2.0% fibrin sheets at early time-points. Conduction velocities peaked at 22 ± 2.1 cm/s (*n*=3) on day 28 in the 0.75% fibrin group and at 13 ± 0.9 (*n*=3) cm/s on day 14 in 2.0% fibrin when samples were paced at 1 Hertz (Hz) (**Fig. 2B**). Similar trends were also noted across several pacing rates. The average maximum captured rate peaked at 4.2 ± 0.6 Hz on the 0.75% fibrin microfibers and 3.5 ± 1.0 Hz on the 2.0% fibrin microfibers (**Fig. 2H**).

The fibers were paced from the center to detect the presence of anisotropy and the 0.75% fibrin fibers exhibit an anisotropy ratio of 2.2 (**Fig. 2C,D**). Action potential durations (APD) at both 80% repolarization (80) and 30% repolarization (30) increased over time in both the 0.75% and 2.0% fibrin concentrations. APD_{80}

at 1 Hz pacing ranged from 133 $\pm$ 19 ms (*n=5*) at day 7 to 229 $\pm$ 51 ms (*n=8*) at day 56 in the 0.75% fibrin group (**Fig. 2F**). A similar trend was noted with the 2.0% fibrin fibers. APD_{30} ranged from 43.6 $\pm$ 6 ms (*n=5*) at day 7 to 59 $\pm$ 12 (*n=8*) at day 56 in the 0.75% fibrin group when paced at 1 Hz (**Fig. 2G**).

NRVCM-seeded fibrin sheets were spontaneously contractile (**Video S1,2**). We measured the spontaneous contractile forces of NRVCMs at Day 14 using custom-designed bioreactors. Cardiomyocytes generated 2.3 $\pm$ 0.7 mN and 1.4 $\pm$ 1 mN of force on 0.75% and 2.0% fibrin microfiber sheets, respectively (**Fig. 3A,B**) at frequencies of 0.4 $\pm$ 0.3 Hz and 0.5 $\pm$ 0.4 Hz respectively. When stimulated at 1 Hz, the stimulated forces of contraction were 1.8 $\pm$ 0.4 mN and 0.9 $\pm$ 0.5 mN on the 0.75% and 2.0% fibers, respectively (**Fig. 3C**). Constructs were paced up to 3 Hz but typically lost capture at higher pacing rates. Fibers were strained up to 20% at 1 Hz pacing to generate force-length relationship data. There was a maxima at ~10% strain in 2.0% fibrin groups (Peak normalized force: 1.3 $\pm$ 0.4), while the maximum force on 0.75% fibrin was measured at 2% strain (Peak normalized force: 1.1 $\pm$ 0.3) (**Fig. 3D**).

3.3 Tri-Cultures of NRVCM:hASC:HUVEC on Fibrin Microfiber Sheets

To engineer vascularized cardiac patches, hASCs and HUVECs were cultured together with the NRVCMs. We utilized our published culture protocol established for cells grown on glass coverslips in which the optimal NRVCM:hASC:HUVEC ratio was 20:2:1 [41]. Therefore, maintaining the NRVCM seeding density at 1500 cells/mm^2, we tested the equivalent ratio (1500:150:75) as well as an additional ratio in which the concentrations of hASCs and HUVECs

were further reduced (1500:75:37.5). At these ratios, the electrophysiological properties of the cells were significantly impaired and the vascular networks were not considered sufficiently extensive or interconnected (**Fig. S4**).

To address this, we followed a step-wise approach to improve the system. (Step 1) We co-cultured NRVCMs and hASCs in the absence of HUVECs and found that 1500:37.5:0 was the highest ratio of hASCs that could be co-cultured with NRVCMs without completely inhibiting the ability of the cultures to be optically mapped (**Fig. S5**). However, electrophysiological properties such as conduction velocity and maximum capture rate of the co-cultures at this ratio were significantly inhibited compared to NRVCM only cultures. (Step 2) We then cultured hASCs and HUVECs in the absence of NRVCMs to assess vascular assembly on the fibers. We used 37.5 hASC/mm^2 to be consistent the cell densities determined in the NRVCM:hASC co-cultures and varied the concentration of HUVECs. Robust vessel assembly was observed on 0.75% and 2.0% fibrin microfiber sheets at the ratios of 0:37.5:75 and 0:37.5:150 (**Fig. S6**). Since the NRVCM cultures required a minimum of 6% serum, we tested vascular assembly in the presence of 6% serum. Quantification of vessel length and interconnectivity yielded similar results as 2% serum (optimal serum concentration for culturing HUVECs).

(Step 3) In addition to determining suitable hASC and HUVEC concentrations, we assessed postponing seeding of hASCs and HUVECs (to a time later than Day 3). Since the NRVCM only cultures exhibited mature electrophysiological characteristics at Day 14, the tri-culture system was

developed in which NRVCMs were seeded at 1500 cells/mm^2 and cultured for 14 days before hASCs/HUVECs were added (**Fig. 4A**). Three groups were studied using the ratios 1500:37.5:37.5, 1500:37.5:75, and 1500:37.5:150 and compared to a NRVCM only (1500:0:0) control. Through CD31 staining, we observed increased vessel length and interconnectivity as the concentration of HUVECs increased (**Fig. 4B-D**). After 21 days of culture, constructs were optically mapped. At 1 Hz pacing, there were no significant differences in the tri-culture conduction velocities on the 0.75% or the 2.0% fibrin groups compared to the respective controls.   Conduction velocities of 0.75% and 2.0% fibrin for the ratio 1500:37.5:37.5, were 13 ± 1.3 cm/s (*n=6*) and 14 ± 1.5 cm/s (*n=4*) respectively. Similarly, the 1500:37.5:75 displayed conduction velocities of 15 ± 1.9 cm/s (*n=6*) and 13 ± 1.5 cm/s (*n=9*) (0.75% and 2.0% respectively) and 1500:37.5:150 had 14 ± 2.3 cm/s (*n=7*) and 14 ± 0.6 cm/s (*n=5*) compared to the controls of 14 ± 2.1 cm/s (*n=6*) and 13 ± 1 cm/s (*n=4*) (**Fig. 4E,F**). We saw similar trends using other pacing rates (**Fig. S7**). We found that there was no statistical difference in action potential duration (both 80% and 30%) between the control groups and the ratio 1500:37.5:150 but the action potentials appeared to be prolonged in the 1500:37.5:37.5 and 1500:37.5:75 after 21 days of total culture time on both stiffness groups (**Fig. 4G,H**). The control group had a maximum captured rate of 3.4 ± 1.3 Hz (*n= 6*) (0.75%) and 3.2 ± 0.4 Hz (*n= 10*) (2.0%) compared to those of the 1500:37.5:150 groups, which achieved higher rates at 3.8 ± 1 Hz (*n= 6*) (0.75%) and 3.9 ± 0.7 Hz (*n= 5*) (2.0%) (**Fig. 4I**). We tested the stimulated force of contraction of the 1500:37.5:150 groups at 1 Hz pacing and found statistically

higher forces on the 2.0% fibrin group (1.1 ± 0.8 mN) compared to the 0.75% fibrin

(0.5 ± 0.1 mN).

3.4 In Vivo Proof-of-Principle Vascularized Cardiac Patch

Preliminary *in vivo* studies showed that both 0.75% and 2.0% fibrin fibers

could be sutured to the rat ventricular walls, however, due to the increased

mechanical integrity of the 2.0% fibrin microfiber sheets, they were easier to handle

and remained stretched across the myocardium better than the 0.75% fibrin

sheets. Preliminary studies were also used to establish the surgical protocol that

included enzymatic removal of the pericardium with 2.5% trypsin, the incorporation

of fibrin hydrogel adhesive, and suturing all four corners of the patch. These

techniques enabled better integration of the patch with the native myocardium and

host vasculature appeared to grow into the patches (**Fig. 5A**). To track the survival

of transplanted NRVCMs, we transduced them with luciferase. We were able to

detect the luminescence of the cultures pre-implantation (not shown) and up to 1

month post-implantation (**Fig. 5B,C**). To test the potential for using these

engineered grafts as cardiac patches, we utilized an established a rat MI model

[40]and applied the 2.0% fibrin microfiber sheets (**Video S3,4**). We cultured

NRVCM:hASC:HUVEC in the 1500:37.5:150 ratio using the previously described

protocol and assessed functional metrics up to 28 days post-MI. The results for 2

rats with identical treatment regimes are presented. In both rats, the ejection

fraction decreased significantly following MI (Rat 1: 78% ➔ 37%; Rat 2: 78% ➔

38%). Following treatment with the patch, the ejection fraction in Rat 1 remained

unchanged, while the ejection fraction in Rat 2 increased to 56% at Day 14 and

68% at Day 28). In the untreated control, the ejection fraction remained at 38%. The values of end diastolic volume and end systolic volume also indicated functional improvements in Rat 2 beginning at Day 14 and continuing through Day 28. At Day 28, the end diastolic volumes were 552 µL (Rat 1) and 298 µL (Rat 2) (Pre-MI: 98 µL; Untreated control: 271 µL). The end systolic volumes were 343 µL (Rat 1) and 97 µL (Rat 2) (Pre-MI: 21 µL; Untreated control: 168 µL) (**Fig. 5C-E**). Using echocardiography, we observed beating of the ventricular walls in Rat 2 from the M-Mode image after 28 days in the host (**Fig. 5F-H).** We did not observe measurable changes in morphologic parameters assessed using the echocardiography (**Fig. S8**). After 1 month in the host, we removed the heart from Rat 2 and used optical mapping to assess integration of the patch. The maximum captured rate was 3Hz (point stimulation) and 7Hz (field stimulation). (**Fig. S9**).

4. DISCUSSION:

The ultimate goal of cardiac tissue engineering is the development a cardiac graft that can be used as a source of functional regeneration of the myocardium. In this present study, we demonstrate that fibrin microfibers cultured with NRVCMs, HUVECs, and hASCs resulted in the development of a vascularized cardiac graft that can be implanted into the infarcted myocardium and maintain survival and improve functional outcomes. This study was broken into several components in which we assessed cardiomyocyte survival and functionality, vascular assembly, vascularized cardiac tissue formation, and acute myocardial treatment with the vascularized cardiac graft.

Electrospun fibrin microfiber sheets provide a unique advantage relative to bulk fibrin hydrogels. Previous researchers have utilized isotropic fibrin hydrogels that rely on cell-generated stresses to create cell alignment[189,190] with limited capacity to tune the mechanical properties. These previous studies utilize tension to allow for the cardiomyocytes to elongate, connect, and form a syncytium. To achieve tension these groups utilize PDMS hexagonal posts, flexible silicon posts, and other types of post to culture the fibrin hydrogels. In contrast to fibrin hydrogels, fibrin microfibers sheets display tunable mechanical properties, provide uniaxial alignment, have flexible geometry, are customizable in dimensions, and can be sutured onto organs like the myocardium[58]. To mimic the mechanical properties of native tissue extracellular matrix during homeostasis and the stiffer state that is present following myocardial infarction as these two conditions will impact the contractile response of cardiomyocytes. Fibrin microfiber sheets are spun using two compositions of fibrinogen under sterile conditions. Electrospun fibrin microfiber sheets were developed at 2 unique tensile moduli, 49 kPa and 90 kPa. Researchers have found the rat myocardium has a tensile modulus in the long myofiber direction, the direction that is parallel to cardiomyocyte alignment, of 43 $\pm$ 9 kPa and the epicardium has a stiffness of 12 kPa at birth in neonatal rats to 39kPa in adult rats [48,191]. The stiffness of the softer substrate has a similar order of magnitude.

Fibrin microfibers grafts were cultured with NRVCMs-only for up to 2 months. Electrophysiological properties, specifically conduction velocity increased over time up until 28 days and gradually decreased after 2 months of culture. We

found that the conduction velocity was significantly higher in the 0.75% fibrin group compared to the 2.0% group over time. This finding was consistent with previous reports indicating that stiffer substrate negatively influenced the maturation and electrophysiology of cardiomyocytes. Specifically, it was shown that cells cultured on softer matrices or near the stiffness of the native myocardium show larger calcium transients, contained more sarcoplasmic calcium stores, and generated more force[75,77,182,185]. While substrate stiffness in NRVCM-only cultures appeared to have an effect on conduction, the time frame in which maximum conduction velocity was achieved could be attributed to the fact that cardiomyocyte maturation in 3D substrates takes a slightly longer time frame than monolayer cultures to achieve faster conduction. These differences can be attributed to cell-matrix interactions and the ability of cells to undergo morphogenic changes and form matrix adhesions that are more *in vivo*-like [192].

Culture of cardiomyocytes on the 0.75% fibrin resulted in an anisotropy ratio similar to the rat myocardium as compared to the 2.0% fibrin microfiber sheets[193] which is near 2.3. Similarly, the 0.75% fibrin microfibers, the softer of the two substrates, exhibited increased force of contraction compared to the 2.0% microfibers. Previous engineered constructs have shown that the force of contraction can range from as high as ~3.0 mN to as low as ~0.1 mN [57,194–196]. In our system, force of contraction is on the higher end of the range at ~2.3 mN of force. To improve the force of contraction, researchers have found that introducing electromechanical stimulation into a culture system has the potential to increase

the force of contraction due to the increase in cardiac troponin and SERC2a expression [119].

Fibrin microfiber sheets also support the development of dense vascular structures. We find that in both the 0.75% and 2.0% fibrin microfiber there is robust vascular assembly. Current literature suggests that softer substrates support HUVEC network formation and substrates at ~25 kPa support proliferation of endothelial cells [197,198]. In our study, we found that vessel assembly occurred at both stiffness ranges and vessel length is relatively similar amongst experimental groups and ratios. This can be possibly explained by the paracrine effects of hASCs and their role as supportive vascular mural cells. Wang et al. suggests that smooth muscle cells, like hASCs, can be highly proliferative in the presence of PDGF and substrate stiffness of ~84 kPa which would ultimately preserve and support vascular assembly and explain the presence of robust dense vascular structures [199,200]. In addition to substrate stiffness, we investigated changing serum concentration from 2% to 6% because the cardiomyocytes are cultured in 6% serum. Serum concentration could potentially play a role in vessel assembly and maintenance of cardiomyocyte functionality. There were no relative differences in vessel length between the two concentrations of serum. Bala *et al* has shown that increasing serum up to 20% can be detrimental to HUVEC morphology and proliferation rate, which would explain that vessel assembly would not be jeopardized until this threshold has been reached with serum concentrations[201].

Developing a contractile, electrically responsive, vascularized cardiac patch required several iterations of cell concentration and seeding time points. In initial

studies we utilized a protocol optimized for tri-culture on tissue culture. We found that culturing cardiomyocytes for 2 days prior to the addition of hASCs and ECs yielded grafts with poor electrophysiological properties although vessel assembly was successful (**Fig. S4**). NRVCMs on the electrospun fibrin microfiber sheets took longer to elongate and form gap junctions with other cardiomyocytes compared to those cultured on traditional tissue culture plastic[202]. To overcome these limitations, it was necessary to increase NRVCM seeding concentrations six-fold, lower the concentration of serum used in the cultures (to mitigate the effects of cardiac fibroblast proliferation), and to reduce the relative ratio of NRVCM:hASCs (20:1) compared to previously reported values. [41] Interesting, while 1,500,000:37,500 (NRVCM:hASC) cultures resulted in reproducible conductivity (CV: 10 cm/s (50kPa) & 6 cm/s (90kPa)), the conduction velocities increased further when HUVECs were included in the 1,500,000:37,500:75,000 cultures (CV: 15 cm/s (50 kPa) & 13 cm/s (90kPa)). This compared favorably with NRVCM-only control samples (14 cm/s (50 kPa) & 13 cm/s (90 kPa). We speculate that paracrine factors secreted by endothelial cells could enhance NRVCM-hASC crosstalk leading to better conduction properties[203]. Previous studies have shown that paracrine signaling from vessel networks promote survival of cardiomyocytes and enhanced electrophysiological properties [49].

After characterizing the tri-culture system *in vitro*, the vascularized cardiac patches were implanted into the myocardium following acute MI. *In vivo* studies were performed primarily with the stiffer scaffolds, which exhibited near identical electrophysiological properties and vessel network characteristics as the softer

scaffolds (**Fig. 4**), but were easier to handle surgically. These studies were performed as proof-of-principle and confirmed the potential for using these grafts to enhance cardiac function. Bioluminescence imaging demonstrated that roughly 10% of the NRVCMs survived at least one month in the ischemic environment. Additionally, there appeared to be anastomosis between the host and implanted vasculature. In one of the rats tested, the cardiac patch demonstrated improvement in ejection fraction, end systolic volume, and end diastolic volume. Additionally, data from optical mapping of the whole heart suggest that the patches potentially integrated with the myocardium. To confirm electrical connectivity between the patch and the heart, future studies will utilize a calcium reporter gene to display the activity of the patch and show the alignment or the dissonance of the patch implanted onto the myocardium.

5. CONCLUSIONS:

We have successfully generated vascularized, electromechanically coupled cardiac patches that could be directly applied to treat infarcted myocardial tissues. To achieve this, we employed uniaxially aligned fibrin microfiber sheets with biomimetic stiffnesses and developed a protocol for successfully co-culturing NRVCMs, hASCs, and HUVECs. These studies confirmed previous reports that NRVCM physiology is enhanced on softer substrates (50 kPa vs. 90 kPa), but also provided novel insight in demonstrating that the effect of substrate stiffness on cardiomyocyte function is not fixed, but is also influenced by heterotypic cell-cell interactions. Ultimately, tri-cultures on the two substrates yielded identical electrophysiological and vessel network characteristics *in vitro* though cells on the

stiffer substrates generated higher contractile forces in response to electrical stimulation. The patches show considerable regenerative potential, improving cardiac function in one of two transplanted rats and anastomosis of transplanted vasculature with little to no observable fibrosis between the host and graft. These studies indicate that fibrin microfiber sheets are a potentially viable source for engineering functional, vascularized cardiac grafts.
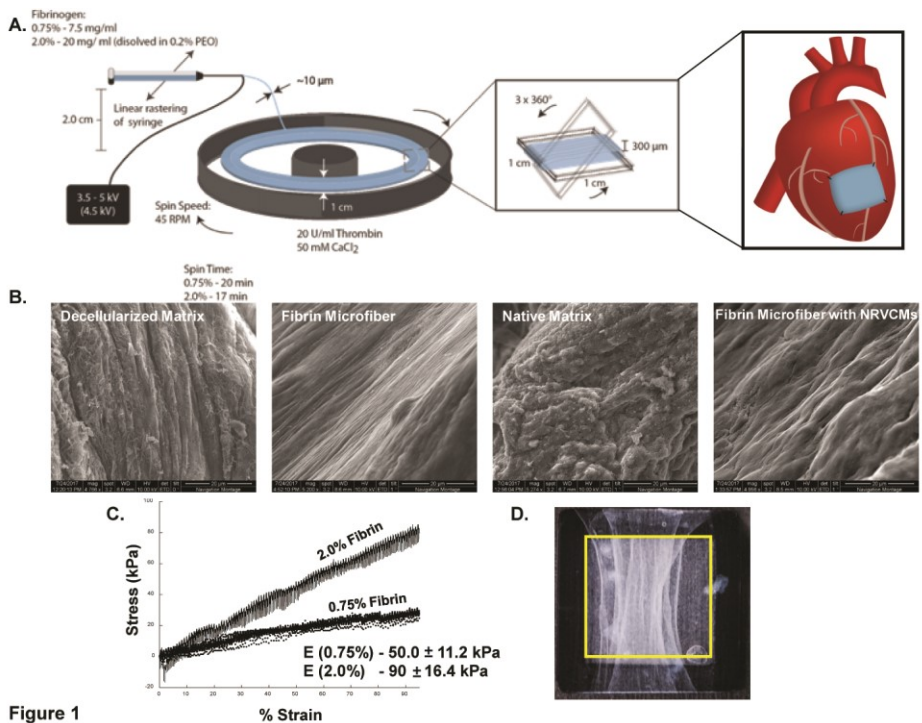
Figure 1

Figure 1: Fibrin microfiber sheet development and characterization A) Schematic illustrating the electrospinning process used to fabricate fibrin microfiber sheets. **B)** Representative SEM images comparing the decellularized or native myocardium to acellular or NRVCM-seeded fibrin microfiber sheets. **C)** Stress strain curve of bulk fibrin microfiber sheets depicting the Young's Modulus of each concentration of fibrin. **D)** Representative image of 1cm × 1cm fibrin

microfiber sheets on mylar frame. Yellow dashed line indicates inner edges of the mylar frame and the boundaries of the scaffold.
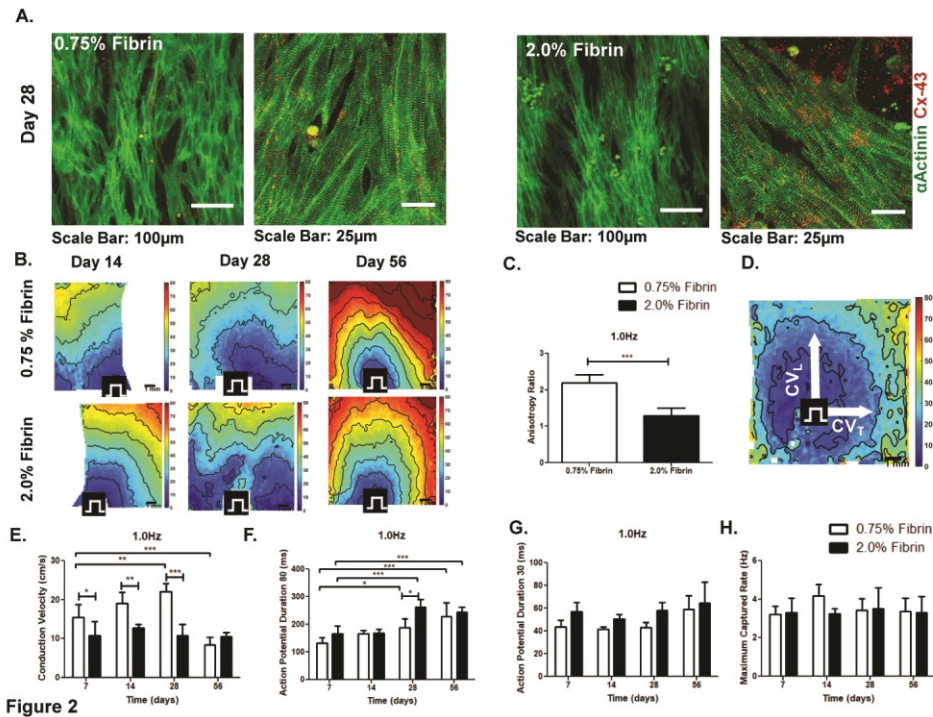
Figure 2: Morphological and Electrophysiological characterization cardiomycoytes on fibrin microfiber sheets. A) Immunofluorescent staining of αActinin (green) and Connexin-43 (red) on both 0.75% and 2.0% fibrin microfiber sheets. Scale Bar is 100µm and 25µm **B)** Representative time course (14, 28, and 56 days) activation maps of selected of 0.75% and 2.0% fibrin microfiber cardiomyocyte only group. **C)** Anisoptropy ratio of 0.75% and 2.0% fibrin microfibers at 1.0 Hz pacing rate after 2 weeks of culture. **D)** Representative activation map of 0.75% fibrin microfiber pacing from the center at 1.0 Hz pacing rate. **E)** Comparison of conduction velocity of .075% and 2.0% fibrin microfibers (*n=4-9*) **F)** Comparison of action potential duration 80% and **G)** 30% amongst

0.75% and 2.0% fibrin microfibers sheets from 7-56 days (*n=4-9*) **H)** Comparison of maximum captured rates between 0.75% and 2.0% fibrin fibers * $p < 0.05$; **$p < 0.01$; ***$p < 0.001$
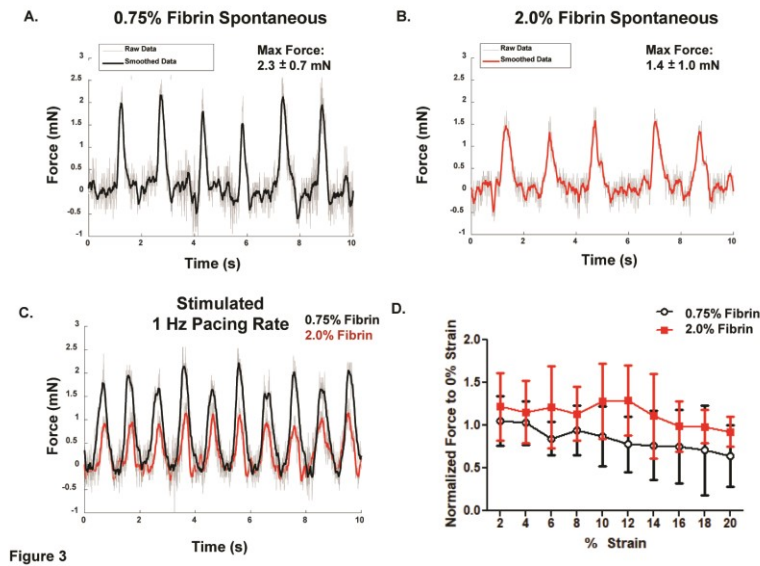
Figure 3: Force of Contraction measurements of Fibrin microfiber sheets. **A)** Representative spontaneous force trace measurement of 0.75% fibrin concentration microfibers. **B)** Representative spontaneous force trace measurement of 2.0% fibrin concentration microfibers. **C)** Representative stimulated force of contraction trace of both 0.75% (black) and 2.0%(red) fibrin microfibers paced at 1 Hz. **D)** Force length relationship of fibrin microfibers up to 20% strain.
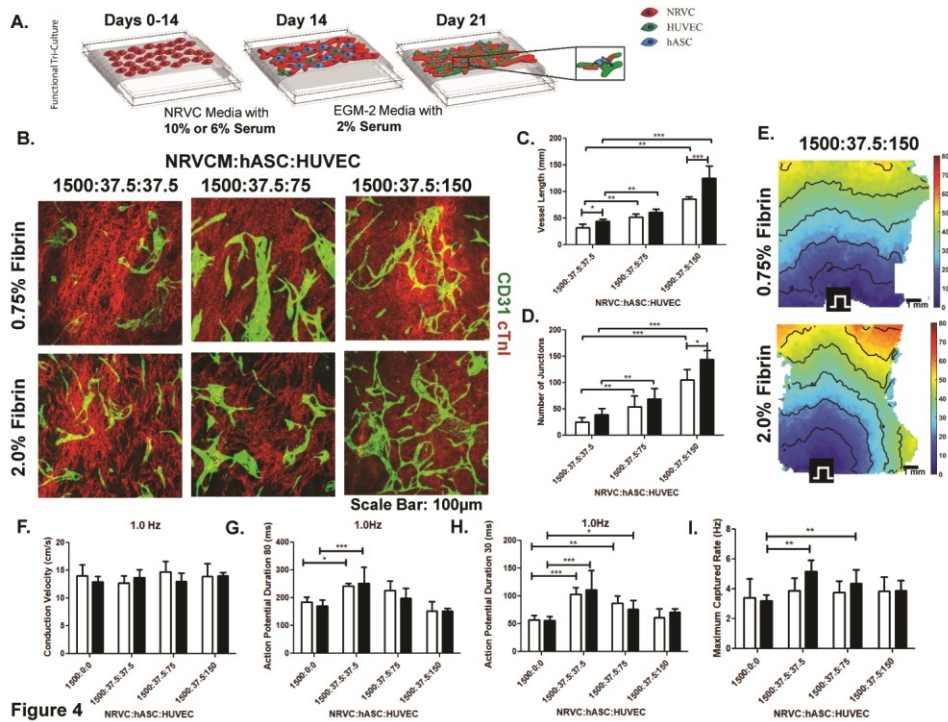
Figure 4: Engineered functional vascularized cardiac graft. A) Schematic showing the additional seeding of supporting cells (hASC and HUVECs) types after 14 days of CM culture. **B)** Immunofluorescent staining of CD31/PECAM-1 (green) vessel structures along with cardiac Troponin I (red) on both the 0.75% and 2.0% fibrin microfibers sheets with cell concentrations ranging from 1500:37.5:37.5-1500:37.5:150. **C)** Comparison of vessel length between tittered endothelial cells in tri-culture **D**) Comparison of the interconnectivity of vessel structures developed in tri-cultures. **E)** Representative activation maps of both 0.75% and 2.0% fibrin microfiber sheets with tri-cultures at the ratio of 1500:37.5:150 **F)** Conduction velocity of tri-cultures compared to NRVCM only cultures in both 0.75% and 2.0% fibrin microfibers **G)** Comparison of Action Potential Duration 80 and **H)** Action Potential Duration 30 of both 0.75% and 2.0% fibrin microfibers **I)** Maximum

captured rates comparing both fiber stiffness and ratios of NRVCM:hASC:HUVECs p < 0.05; **p < 0.01; ***p < 0.001
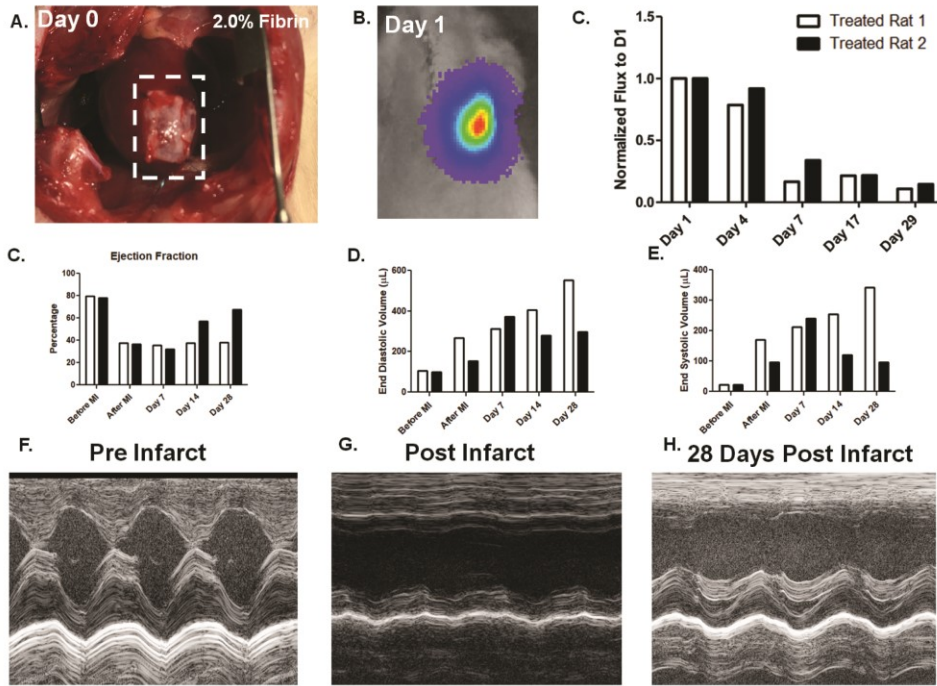
Figure 5

Figure 5: Implantation of Function Vascularized Cardiac Patch. A) Image of fibrin microfiber attached to myocardium post infarction after implantation **B)** Image of bioluminescence of vascularized cardiac patch implanted onto infarcted myocardium **C)** Quantified flux of fibrin microfibers over time **E)** Ejection Fraction measurements over time of treated rats **F)** End diastolic volume measurements over time **G)** End systolic volume measurements over time **H)** M-mode image of myocardium pre-infarct **I)** M-mode image of myocardium 24 hours post-infarct **J)** M-mode image of myocardium 28 days post-infarct
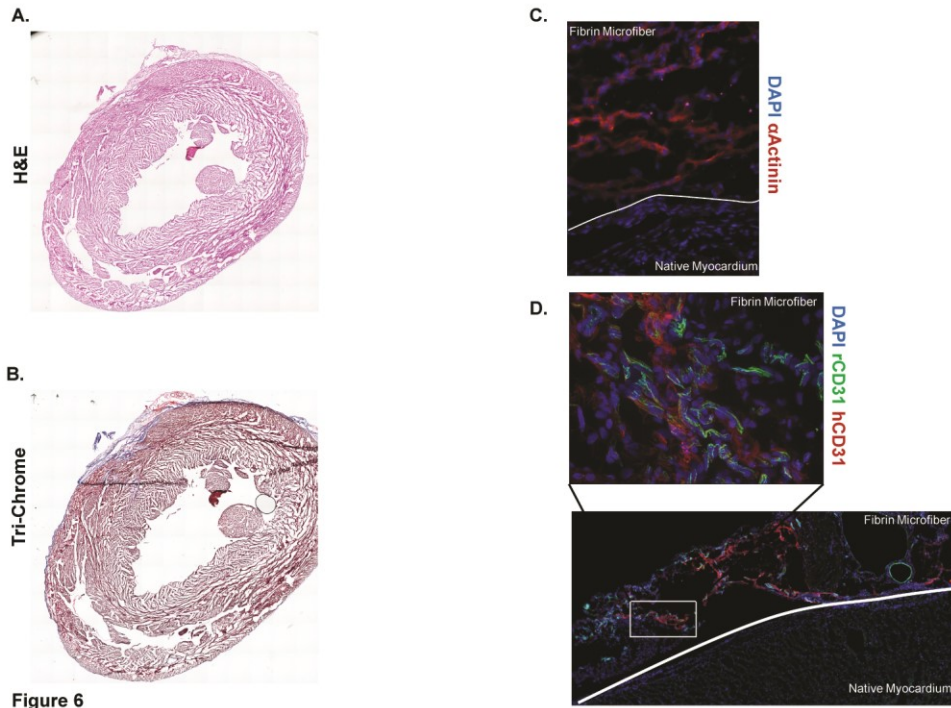
Figure 6: *Histology and Immunostaining of Implanted Vascularized Cardiac Patch*. **A)** H&E staining of 5μm slice of patch placed on myocardium. **B)** Masson's tri-chrome staining of 5μm slice of patch placed on myocardium.**C)** Immunostaining of 5μm patch 29 days post implantation for αActinin (cardiomyocytes) and DAPI **D)** Immunostaining of 5μm patch 29 days post implantation for rat CD31(green) for host vasculature, human CD31 (red) for engineered vasculature and DAPI
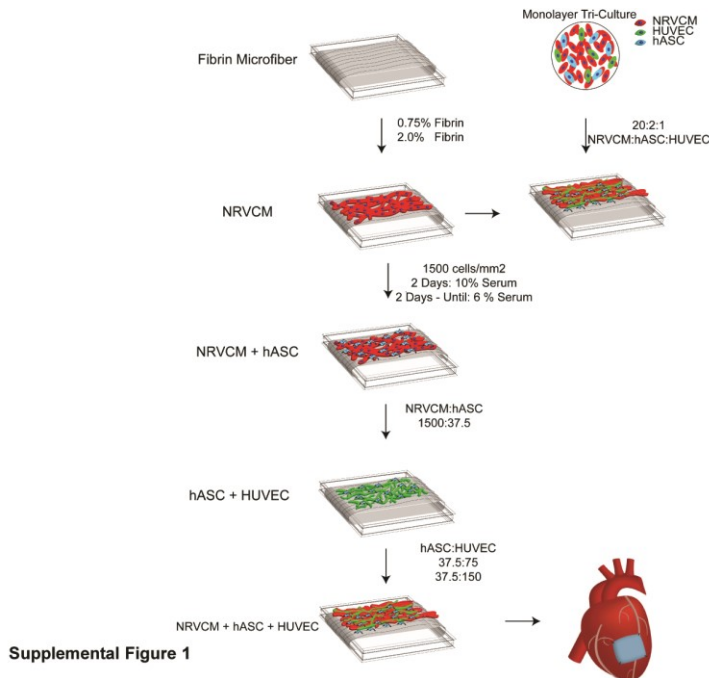
Supplemental Figure 1: Schematic of experimental design. Fibrin microfiber sheets were characterized 0.75% and 2.0% fibrin microfibers were used for the remaining studies. NRVCMs were characterized on fibrin microfibers and resulted in the concentration of cardiomyocytes and culture conditions. NRVCMs and hASCs consistently mapped at the ratio of 1500:37.5:0. Vessel development was characterized at the ratio of 0:37.5:75 and 0:37.5:150. This information resulted in the tri-culture conditions and ultimately the patch implanted onto the infarcted myocardium.
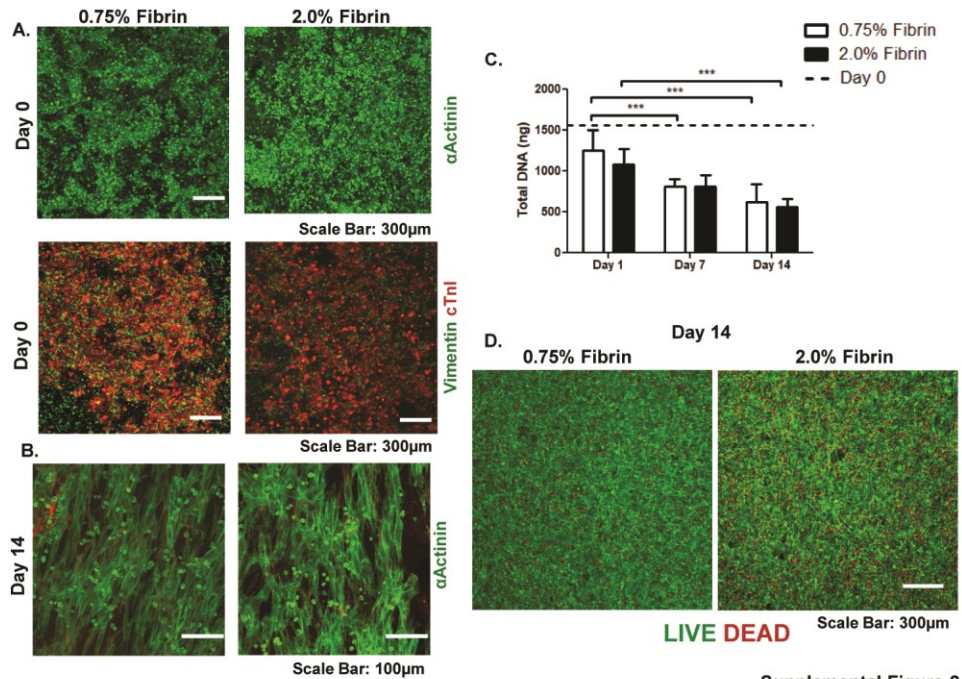
Supplemental Figure 2: Survival of cardiomyocytes on fibrin microfiber sheets. **A)** Immunofluorescent staining of cardiomyocytes on fibrin microfibers at Day 0 alpha Actinin (cardiomyocytes) in green on top panel and immediately below vimentin (fibroblast) in green and cardiac troponin I (cardiomyocytes) in red. **B)** Immunofluorescent staining of 0.75% and 2.0% fibrin microfiber sheets **C)** DNA quantification of cardiomyocytes on fibrin microfiber sheets (0.75% and 2.0%) over 14 days relative to Day 0. **D)** Representative images of calcein AM and ethydium bromide stained fibers to qualitatively examine cardiomyocyte survival. ***p < 0.001
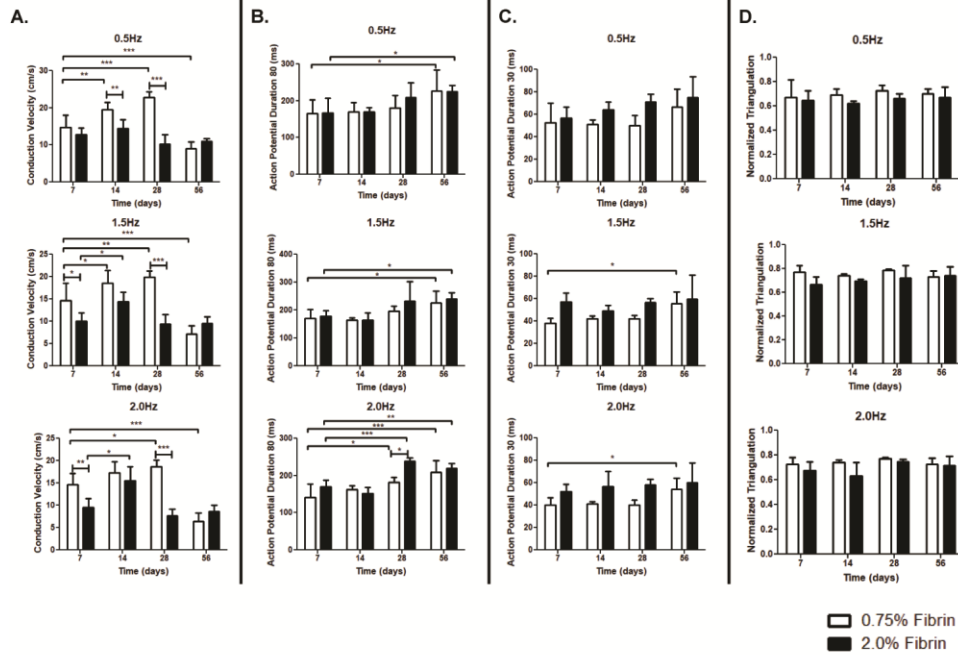
Supplemental Figure 3

Supplemental Figure 3: Electrophysiological characterization of cardiomyocytes at 0.5, 1.5, and 2.0 Hz Pacing A) Conduction velocity of both 0.75% and 2.0% fibrin over time **B)** Action potential duration 80 of both 0.75% and 2.0% fibrin over time **C)** Action potential duration 30 of both 0.75% and 2.0% fibrin over time **D)** Normalized triangulation over time.
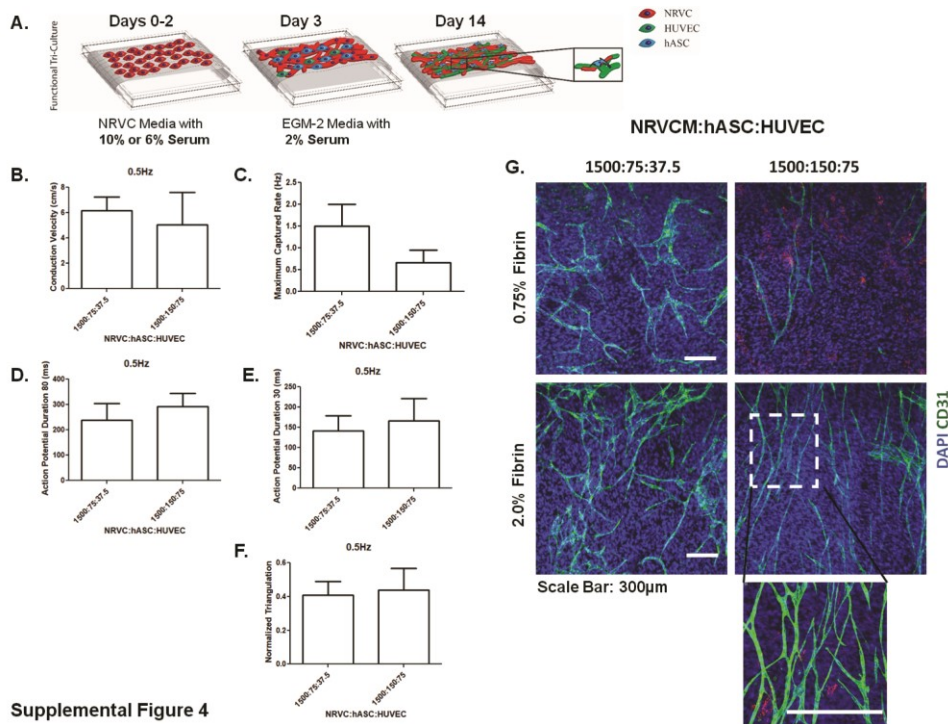
Supplemental Figure 4: *Development of functional tri-culture*. **A)** Schematic showing the additional seeding of supporting cells types after 2 days of CM culture. **B)** Conduction Velocity of tri-culture **C)** Maximum captured rate **D)** Action Potential Duration 80 **E)** Action Potential Duration 30 **F)** Normalized Triangulation **G)** Immunofluorescent staining of CD31/PECAM-1 vessel structures.

Supplemental Figure 5

Supplemental Figure 5: Cardiomyocyte and hASC co-cultures on fibrin microfiber sheets. A) Schematic of sequential seeding of hASCs after cardiomyocytes. 0.75% fibrin microfibers at several pacing rates **B)** Conduction velocity **C)** Action potential duration 80 **D)** Action potential duration 30 **E)** Normalized Triangulation. 2.0% fibrin microfibers at several pacing rates **F)** Conduction velocity **G)** Action potential duration 80% **H)** Action potential duration 30% **I)** Normalized Triangulation.

These parameters were consisted of conduction velocity at 10 $\pm$ 1.4 cm/s (*n=3*), APD 80 261 $\pm$ 28 ms (*n=3*), APD 30 85 $\pm$ 11 ms (*n=3*), and a normalized triangulation of 0.7 $\pm$ 0.02 (*n=3*) (**Supplemental Figure 6**). The 2.0% fibrin group seeded similarly to the 0.75% fibers displayed similar electrophysiological characteristics (**Supplemental Figure 6**).

Supplemental Figure 6: Characterization of vessel development on fibrin microfiber sheets. **A)** Schematic of vessel development on fibrin microfibers **B)** Immunostaining of vessel assembly after several 7 days of culture **C)** Vessel length of assembled vasculature with both 2% and 6% serum **D)** Interconnectivity of assembled vasculature with both 2% and 6% serum

Vessel lengths and interconnectivity were slightly greater in the 0:37.5:75 ratio compared to the 0:37:150, which peaked at 80 ± 14 mm and 940 ± 408 respectively.
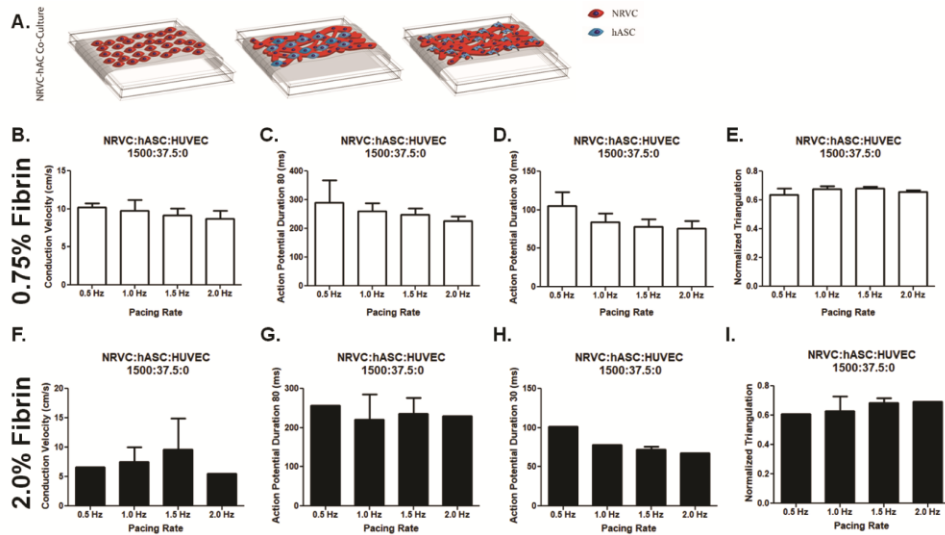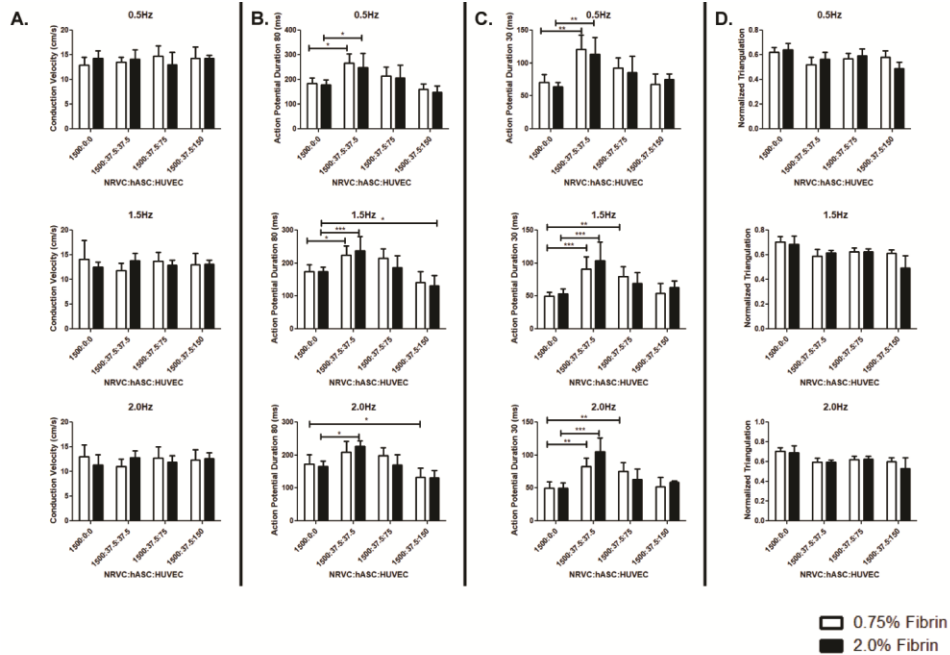
Supplemental Figure 7

Supplemental Figure 7: Electrophysiological characterization of tri-cultures at 0.5, 1.5, and 2.0 Hz Pacing A) Conduction velocity of both 0.75% and 2.0% fibrin over time **B)** Action potential duration 80 of both 0.75% and 2.0% fibrin over time **C)** Action potential duration 30 of both 0.75% and 2.0% fibrin over time **D)** Normalized triangulation over time.
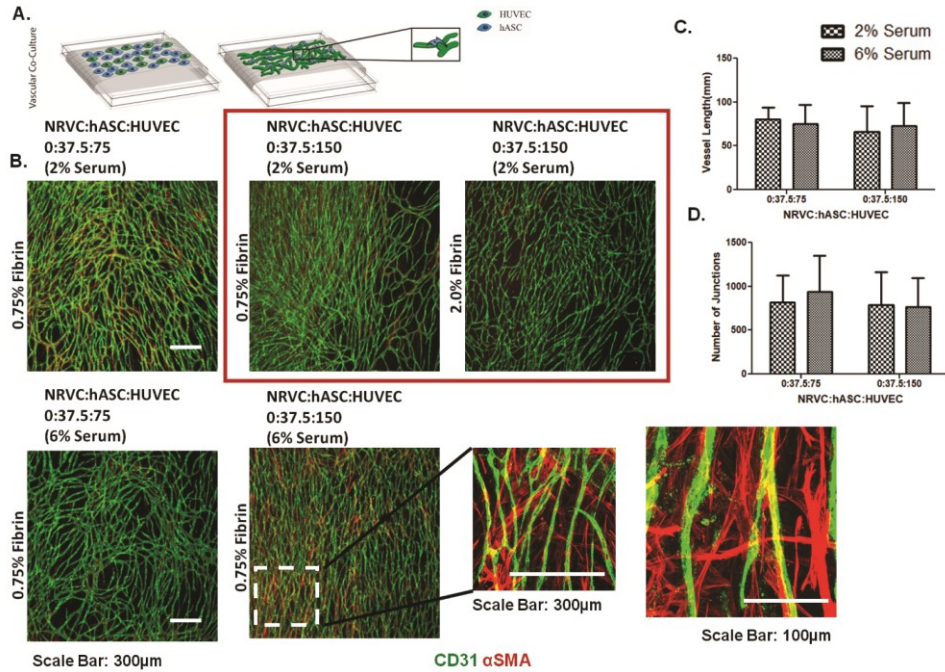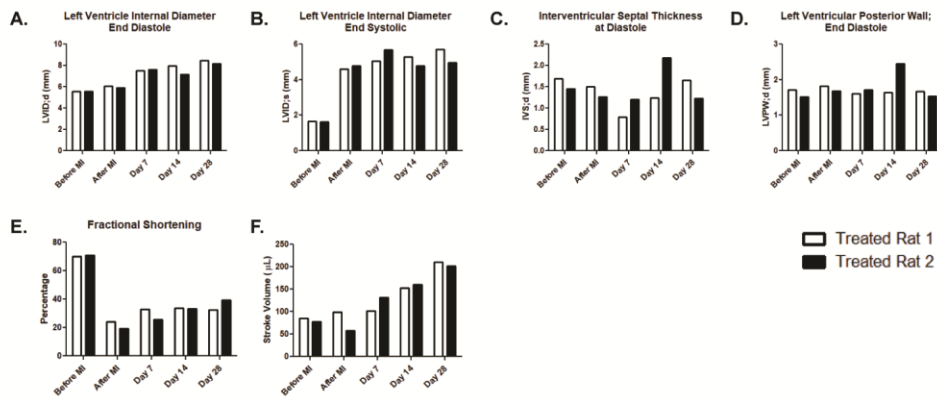
Supplemental Figure 8

Supplemental Figure 8: Implantation of Vascularized Cardiac Patch. A) LVID;d over time **B)** LVID;s over time **C)** IVS;d over time **D)** LVPW;d over time **E)** Fractional shortening **F)** Stroke volume over time **G)** M-mode image of myocardium pre-infarct of Rat 1 **H)** M-mode image of myocardium 24 hours post-infarct of Rat 1 **I)** M-mode image of myocardium 28 days post-infarct of Rat 1
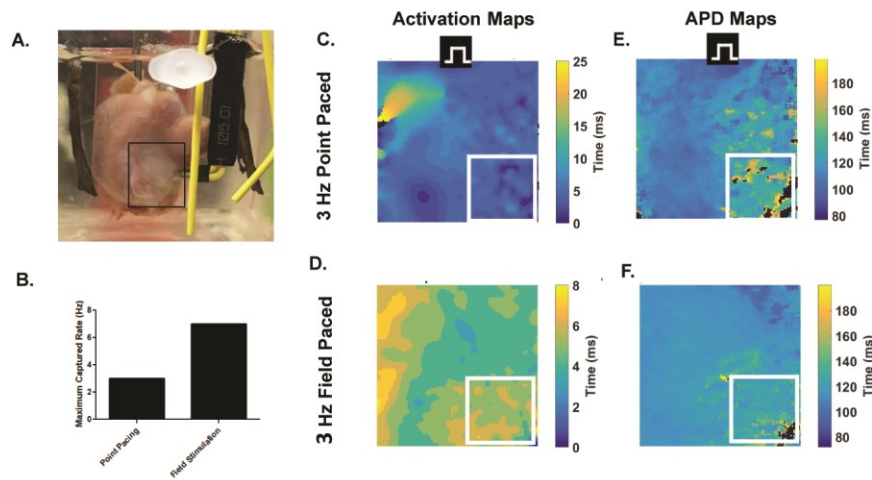
Supplemental Figure 9: Whole Heart Optical Mapping of Vascularized Cardiac Patch. A) Treated rat heart on Langendorff perfusion chamber for optical mapping **B)** Maximum captured rate of point paced and field paced heart **C)** Activation Map of 3 Hz point paced myocardium **D)** Activation Map of 3 Hz field paced myocardium **E)** Action potential duration map of point paced and **F)** field paced.
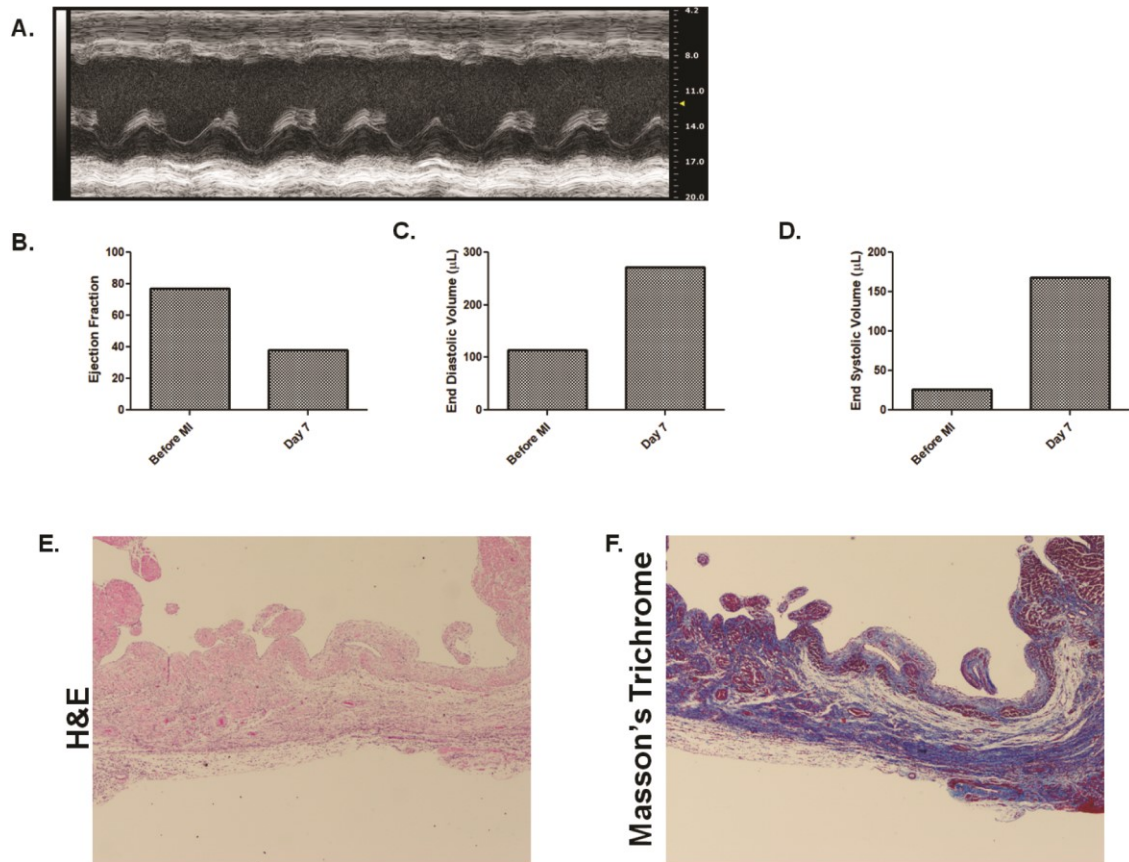
Supplemental Figure 10: Infarct model characterization . A) M-mode image of myocardium post-infarction **B)** Ejection Fraction measurements over time of infarcted rat **C)** End diastolic volume measurements over time **D)** End systolic volume measurements over time **E)** H&E staining of infarct after 7 days **F)** Masson's trichrome staining of infarct after 7 days

A.

B. 0.75% Fibrin

Day 0
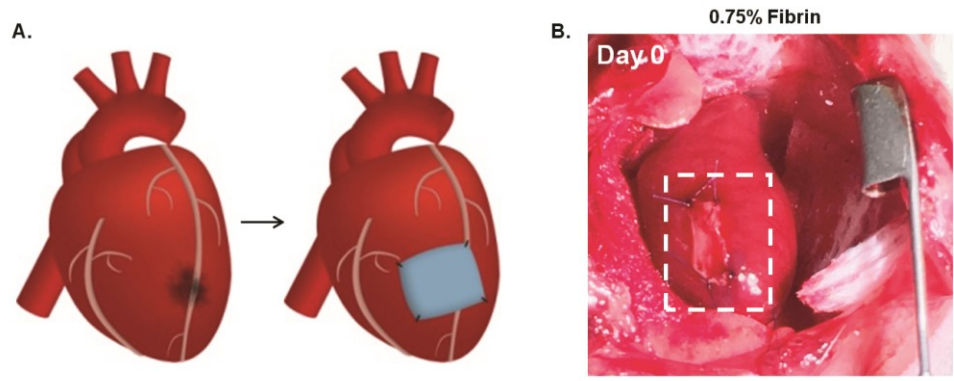
Supplemental Figure 11

Supplemental Figure 11: Infarct model schematic

4

Cell-Cell Interaction of Adipose Derived Stem/Stromal Cells with Human Cardiomyocytes and Human Endothelial Cells

1. INTRODUCTION:

In the United States (US) nearly 800,000 new cases of myocardial infarction occur per year.[1] With a shortage of donor hearts and the inherent limited endogenous repair of the native myocardium, there is a critical need for new therapeutic approaches to regenerate the injured myocardium. Tissue engineering offers a method to engineer cardiac tissue that mimics the native cellular make-up and could potentially be used to restore lost functionality.[6,152] The native myocardium is mainly composed of cardiomyocytes, endothelial cells, and fibroblasts. More recently, it has been discovered that endothelial cells make up the largest number of cells found in the myocardium due to the highly metabolic nature of cardiomyocytes.[186] While supporting cell types are important, finding a suitable cardiomyocyte source, which is the primary electrically excitable cell in the heart, is essential for functionality. This is a critical problem because cardiomyocytes have a life-span of nearly 100 years and do not often divide to repair damaged regions of the myocardium.

Early discoveries have utilized human embryonic stem cells (hESCs) as a promising cell source for generating functional cardiomyocytes. While a promising cell

source, hESCs have drawbacks which include ethics, the potential to form teratomas when implanted *in vivo,* and genetic instability.[204] More recently induced pluripotent stem cells have been developed with the promise of offering similar differentiating potential to embryonic stem cells but the ability to be patient specific and developed in larger quantities. [205,206] Cardiomyocytes derived from human pluripotent stem cells (hiPSC-CMs) are a promising cell source that can be utilized for *in vitro* cardiac electrophysiology studies, investigation of cardiac drugs (respond to cardioactive drugs), models of disease, and patient-specific therapeutic applications. [207] Although hiPSC-CMs are a promising cell source, there are still roadblocks with these cells. hiPSC-CMs are immature in their cardiac development with respect to morphology, electrophysiology, ion channels location and function, and gap junction localization.

Currently studies have indicated that non-myocyte co-cultures can aid in the maturation of cardiomyocytes. Particularly the development of a vascularized cardiac system *in vitro* with hiPSC-CMs has shown an increase in gene expression of cardiac markers and morphological changes of cardiomyocytes. (Vuorenpaa H. et al. 2014) From this study we learn that there is also a need to investigate endothelial cells that have unlimited self renewal capacity and have the potential to be patient specific. Currently human umbilical vein endothelial cells (HUVECs) and endothelial progenitor cells/endothelial colony forming cells (EPCs/ECFCs) are used for vessel development studies. HUVECs are not clinically translatable cells because they come from the umbilical cord and are allogenic. EPCs/ECFCs are clinically relevant and can be obtained from peripheral blood, but are slow growing initially and require many passages to achieve large number of cells.[128,141,208] Similar to cardiomyocytes, researchers have differentiated pluripotent stem cells into endothelial cells.[209] ESC/iPSC derived endothelial cells express phenotypic markers that are similar to both HUVECs and ECFCs. hiPSCs have unlimited self-renewal potential which could ultimately provide an

abundant source of endothelial cells.   Differentiated hESC/hiPSC-ECs have the ability to form cord like structures when culture in 2D and develop 3D lumens when cultured in hydrogels. hESC/hiPSC-EC derived endothelial cells can anastomose with host vasculature when implanted *in vivo*. hiPSC-ECs can be autologous and/or disease specific and also have the ability to be differentiated towards the arterial and venous lineage.

In an effort to develop a vascularized cardiac tissue, the tri-culture system consists of cardiomyocytes, endothelial cells, and a stromal cell. Research has shown that human adipose derived stem/stromal cells have the ability to serve as the non-myocyte support cell for cardiomyocytes as well as the vascular support cell for vessel stabilization. Stromal cells like hASCs can aid with matrix deposition and signal transduction when coupled with cardiomyocytes. Stromal cells, like fibroblasts, have shown improved contractile force in co-culture with pluripotent stem cell derived cardiomyocytes. In addition, fibroblasts co-cultured with hiPSC-CMs have shown to reduce calcium transients and upregulated sarcoplasmic reticulum calcium uptake which is more adult like. (Kane C, et al. 2016). We compared the electrophysiological properties of suitable stromal cells (bone-marrow mesenchymal stem cells (BM-MSCs), dermal fibroblasts, and cardiac fibroblasts) to hASCs. Similarly, with vasculature development and stabilization, we compared supporting cell types to hASC in co-cultures with endothelial cells. The results could ultimately be combined to determine a vascularized cardiac model.

2. MATERIALS and METHODS:

2.1 Human Cardiomyocyte Differentiation:

hESC-CM (H9 cell line, wild type) differentiated by a monolayer-based protocol. Undifferentiated hESC monolayers were maintained in E8 media (Thermofisher Scientific, USA) on 1:200 diluted GelTrex (Thermofisher Scientific, USA)-coated 6-well tissue culture plates prior to differentiation. A directed differentiation protocol was used to differentiate hESC into the cardiac lineage once cells reached near 80% confluency. At day 0 of differentiation (d0), media was switched to RPMI 1640 (Thermofisher Scientific, USA) with B27 without insulin (Thermofisher Scientific) until day 9 (d9). Media was supplemented with 6μM CHIR99021 (Selleckchem, USA) for 48 hours (d0-2), then 5μM IWR-1 (Sigma-Aldrich, USA) for 48 hrs (d3-5). On day 9, media was switched to RPMI 1640 with B27 with insulin (Thermofisher Scientific, USA). Cardiomyocytes began to spontaneously beat starting from d7 to d10. On day 10-12, cells were dissociated using 0.05% trypsin and re-plated on 1:200 GelTrex-coated tissue culture plates at a density of 250,000 cells/cm^2 to form confluent monolayers [210].

hiPSCs were generated from a healthy patient (JHUCCL2 line, wild type) and plated onto 6-well plates coated 1:200 GelTrex:DMEM/F-12. The same differentiation protocol for hESC-CMs was used for hiPSC-CMs.

2.2 Human Adipose Derived Stem/Stromal Cells:

Human adipose derived stem/stromal cells (hASCs) isolation was performed at the Johns Hopkins University, under an Institutional Review Board approved protocol according to published methods. Briefly, fresh human subcutaneous

adipose lipoaspirates were obtained under informed consent from healthy donors undergoing elective liposuction. The lipoaspirate tissue was extensively washed with warm phosphate buffer saline solution to remove erythrocytes and then digested in PBS supplemented with 0.1% Collagenase Type I (Worthington), 1% BSA, and 2 mM CaCl2 for one hour at 37°C. Following room temperature centrifugation at 300G and resuspended in stromal vascular fraction medium (DMEM/F-12) (Life Technologies) supplemented with 10% FBS (Atlanta Biologicals) and 1% penicillin/streptomycin), the stromal vascular pellet obtained from 35mL of lipoaspirate digest was plated in a T175 flask (0.2mL per cm2). After 24 hour of incubation at 37°C, 5% CO2, the adherent cells were washed with warm PBS and maintained in stromal medium until 80-90% confluent. The adherent population ("passage 0") was harvested by digestion with trypsin (0.05%)/EDTA(1mM) at 37°C for five minutes, washed with Stromal Medium and cryopreserved. Prior studies have shown that there are no deleterious effects on hASCs due to cryopreservation, such as loss of viability or multipotency [164] . For expansion, hASCs were thawed and cultured in expansion medium which includes DMEM high glucose (Life Technologies, USA), 10% FBS (Atlanta Biologicals, USA), 0.5%penicillin/streptomyocin (Cellgro, USA), 0.5%antibiotic/antimycotic, 1ng/mL FGF2 (PeproTech). Cells were utilized at passage 2.

2.3 Human Endothelial Cell Differentiation:

To initiate mesodermal induction, Essential 6 medium (Gibco, USA) supplemented with 6 µM CHIR-99021 (STEMCELL Technologies, USA) was

added to one well of hiPSCs (BC1 cell line, wild type) at 70% confluence. In early

vascular differentiation, cells were plated onto collagen IV (Corning, USA) coated

plates at 2 x10^4 cells/cm^2 with ROCK inhibitor and cultured in endothelial cell

growth medium (Promocell, USA) supplemented with 50 ng/mL VEGF (R&D,

USA) and SB-431542 (Sigma-Aldrich, USA), internally referred to as high VEGF

media. Early Endothelial Cells (day 8) were magnetically sorted using VE

cadherin-PE (BD Biosciences, USA) and the MACS sorting system (Miltenyi

Biotech, USA) according to the manufacturer's instructions. Sorted ECs were

cultured on collagen IV coated plates in high VEGF media to mature [133,135].

2.4 Human Dermal Fibroblast (hNDF) Culture:

Adult Human Normal Dermal Fibroblast (hNDF) (ATCC, USA) were expanded in

tissue culture flasks up to passage 3 (P3) using Fibroblast Basal Media (ATCC,

USA) and Fibroblast Growth Kit Low Serum which contains 2% FBS (ATCC,

USA), 5 ng/mL rhFGF-2, 7.5mM L-glutamine, 50 μg/mL Ascorbic Acid,1μg/mL

Hydrocortisone Hemisuccinate, 5 μg/mL recombinant human Insulin, and 1.0%

antibiotic/antimycotic (Life Technologies, USA). NHDFs were used between

passage 3-4.

2.5 Human Cardiac Fibroblast-Ventricular (hNCF-V) Culture:

Adult normal human cardiac fibroblast-ventricular (Lonza, USA) were expanded

in tissue culture flasks and cultured with Fibroblast Basal Medium (Lonza,USA)

and the Fibroblast Growth Medium-3 (FGM-3) Bullet Kit which contains 10%

FBS. NHCF-Vs were used at between Passages 2-3.

2.6 Human Bone-Marrow Derived Stem Cells (hBM-MSC) Culture:

Human bone-marrow derived stem cells (Lonza) were expanded from passage 0 to passage 2 using expansion medium which consisted of Dulbecco's modified Eagle medium (DMEM) with 4.5 g/l glucose (Life Technologies, USA) supplemented with 10% (vol/vol) fetal bovine serum (FBS; Atlanta Biologicals, USA), 100 U/ml penicillin and 100 μg/ml streptomycin (Cellgro, USA), and 1 ng/ml basic fibroblast growth factor (FGF-2) (PeproTech, USA). hBM-MSCs were used at between Passages 3-4

2.7 Human Umbilical Vein Endothelial Cell Culture (HUVEC) Culture:

A vial of pooled human umbilical vein endothelial cells (HUVECs) (Lonza, USA) were expanded in tissue culture flasks up to passage 3-5 using Endothelial Basal Medium 2 (EBM-2) culture medium (Lonza, USA) supplemented with the Endothelial Growth Medium-2 (EGM-2) Bullet Kit (Hydrocortisone, human fibroblast growth factor (hFGF)-2, vascular endothelial growth factor (VEGF), R3-insulin-lke growth factor (IGF)-1, ascorbic acid, human epidermal growth factor (hEGF), gentamicin & amphotericin (GA-1000), and Heparin) and 2% FBS. HUVECs were used for experimentation at Passage 4-6.

2.8 Human Endothelial Colony Forming Cells (hECFC) Culture:

Human endothelial colony forming cells (hECFCs) (Lonza, USA) were used for experiments between passages 5 and 9. hECFCs were expanded in flasks coated with type I collagen (BD Biosciences, USA) in Endothelial Basal Medium-2 (EBM-2; Lonza USA) supplemented with EGM-2 Bulletkit (Lonza) and 10%

fetal bovine serum (FBS; Hyclone, USA). ECFCs were fed every other day, passaged every 5 to 7 days using 0.05% trypsin/0.1% ethylenediaminetetraacetic acid (EDTA; Invitrogen, USA).

2.9 Flow Cytometry Analysis of hASCs, hNDFs, hNCFs-V, and hBM-MSCs:

Cells were detached with 0.25% Trypsin/EDTA and washed with phosphate buffer saline (DPBS) containing 2% FBS. They were then incubated with monoclonal antibodies for mesenchymal markers (CD73 and CD105) and vascular markers, (CD31, CD34, and CD309 (VEGFR2)), hematopoietic marker (CD45), and MHC receptor (HLA-DR) and isotype controls (BD Biosciences) were conjugated to fluorescein isothiocyanate (FITC), phycoerythrin (PE), and Per CP-Cy 5.5 for 30 minutes at 4 °C. Cells were analyzed with the BD Accuri C6 flow cytometer.

2.10 Optical Mapping:

Optical mapping was performed on days 14-28. Cell monolayers were stained with 10 µM of the voltage-sensitive dye di-4-ANEPPS (Invitrogen), in Tyrode's solution for 10 minutes at 37 °C while being protected from light. After staining, the dye solution was removed, cells were washed with Tyrode's solution, and placed on a heated stage in Tyrode's solution with 5 µM blebbistatin to prevent motion artifacts due to contraction. Optical mapping was performed using a CMOS camera (MiCAM Ultima, Scimedia, Costa Mesa, CA). Cells were electrically stimulated by placing a bipolar point electrode near the edge of the coverslip, out of the field of view of the camera, and paced starting at 0.5 Hz and incrementally increased several intervals. At each new pacing rate, the cell monolayers were stimulated for 1 minute to achieve steady state before an optical recording was taken.

2.11 DNA Assay:

500μL Deoxyribonucleic Acid (DNA) lysing solution (10mM Tris, 1mM EDTA, 0.1% Triton X-100, and 0.1 mg/mL proteinase K) was placed on monolayers and removed and placed into Eppendorf tubes and frozen at -20°C. Samples were subsequently heated at 50 °C overnight to digest proteins and inactivate nucleases. PicoGreen dsDNA quantification assay was carried out according to the manufacturer's instructions. Briefly, the samples were combined with PicoGreen reagent (100 μL sample + 100 μL PicoGreen) and transferred (200 μL) into a black 96-well plate along with DNA standards. Fluorescence was measured at excitation 485nm / emission 528 nm using a fluorescent plate reader.

2.12 Fluorescence Recovery After Photobleaching (FRAP):

hCMs were plated at low density (100,000 cells per 35 mm MatTek dish) and cultured for 14 days. DiI (Life Technologies, USA) stained non-myocytes (hASCs) were added to culture two days before experiment. Cells were incubated with 0.5 uM calcein AM (Life Technologies, USA) for 20 minutes at 37C, rinsed with DPBS and culture media was added to the stained cells. In pairs of cells (one CM and one DiI-labelled non-myocyte) or in groups of cells (one DiI-labelled non-myocyte surrounded by CMs), the non-myocytes were photbleached with a 488 laser and consecutive images were taken for up to 7 minutes to determine the recovery of fluorescence.

2.13 Immunocytochemistry:

Cells were fixed with 4% paraformaldehyde for 20 minutes at room temperature. Formaldehyde was washed three times with DPBS for 30 minutes each time. Samples were permeabilized with 0.2% triton X-100 for 10 minutes and then blocked with 10% normal donkey serum (Sigma Aldrich, USA) for 30 minutes. The samples were incubated overnight with goat anti-CD31 (Santa Cruz Technologies, USA) and rabbit anti-von Willebrand Factor (Sigma Aldrich, USA) primary antibodies diluted in 10% normal donkey serum at 4°C. Primary antibody was washed three times with DPBS. Samples were incubated with secondary antibodies AlexFluor 488-conjugated donkey and AlexaFluor 647-conjugated donkey anti-rabbit (Jackson ImmunoResearch, USA). Samples were washed three times with DPBS. Samples were incubated with DAPI (Sigma Aldrich) diluted in DPBS. Petri dishes were imaged under Zeiss Axio Observer inverted fluorescence microscope and the Zeiss LSM 510 confocal.

2.14 Image Analysis:

Vascular assembly images were taken at 2.5x on a Zeiss Axio Observer inverted fluorescence microscope, which the conversion of the images is 4.0145 μm/pixel. Thresholded images were subsequently analyzed with AngioQuant software to determine the total vessel length, area, and interconnectivity.

2.15 Statistical Analysis:

Quantitative data is reported as the mean $\pm$ the standard deviation. One-way ANOVA with Dunnett's post-hoc test or Tukey's post-hoc test was performed to

determine statistical difference between testing groups. Differences were considered statistically significant at $*p < 0.05$; $**p < 0.01$; $***p < 0.001$.

3. RESULTS:

3.1 Effect of hASCs on human stem cell derived cardiomyocyte electrophysiology:

Both human embryonic stem cell derived cardiomyocytes (hESC-CMs) and human induced pluripotent derived cardiomyocytes (hiPSC-CMs) were cultured for a week prior to the addition of hASCs. After culturing the cardiomyocytes for 7 days to establish cell-cell contact, hASCs were seeded at various ratios from 300:30:0, 300:60:0, 300:150:0, and 300:300:0 (hCM:hASC:hEC). In the hESC-CMs co-cultured with hASCs group, the conduction velocity increased with the addition of hASCs in co-culture slightly in the presence of hASCs as compared to the control. At 1 Hz pacing rate, conduction velocity ranged from 14 ± 6 cm/s (*n=11*) (control) to a peak of 18 ± 2 cm/s (*n=7*) (300:150:0) **(Supplemental Figure 2B)**. It is noteworthy that within the 0.5 Hz and 0.7 Hz there was a similar trend in conduction velocity but there was statistical significance between the 300:150:0 group compared to 300:0:0 **(Supplemental Figure 3A)**.

Action potential duration at 80% repolarization (APD_{80}) ranged from the control of 321 ± 66 ms (300:0:0) to highest at 377 ± 80 ms (300:300:0) **(Supplemental Figure 2C)**. There were no statistical differences amongst APD_{80} with the control and the varied hASC ratios. We notice similar trends in the APD_{30} which ranged from 167 ± 20 ms (300:30:0) to 185 ± 30 ms (300:300:0)

(Supplemental Figure 2D). In addition, there is statistical significance in the normalized triangulation comparing the control (300:0:0) of 0.43 ± 0.06 to the ratio 300:300:0 of 0.5 ± 0.03 **(Supplemental Figure 2E)**. These rates were acquired at 1 Hz pacing. We observe similar findings at other pacing rates of 0.5 Hz and 0.7 Hz **(Supplementary Figure 3B-D)**. The maximum captured rate tended to be increased with the presence of hASCs which maxed at 2.4 ± 0.2 Hz (300:300:0) as compared to 1.8 ± 0.5 Hz (300:0:0).

Similarly to hESC-CM, hiPSC-CMs displayed slightly increased electrophysiological properties as compared to the control group (300:0:0). At 1 Hz pacing, the conduction velocity peaked at 16 ± 2 cm/s (*n=12*) (300:300:0) and lowest at 14 ± 2 cm/s (*n=11*) (300:60:0) **(Figure 2B)**. Similar trends exist at other pacing rates and we also find that at increased concentrations of hASCs increased the conduction velocity when paired with hiPSC derived CMs **(Supplementary Figure 2A)**. APD_{80} increased as to a maximum of 321 ± 52 ms (*n=12*) at the ratio of 300:300:0 and was lowest at 261 ± 50 ms (*n=8*) (300:30:0) **(Figure 2C)**. APD_{30} ranged from 104 ± 35 ms (*n=11*) (300:60:0) and 171 ± 52 ms (*n=12*) (300:300:0) **(Figure 2D)**. There were no statistical differences in conduction velocity, APD 80 and 30, or normalized triangulation. Similar to hESC-CMs, hiPSC-CMs coupled with hASCs displayed increased maximum captured rates. While maximum captured rate was higher than the control group in all ratios, the 2 ratios that were statistically significant compared to the control were 300:60:0 and 300:150:0 which rates were 3.4 ± 0.4 Hz (*n=12*) and 3.0 ± 0.9 Hz (*n=7*) respectively **(Figure 2F)**. The DNA assay data demonstrated that the

paracrine effects of hASC did not increase cardiomyocyte proliferation (**Supplemental Figure 6**), which lead us to further believe that the increases in conduction can be attributed to another mechanism. In **Supplemental Figure 7,** the fluorescent recovery after photobleaching (FRAP) suggested that slight recovery was occurring in the hASCs that were connected to cardiomyocytes. This leads to the potential that hASCs could develop gap junctions with cardiomyocytes and aid in signal transduction.

3.2 Effect of hBM-MSC, hNDF, and hNCF-V on human stem cell derived cardiomyocyte electrophysiology:

In an effort to understand the role of mural cell types other than hASCs, we compared cardiomyocyte electrophysiology amongst hBM-MSCs, hNDF, hNCF-V, and pluripotent stem cells (PSCs) in co-culture with either hESC-CMs or hiPSC-CMs. We initially characterized the surface markers of hASCs, hBM-MSCs, and hNCF-V and found that the cells were positive for mesenchymal markers CD73 (99.8%-hASCs, 99.9%-hBM-MSCs, and 91.9%-nHCF-V) and CD105 (99.3%-hASCs, 95.8%-hBM-MSCs, and 99.9%-nHCF-V), slight to no expression of endothelial markers CD31(0.16%-hASCs, 0.45%-hBM-MSCs, and 1.83%-nHCF-V), CD34 (3.21%-hASCs, 0.006%-hBM-MSCs, and 8.28%-nHCF-V), and VEGFR2 (0.06%-hASCs, 0.07%-hBM-MSCs, and 1.54%-nHCF-V). All supporting cell types were negative for hematopoietic marker CD45 and only hBM-MSCs were positive for HLA-DR at 20.2%. (**Supplementary Figure 4**)

After sequential addition of supporting cells types, electrophysiologically we have discovered that supporting when coupled with hESC-CM or hiPSC-CMs

conduction velocity is lower than the control samples at 1 Hz pacing rate.

Although not statistically significant, it appeared that supporting cell types hBM-MSC, hNDF, and hNCF-V coupled with hESC-CMs displayed conduction velocities that were slower than the control group. The conduction velocities were as follows, hBM-MSC (7 ± 0.8 cm/s) (*n=16*), hNDF (8 ± 1.2 cm/s) (*n=11*), hNCF-V (8 ± 1.3 cm/s) (*n=6*) which were compared to the control (9 ± 2 cm/s) (*n=12*) **(Supplemental Figure 5B)** . Pluripotent stem cells hPSC (10 ± 1 cm/s) (*n=6*) appeared to increase conduction velocity as compared to the control. We notice similar relationships with other pacing rates. hiPSC-CM samples displayed trends that mirrored hESC-CMs. These conduction velocities were hBM-MSC (7 ± 0.6 cm/s) (*n=9*), hNDF (8 ± 1.7 cm/s) (*n=11*), hNCF-V (6 ± 0.8 cm/s) (*n=8*), hPSC (9 ± 0.8 cm/s) (*n=4*) compared to the control of 8 cm/s **(Supplemental Figure 5F)**.

Action potential duration both 80 and 30 were not statistically significant when comparing hBM-MSC, hNDF, hNCF-V, or hPSC in co-culture with hESC-CMs. The APD_{80} values ranged from a minimum of 321 ± 66 ms (hBM-MSC) (*n=16*) to a maximum of 362 ± 72 ms (hNDF) (*n=11*) at 1 Hz pacing **(Supplemental Figure 5B)**. We noted similar trends with APD_{30} as APD_{80} which resulted in no statistical increases or decreases in duration as compared to the control samples **(Supplemental Figure 5C)**. The normalized triangulation was also not statistically different amongst the various cells types in co-culture with CMs **(Supplemental Figure 5D)**. Maximum captured rate peaked at 2.4 ± 0.7 Hz (hPSC) (*n=6*) but there was no statistical difference amongst other cell types compared to the hESC-CM control **(Supplemental Figure 5E)**. Supporting cells

co-cultured with hiPSC-CMs resulted in action potential duration 80 that were

282 ± 25 ms (hBM-MSC) (*n=9*), 344 ± 36 ms (hNDF) (*n=11*), 326 ± 28 ms

(hNCF-V) (*n=8*), and 351 ± 26 ms (hPSC) (*n=4*) compared to control of 310 ms

at 1 Hz pacing rate **(Figure 3C)**. APD_{30} resulted in 142 ± 13 ms (hBM-MSC)

(*n=9*), 176 ± 23 ms (hNDF) (*n=11*), 172 ± 11 ms (hNCF-V) (*n=8*), and 214 ± 14

ms (hPSC) (*n=4*) compared to control of 139 ms at 1 Hz pacing rate. There were

no statistical differences in normalized triangulation **(Figure 3D)**. The maximum

captured rate was greatest with hNDF at 2.4 ± 0.7 Hz **(Figure 3E).**

3.3 Effect of hASC co-cultured with hECFC, HUVEC, or hiPSC-EC on

vascular assembly:

In an effort to determine vascular assembly of mature endothelial cells and

progenitor endothelial cells, we held hASCs constant at 230,000 cells/cm^2,

92,000 cells/cm^2, or 46,000 cells/cm^2 and tittered endothelial cells to determine

the vascular assembly coupled with cellular concentration. These co-cultures

would be used to generate a range of concentrations for vascular development

with hiPSC-EC as the primary endothelial cell. We show that hECFCs and

HUVECs formed similar vessel lengths and interconnectivity at various ratios. At

a 1:1 ratio (~i.e 0:60:60) we observe that there are clusters of endothelial cells

that are not contributing to vessel network formation. Vessel lengths were as

follows for the ratios of 0:60:6, 0:60:12, 0:60:30, 0:60:60 were 162 ± 79 mm, 168

± 13 mm, 225 ± 28 mm, and 292 ± 63 mm (*n=4*) (hECFC) (**Supplemental Figure**

9) and 221 ± 16 mm, 240 ± 70 mm, 316 ± 22 mm , and 321 ± 22 mm (*n=3-4*)

respectively **(Supplemental Figure 9)**. Interconnectivity of vasculature ranged

from 270 ± 160 junctions to 2,074 ± 726 junctions in hASC:hECFC co-cultures

and displayed similar trends in hASC:HUVEC co-cultures (**Supplemental Figure**

9). Learning from the information of hASC:hECFC/HUVEC co-cultures, hiPSC-

EC co-cultures studies were carried out in the range of 0:150:15 to 0:150:150

(hCM:hASC:hEC) and characterized for vessel length and interconnectivity

(Figure 4A). With increasing endothelial cells, there was increase in vessel

network and number of junctions formed. The peak vessel length at 0:150:150

was 280 ± 20 mm (*n=3*) and 1525 ± 330 junction s (*n=3*) (**Figure 4B,C).**

3.4 Effect of hBM-MSC, hNDF, or hNCF-V co-cultured with hiPSC-EC on

vascular assembly:

In addition to electrophysiological effects of hBM-MSCs, hNDFs, or

hNCFs-V when coupled with cardiomyocytes, we assessed their effects of vessel

network assembly when coupled with hiPSC-ECs. We found that hBM-MSCs and

hNCFs-V displayed cord like structures that were seen with hASC:hiPSC-ECs

co-cultures **(Figure 5).** With respect to hNDF, we found that there were only

small areas of vessel network assembly, but majority of the field of view

consisted of endothelial cells clustered together. These cultures were seeded at

the ratio of 0:150:150 and comparing vessel lengths with hASCs cultured at this

same ratio, we find that they generate greater interconnectivity and comparable

vessel lengths. Interconnectivity for these fibroblast-like cells were hBM-MSC

(1356 ± 546) (*n=5*), hNCF-V (628 ± 266) (*n=4*), and hASC (1525 ± 330) (*n=3*)

(Figure 5). Vessel lengths for these cell types were hBM-MSC (296 ± 43 mm)

(*n=5*), hNCF-V (240 ± 43 mm) (*n=4*), and hASC (280 ± 20 mm) (*n=3*) **(Figure 5).**

4. DISCUSSION:

To develop a system that resembles the native make-up of the native myocardium requires the use of several different cell types. Previous efforts have used rodent or human cardiomycotyes (hESC or hiPSC), typically dermal fibroblasts or stromal cells, and endothelial cells.[44,49,57,142] Previous studies have demonstrated that the presence of non-myocytes improves the electrophysiological maturation of CMs as well as increase the generated force of CMs.[211–215] In addition, non-myocytes (stromal cells) can also potentially prolong survival of CMs when implanted *in vivo*. Stromal cells are also necessary for vascular stabilization. Therefore, we investigated the role of hASCs as a suitable stromal cell source for hPSC-CM and hPSC-EC cultures. The co-culture of these cell types, hPSC-CMs with hASCs and hASCs with hPSC-ECs, has not been well studied and established. With the enhanced benefits of hASCs in previous cardiac and vascular studies, there is a need to establish these models.

Similarly to neonatal rat cardiomyocytes co-cultured with fibroblasts, hESC/hiPSC-CMs are co-cultured with fibroblasts. hASCs have shown to maintain electrophysiological properties of neonatal rat cardiomyocytes when co-cultured, while hNDF were deleterious. [41] These interactions have not been studied with hESC/hiPSC-CM in co-cultures. While both embryonic stem cell derived and induced pluripotent stem cell derived cardiomyocytes are not inherently adult-like in their initial differentiation, they provide a vast resource for generating large amounts of cells and hold the promise of maturing through biochemical factors, electro-mechanical stimulation, and multi-cellular

cultures.(Lundy, Zhu, Regnier, & Laflamme, 2013) We simultaneously compare hESC-CMs and hiPSC-CMs to show similar effects in multiple lines of pluripotent stem cells.

While hESC and hiPSC-CMs are phenotypically similar, hiPSC-CM provide functionally similar cardiomyocytes that do not have the ethical hurdles and can be completely autologous.[217] Co-culture of hESC-CMs with hASCs proved to increase conduction velocity, while maintaining the action potential duration at both 30% and 80% repolarization relative to the cardiomyocyte control. Increased conduction velocity and increased maximum captured rate can potentially be attributed to improved calcium handling amongst the myocytes.[212] In addition, we have previously demonstrated that hASCs express connexin-43 and the increased presence of gap junctions could explain the increased electrophysiological outputs[57,218]. Similar effects were noted with the hiPSC-CMs.

The myocardium has a large fibroblast population, there was a need to compare phenotypically similar cells of hASCs to ensure that hASCs are the most beneficial cell source for supporting cardiomyocytes and vascular stabilization. Therefore, other fibroblast-like cells (hBM-MSCs, hNDFs, and hNCF-V) were examined to determine their electrophysiological effects on co-cultures with cardiomyocytes. This would determine if hASCs are truly superior to other stromal cells.   We found that conduction velocity of cardiomycoytes was slightly decreased in the presence of hBM-MSCs and hNCF-V. hNDFs seem to slightly increase the conduction velocity. The action potential duration appears to

be relatively similar amongst supporting cell types. Previous studies have shown that the incorporation of fibroblasts can maintain electrophysiological properties of neonatal rat cardiomyocytes and mouse embryonic stem cell derived myocytes.[219,220] In addition, the literature suggests that hBM-MSCs and atrial cardiac fibroblasts that are in co-culture with hiPSC-CMs appear to increase action potential duration. [221] Comparing these effects of hASCs to other supporting cell types, hASCs appear to maintain or slightly enhance the electrophysiological properties of cardiomyocytes. Pericytes were not included because previous researchers have shown that they are phenotypically similar to hBM-MSCs and have similar effects on cardiomyocytes and vasculature [222].

After investigating the role of hASCs paired with human cardiomyocytes, we investigated the role of hASC:hEC co-cultures in vessel assembly. These studies were initiated by determining a suitable cellular concentration range to culture hASC: hiPSC-EC co-cultures and establish cord like structures. To establish the cellular concentration, both hECFCs and HUVECs were utilized as the initial endothelial cell source. Previous researchers have explained that hiPSC-ECs generally express both progenitor and mature endothelial cell markers making both hECFC and HUVECs applicable to determining appropriate cell range.[15] By utilizing both a progenitor cell (hECFC) and a mature endothelial cell (HUVECs), our hopes were to extrapolate a suitable range for culturing hiPSC-ECs.[20] It is understood that vascular structures need a mural cell to maintain and support developed structures, hence the use hASCs[30].

Similar trends in vascular development occurred between hECFCs and

HUVECs. Noticeably in both groups at the 1:1 ratio of the 230,000 cells/cm^2 and 92,000 cells/cm^2, vascular development contains both cord-like structures coupled with clustering of endothelial cells. In previous reports, cellular concentrations are imperative to the development of vascular structures. By observing similar trends amongst groups, proceeding forward hASCs were held constant at 92,000 cells/cm^2 and hiPSC-ECs were tittered. In these cultures, it appeared that the presence of more endothelial cells resulted in increased vessel length and increased junctions. The development of robust vessel structures was present in these cultures. Similar to hASCs, hBM-MSCs have previously have been characterized for its perivascular potential and shown to develop robust vasculature when co-cultured with endothelial cells. [25,26,137] In addition, we find that cardiac fibroblast support vessel network formation, although not as robust as hASCs and hBM-MSCs.

Ultimately the supportive nature of hASCs in co-culture with pluripotent stem cell derived cardiomyocytes and their perivascular potential when co-cultured with pluripotent stem cell endothelial cells offers the promise of developing an autologous vascularized cardiac tissue.

5. CONCLUSIONS:

Due to the limited endogenous regenerative potential of the native myocardium, it is important to find alternative sources to ameliorate damage caused by cardiac events like myocardial infarction. Human induced pluripotent stem cells are attractive cell sources that can be used to generate patient specific cells that can be differentiated into the lineage of interest. Specifically in this

study, we examine the effects of recapitulating the native cellular make of the myocardium by exploring hiPSC-CMs coupled with human adipose derived stem/stromal cells as well hiPSC-ECs coupled with hASCs. From this study, we were able to examine the effects of hASCs on cardiomyocyte electrophysiology as well vasculature development. We saw that hASCs were not deleterious to electrophysiological properties of cardiomyocytes and in some cases have the potential to enhance them. When comparing similar fibroblast-like cells, we find that there may be detraction of electrophysiology (i.e conduction velocity). Vascular assembly proved to be robust in the presence of hASCs. While hBM-MSCs have the potential to generate robust vessels like hASCs, these effects are diminished with the loss of electrophysiological properties when coupled with cardiomyocytes. It appears that hASCs prove to be a supportive cell that can be used to regenerate the damaged myocardium in a tri-culture system that can be clinically translatable and patient specific.
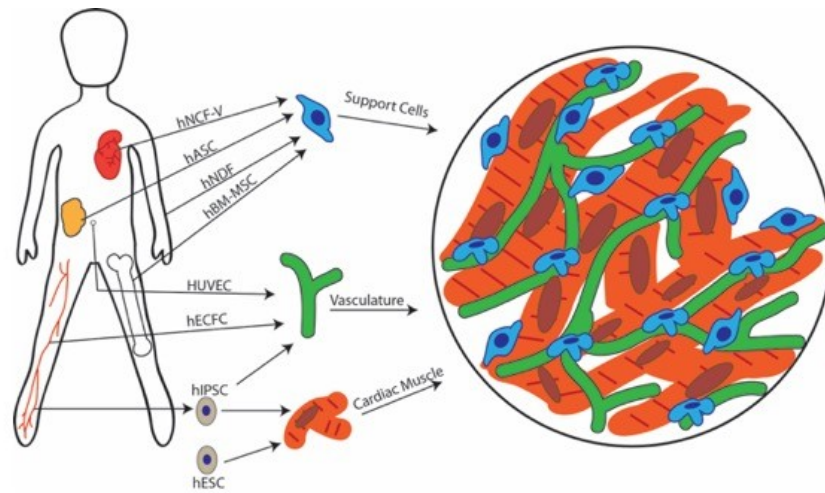
Figure 1

Figure 1: Schematic of cell sources for engineering a vascularized cardiac tissue.
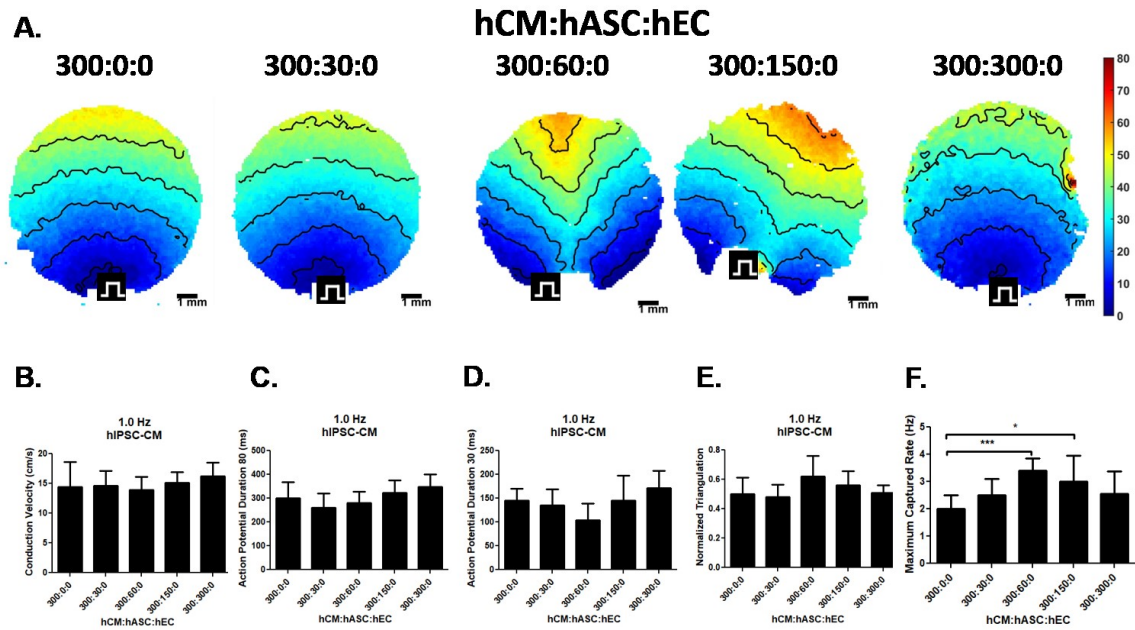
Figure 2

Figure 2: Effects of hCM:hASC ratios on electrophysiological function. (**A**) Activation maps of cardiomyocyte co-cultures with hASCs (**B**) Conduction velocity of hiPSC-CM:hASC at 1 Hz pacing (*n=7-12*), (**C**) APD_{80} and (**D**) APD_{30} values for various hiPSC-CM:hASC ratios at a pacing rate of 1 Hz (*n=7-12*), (**E**) Normalized triangulation of hiPSC-CM:hASC ratios (*n=7-12*), (**F**) Maximum captured rates *= $p < 0.05$; **$p < 0.01$; ***$p < 0.001$.
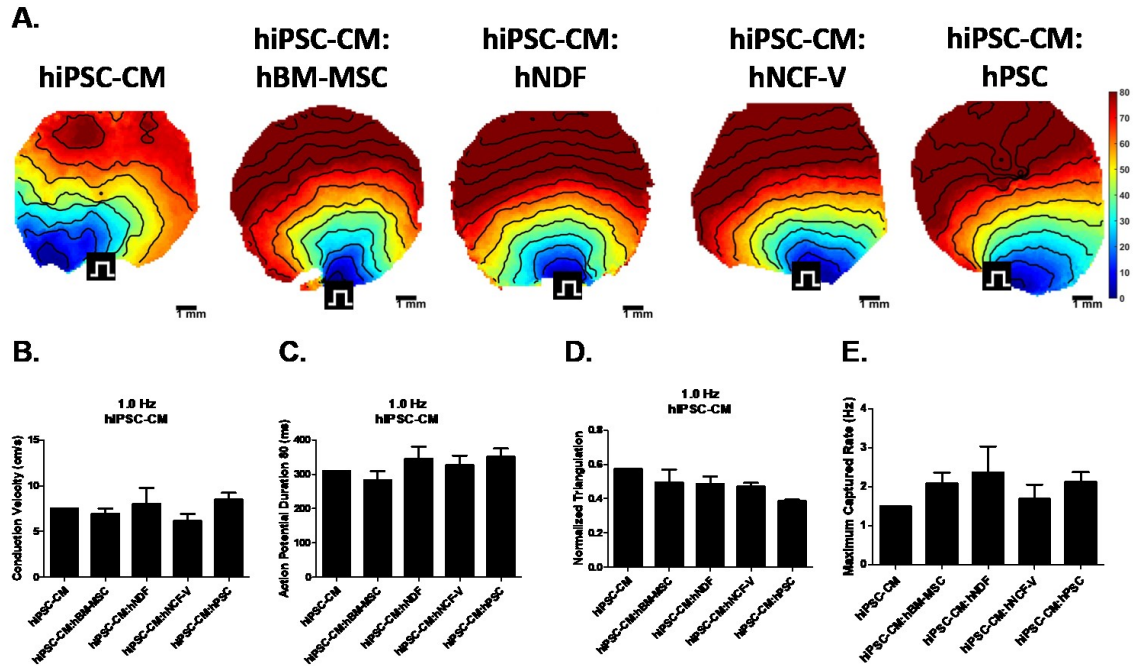
Figure 3

Figure 3: Effects of hiPSC-CM and hBM-MSC, hNDF, hNCF-V, or hPSC co-cultures on electrophysiological function. (**A**)Conduction Velocity of hiPSC-CM co-cultures at 1.0 Hz pacing (*n=6-12*), (**B**) APD_{80} and (**C**) APD_{30} values for various hIPSC-CM co-cultures at 1 Hz pacing/ratios at a pacing rate (*n=6-12)*, (**D**) Normalized triangulation of hIPSC-CM co-cultures at 1 Hz pacing (*n=6-12*) (*E*) Maximum captured rate (*n=6-12*)
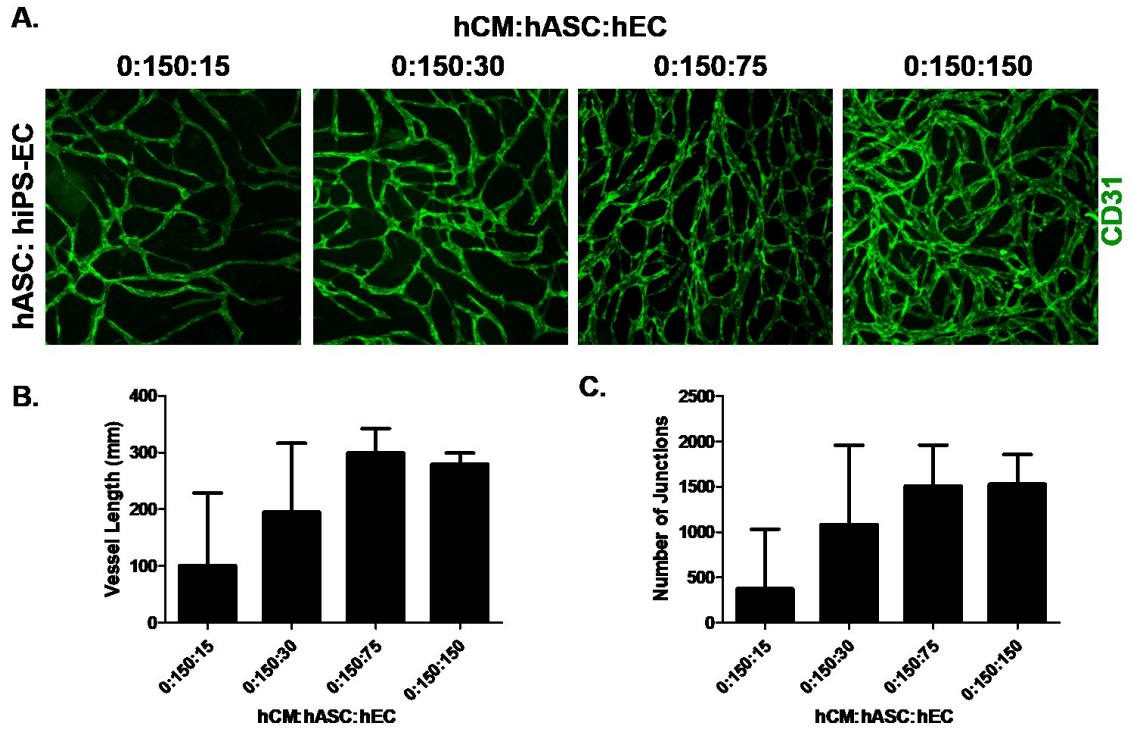
Figure 4

Figure 4: Vascular Assembly with hiPSC-ECs co-cultured with hASCs. (**A**) Immunostaining of PECAM-1/CD31 of various ratios of hASC:hiPSC-EC co-cultures , (**B**) Total vessel length of ratios of hASC:hiPSC-EC co-cultures (*n=3-4*), (**C**) Interconnectivity of ratios of hASC:hiPSC-EC co-cultures (*n=3-4*).
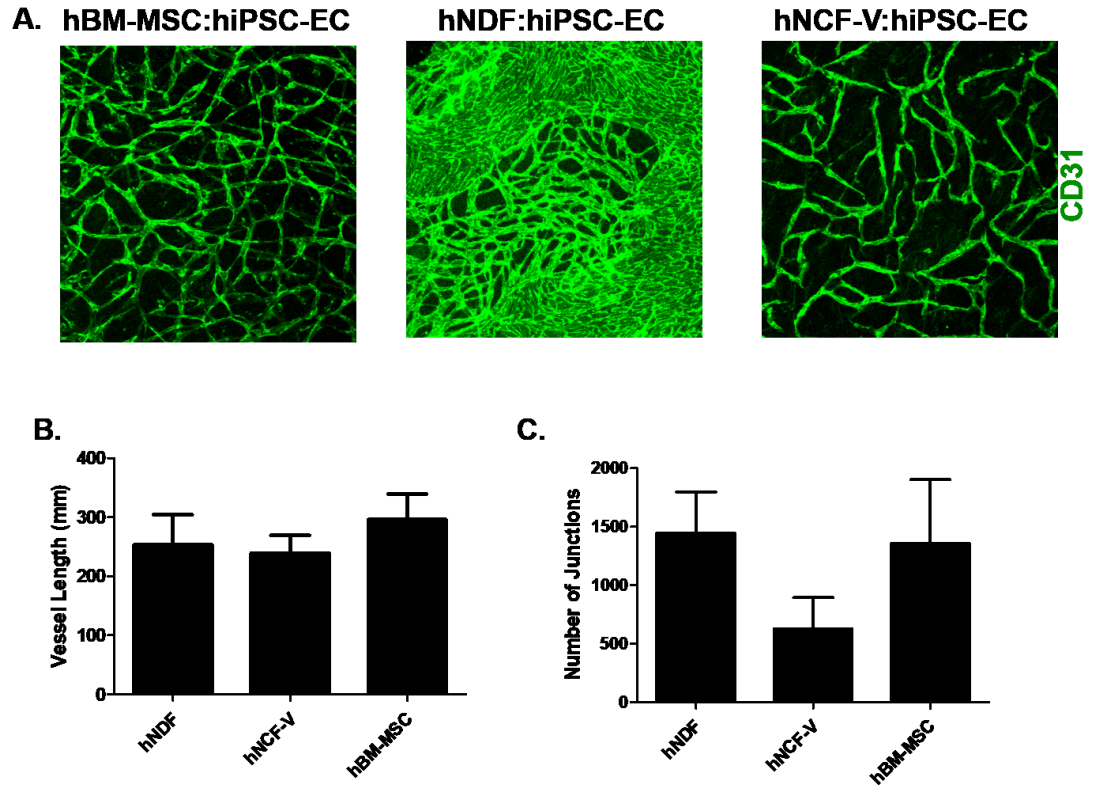
Figure 5

Figure 5: Vascular Assembly with hiPSC-ECs co-cultured with hBM-MSCs, hNDFs, or hNCF-V. (**A**) Immunostaining of CD31 of hBM-MSC:hIPSC-EC co-cultures, hNDF:hIPSC-EC co-cultures, and hNCF-V:hIPSC-EC co-cultures, (**B**) Total vessel length of ratios of hBM-MSC/hNDF/hNCF-V:hIPSC-EC co-cultures (*n=3-4*), (**C**) Interconnectivity of ratios of hBM-MSC/hNDF/hNCF-V:hIPSC-EC co-cultures (*n=3-4*).
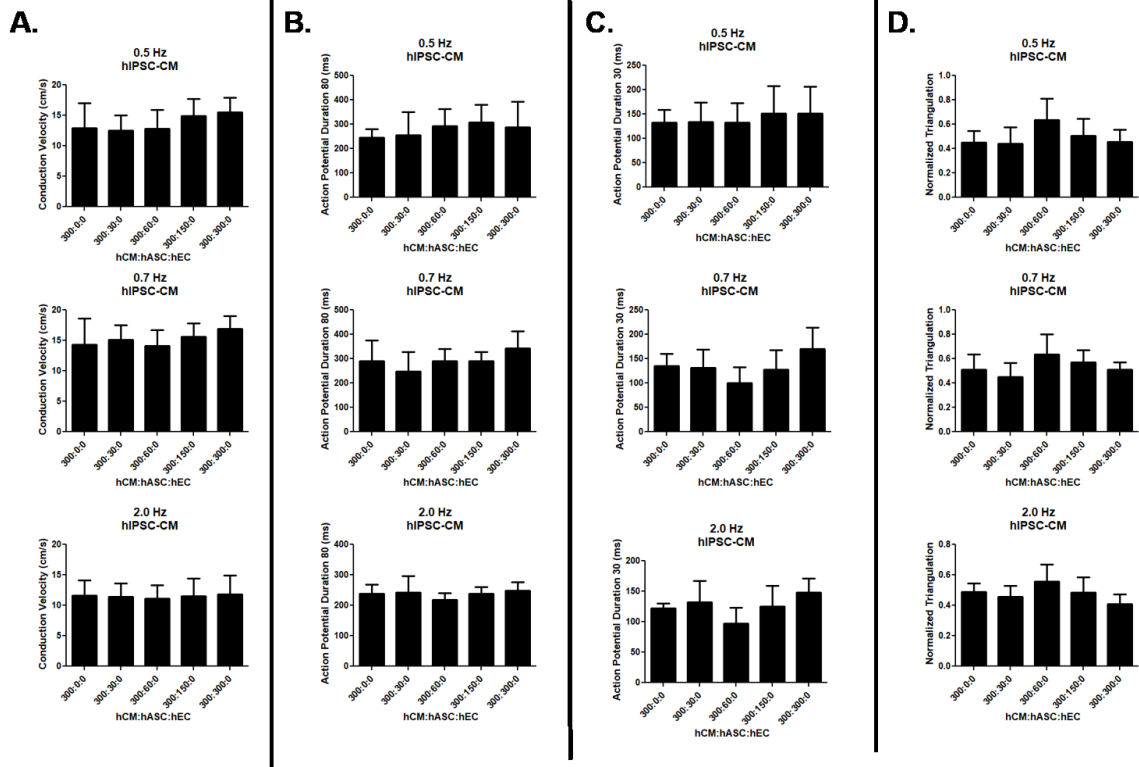
Supplemental Figure 1

Supplementary Figure 1: hiPSC-CM co-cultured with hASCs at various pacing rates. (**A**) Conduction Velocity, (**B**) Action potential duration 80% (**C**) Action potential duration 30%, (**D**) Normalized triangulation

A. hESC-CM 300:0:0 | hCM:hASC:hEC 300:30:0 | 300:60:0 | 300:150:0 | 300:300:0
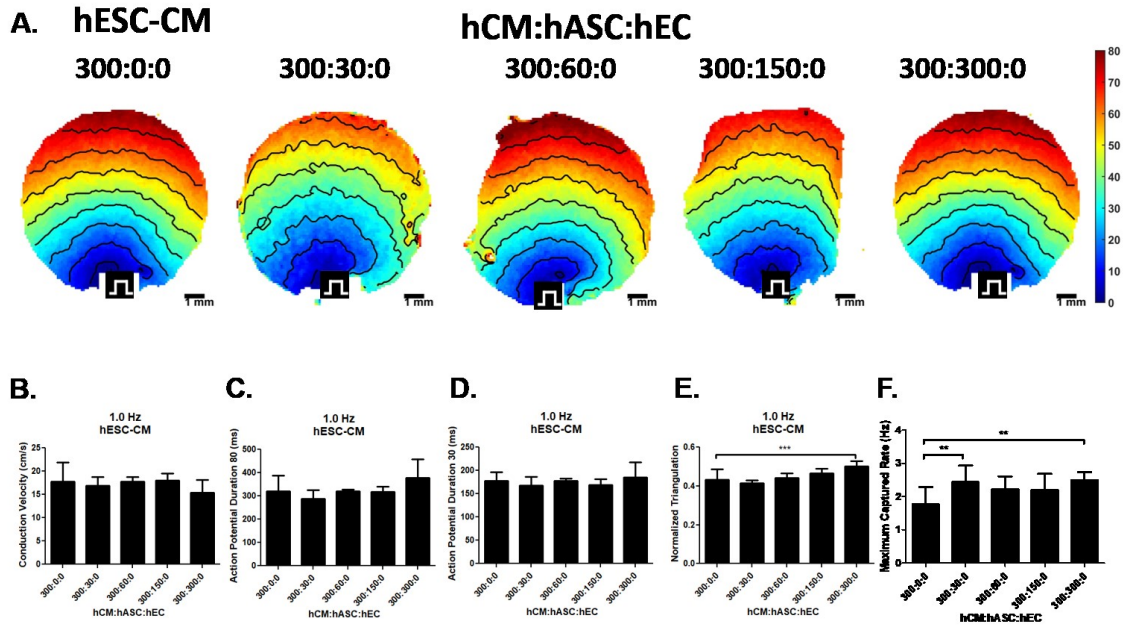
Supplementary Figure 2

Supplementary Figure 2: Effects of hCM:hASC ratios on electrophysiological function. (**A**) Activation maps of cardiomyocyte co-cultures with hASCs Conduction Velocity of hESC-CM:hASC co-cultures at 1 Hz pacing (*n=5-11*), (**B**) APD$_{80}$ and (**C**) APD$_{30}$ values for various hESC-CM:hASC ratios at a pacing rate of 1 Hz (*n=5-11*), (**D**) Normalized triangulation of hESC-CM:hASC ratios (*n=5-11*),
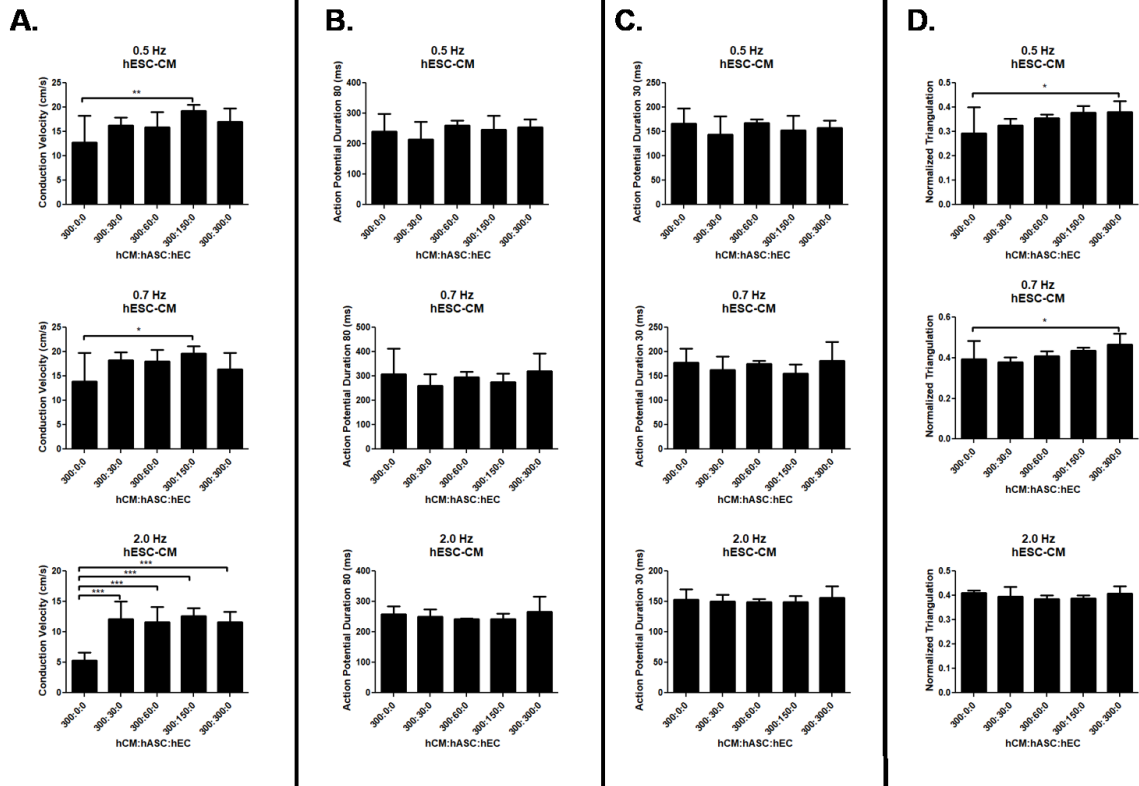
Supplemental Figure 3

Supplementary Figure 3: hESC-CM co-cultured with hASCs at various pacing rates. (**A**) Conduction Velocity, (**B**) Action potential duration 80% (**C**) Action potential duration 30%, (**D**) Normalized triangulation
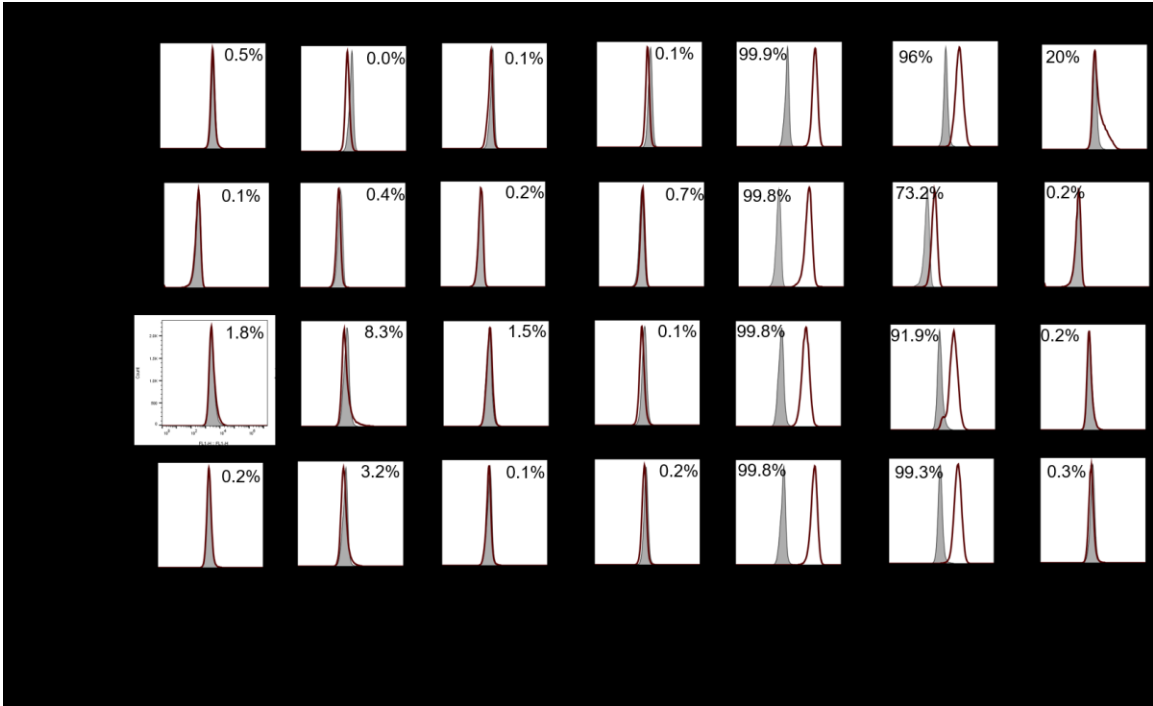
Supplementary Figure 4: Phenotypic profile of hBM-MSC, hNDFs, hNCF-V, and hASCs.

Mesenchymal markers are CD73 and CD105, vascular markers are CD31, CD34, and VEGFR2, and hematopoietic markers CD45 and HLA-DR
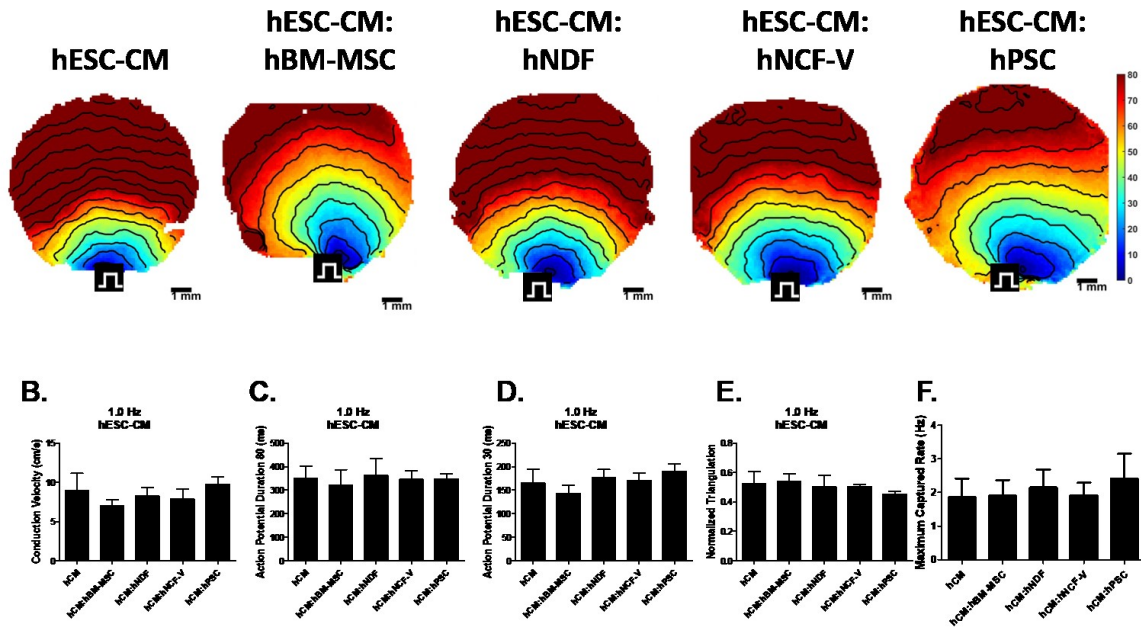
Supplemental Figure 5

Supplementary Figure 5: Effects of hESC-CM and hBM-MSC, hNDF, hNCF-V, or hPSC co-cultures on electrophysiological function. (**A**) Actiavtion Maps (**B**) Conduction Velocity of hESC-CM co-cultures at 1.0 Hz pacing (*n=6-12*), (**C**) APD_{80} and (**D**) APD_{30} values for various hESC-CM co-cultures at 1 Hz pacing (*n=6-12)*, (**E**) Normalized triangulation of hESC-CM co-cultures at 1 Hz pacing (*n=6-12) (***F**) Maximum captured rate (*n=6-12*)
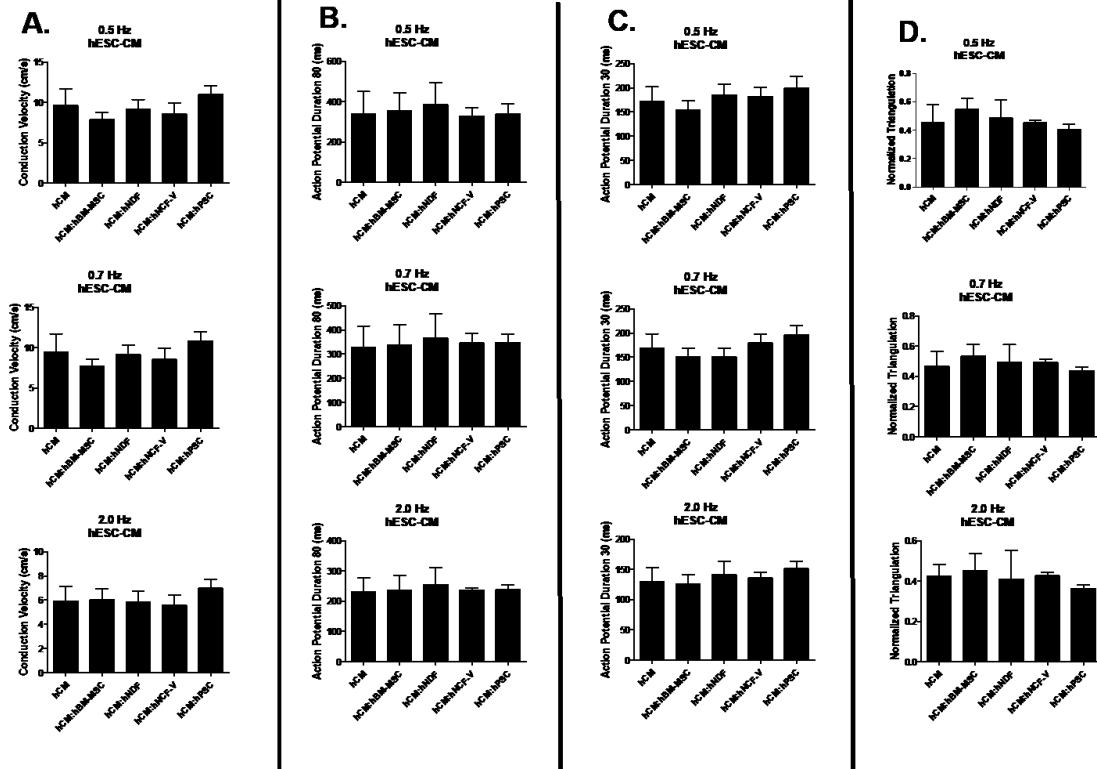
Supplementary Figure 6

Supplementary Figure 6: Effects of hESC-CM and hBM-MSC, hNDF, hNCF-V, or hPSC co-cultures on electrophysiological function at various pacing rates. (**A**) Conduction Velocity of hESC-CM co-cultures (*n=6-12*), (**B**) APD$_{80}$ and (**C**) APD$_{30}$ values for various hESC-CM co-cultures (*n=6-12)*, (**E**) Normalized triangulation of hESC-CM co-cultures

A.
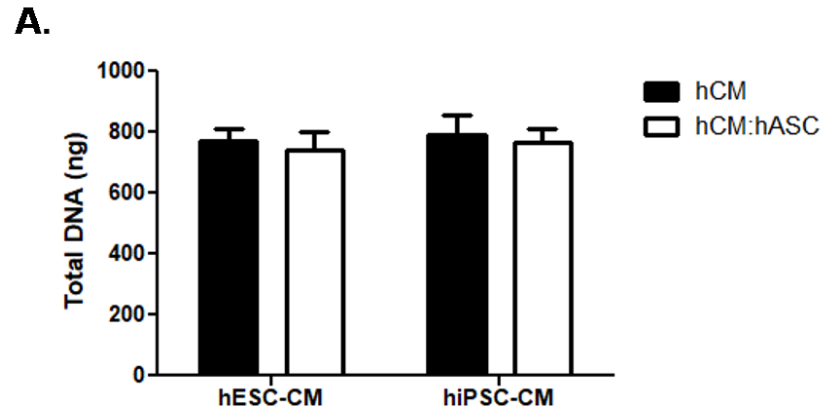
Supplementary Figure 7

Supplementary Figure 7: DNA quantification of hESC-CMs and hiPSC-CMs cultured with hASCs in transwell inserts.

A.
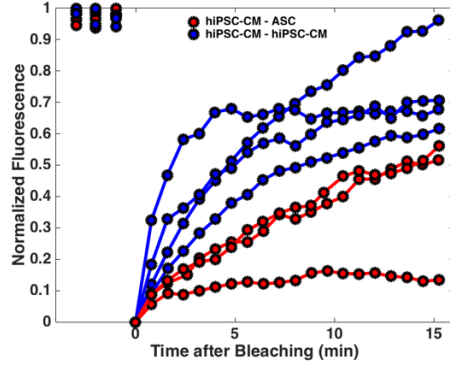
B.
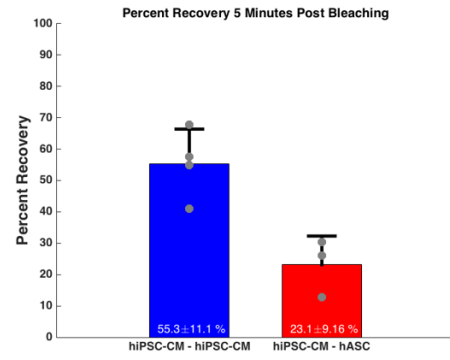
Supplementary Figure 8

Supplementary Figure 8: Fluorescent Recovery After Photobleaching of hCM only cultures and hCM-hASC co-cultures

A. hCM:hASC:hEC

0:150:150 0:150:75 0:150:30 0:150:15

hASC:hECFC

Von Willebrand Factor

B. hCM:hASC:hEC

0:60:60 0:60:30 0:60:12 0:60:6

hASC:hECFC

hASC:HUVEC

Von Willebrand Factor

C.

hCM:hASC:hEC

0:30:30 | 0:30:15 | 0:30:6 | 0:30:3

hASC:hECFC

hASC:HUVEC

Von Willebrand Factor
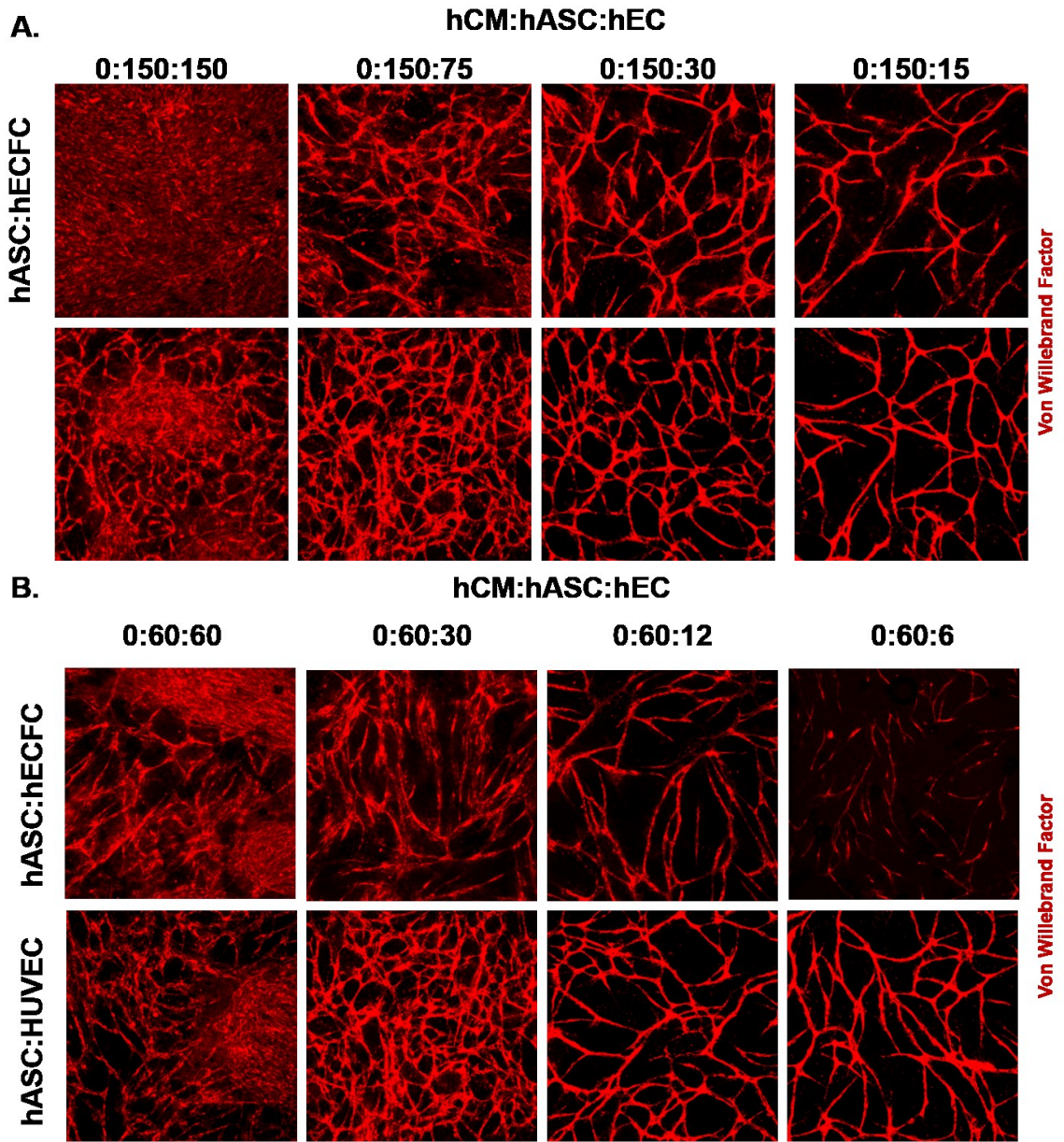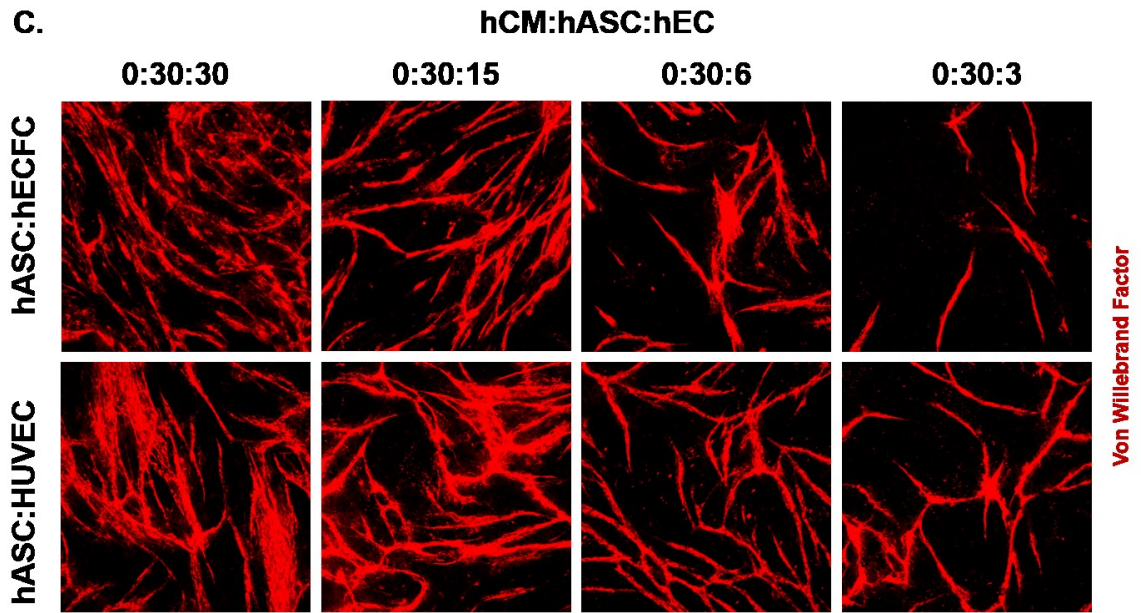
Supplementary Figure 9: Immunofluorescent staining of vWF in

hASC:hECFC/HUVEC co-cultures.

5

Conclusions

Conclusions and Future Perspectives

The data presented in this thesis demonstrates that contractile vascularized cardiac grafts can be developed utilizing adipose derived stem/stromal cells as the vascular mural cell source. The hASCs are able to promote vascular stability and networks with the ability to anastomose with host vasculature when implanted *in vivo* while also maintaining the electrophysiological properties of cardiomyocytes.

5.1 Specific Aim 1 Conclusions:

Chapter 2 describes the ability of hASCs to maintain the electrophysioogical properties of NRVCMs better than hDFs. After discovering the maximum number of hASCs that could be cultured with cardiomyocytes without impeding electrophysiological properties, this information was used to establish ratios to maximize vessel networks interconnectivity and vessel lengths. We directly compared vessel network formation of hASCs to hDFs. We found that hASC co-cultures resulted in the development of more robust vascular networks compared to those formed in hDF co-cultures. By combining the ratios from the NRVCM-hASC co-cultures with the hASC-HUVEC co-cultures, we developed a vascularized tri-culture system consisting of NRCVM-hASC-HUVECs. We found that ultimately at the ratio of 500:50:25 we developed robust vessel networks that were electrophysiologically similar to the NRVCM only control. This data could be

used to develop a vascularized cardiac graft. This work resulted in the development of a first author publication.

5.2 Specific Aim 2 Conclusions:

Chapter 3 described the development of vascularized cardiac grafts. The initial study characterized the development of fibrin microfiber sheets that served as a mechanically tunable scaffold to culture cardiomyocytes. We then assessed the viability and morphology of cardiomyocytes on the fibrin microfiber sheets of two different stiffnesses. NRVCMs were able to be cultured for up to two months on fibrin microfibers and we noticed higher conduction velocities over time on the softer matrix compared to the stiffer matrix. We also found that fibrin microfibers supported robust vascular assembly. After assessing the cardiomyocytes and vascular development independently, we combined all three cell types to develop vascularized cardiac grafts. These vascularized cardiac grafts were able to be implanted into a rodent infarct model and cardiomyocyte survival was tracked for a month. In addition, we were able to assess function of the myocardium through echocardiography and optically map the whole heart pacing from the site of the patch. This work will result in the submittal of a first-authored publication.

5.3 Specific Aim 3 Conclusions:

The studies reported in Chapter 4 assessed the ability of human stem cell derived cardiomyocytes and endothelial cells, cell-cell interactions with hASCs. Initially, pluripotent stem cells derived cardiomyocytes were co-cultured with hASCs and electrophysiology was assessed. Using hESC/hiPSC-CMs, we found that the presence of hASCs did not impede the electrophysiological parameters of

cardiomyocytes but enhanced the conduction velocity of hiPSC-CMs. We investigated whether hASCs were superior to commonly used fibroblast-like cells, hBM-MSCs, hNDFs, hNCF-Vs, and pluripotent stem cells. We discovered that other supporting cell types typically reduced the electrophysiologic potential of both hESC-CMs and hiPSC-CMs. We examined the vasculature development of HUVECs and hECFCs with similar ratios used in the hCM-hASC co-cultures. This data was used to assess the vascular development of hASC-hiPSC-EC co-cultures. hASCs-hEC co-cultures resulted in dense vessel networks. Fibroblast-like cells, hBM-MSCs, hNDFs, hNCF-Vs, and pluripotent stem cells were co-cultured to determine vascular assembly with hiPSC-ECs.

5.4 Future Perspectives:

The studies described in this thesis assessed our ability to form vascularized cardiac patches using hASCs as the vascular mural cell. After evaluating the cellular interactions independently and in the presence of a biomaterial, we assessed the utility of the approach for a completely human cell system. The next step to these experiments are implementing this tri-culture system using hiPSC-CMs and hiPSC-ECs coupled with hASCs to move toward a patient specific therapeutic treatment.

Initial studies would include the culture of hiPSC-CMs on fibrin microfibers to assess the viability, morphology, electrophysiology, and contractility. While hiPSC-CMs are a promising cell source, they are fundamentally immature and require maturation to integrate with the human myocardium. By incorporating mechanical and electrical stimulation into the system, CMs can undergo

maturation. Also, vascular development with hASC-hiPSC-EC co-cultures should be assessed on fibrin microfibers. This information can be combined to develop a human vascularized cardiac patch that can be assessed an *in vivo* setting in both immunosuppressed and immunocompetent models.

To investigate developing a thicker graft, we propose stacking multiple fibrin microfibers utilizing fibrin hydrogels as the adhesive source. We also propose incorporating hASCs and endothelial cells into the hydrogels to promote vasculature between the layers to aid in survival.

Appendix

1. Appendix Materials and Methods:

A2.1 hASC & HUVEC Culture on Fibrin Microfiber Sheets:

hASCs and HUVECs were mixed together in ratios of 0:100:100, 0:100:50, 0:100:20, 0:100:10, 0 and seeded in 80μL onto fibrin microfiber sheets (1cm^2) were seeded onto agarose coated culture plates to prevent cells f rom attached to tissue culture plastic. The constructs were cultured *in vitro* for 7 days and fed every other day with EGM-2 (Lonza).

A2.2 Viability Assessment

To determine cell viability on fibrin μfibers, the microfiber sheets were removed from frames and placed into 500µL Deoxyribonucleic Acid (DNA) lysing solution (10mM Tris, 1mM EDTA, 0.1% Triton X-100, and 0.1 mg/mL proteinase K) and frozen at -20°C. Samples were subsequently heated at 50 °C overnight to digest proteins and inactivate nucleases. PicoGreen dsDNA quantification assay was carried out according to the manufacturer's instructions. Briefly, the samples were combined with PicoGreen reagent (100 µL sample + 100 µL PicoGreen) and transferred (200 µL) into a black 96-well plate along with DNA standards. Fluorescence was measured at excitation 485nm/ emission 528 nm using a fluorescent plate reader. Sampling days included day 0, day 1, day 7, and day 14. Live/Dead viability assay assesses cell viability using calcein AM. Calcein AM is a cytoplasmic dye cleaved by cytoplasmic esterases ultimately stains the cytoplasm green was used at a concentration of 5μM. Ethidium Bromide is a nuclear stain

that only penetrates dying or dead cells and emits red was used at a concentration of 2μM. Both dyes were mixed in NRVCM media and incubated at 37°C for 20 minutes and washed with DPBS. Cells were imaged on the LSM-510 confocal.

A2.3 BLI Imaging Lentiviral Production and NRVM Transduction

Human embryonic kidney 293T cells were transfected with a CMV-mCherry-Luciferase plasmid (kindly provided by Dr. Assaf Gilad) using the Pantropic ViraSafe Lentiviral Packaging System (Cell Biolabs, Inc.). Cells were transfected for 3 hours, and then cultured in stromal medium (High Glucose DMEM with 10% FBS and 1% penicillin-streptomycin) for 24 hours to allow for lentiviral production to occur. Viral supernatant was collected and filtered through a 0.45 μm membrane daily up to 72 hours after transfection. Lentivirus was concentrated by centrifuging the supernatant in a SW 28 Ti rotor (Beckman Coulter, Inc.) at 24,000 g for 1.5 hours. Concentrated virus was resuspended in stromal medium and frozen at -80°C until transduction.

NRVCs on fibrin constructs were transduced with CMV-mCherry-Luciferase lentivirus in NRVCM medium containing 5 μg/mL polybrene (MOI 6). Transduction medium was removed after 48 hours, and constructs were cultured according to standard protocol until *in vivo* transplantation.

Cell retention in implanted fibrin constructs was monitored using bioluminescence imaging. Rats were anesthetized with isoflurane and injected intraperitoneally with 150 mg/kg of D-Luciferin Potassium Salt (Gold Biotechnology, Inc.) 10 minutes prior to imaging. Bioluminescent images of the implanted constructs were acquired with an IVIS Spectrum (PerkinElmer Inc.) using 1 min exposure and medium

binning. Images were acquired every 5 minutes until peak luminescence was observed. Total proton flux of the implant region was quantified using Living Image Software (Perkin Elmer Inc.).

A2.4 Whole Heart Optical Mapping & Analysis:

Adult rats (Nude) were anesthetized with sodium pentobarbital and sacrificed via midline thoracotomy. The hearts were excised, Langendorff-perfused, and stained with 10 µM di-4-ANEPPS for 10 minutes. Blebbistatin (10 µM) was used to eliminate motion artifacts during optical mapping (MiCAM Ultima Camera, SciMedia) of the left ventricular epicardial surface. The patch was positioned in half of the field of view to allow imaging of conduction in native and implanted cells. Custom platinum plate electrodes outside the left ventricular free wall were used for field stimulation, and a stainless steel bipolar electrode was used for point stimulation

AA1.1 hASC-HUVEC Co-Culture Concentration Study:

ECs (passage 5-6) and ASCs (passage 4) were suspended in 10mg/mL fibrinogen solution (dissolved in DPBS). The cell solution was then mixed with 2U/mL thrombin diluted in DPBS, containing Ca^{2+}/Mg^{2+}, to begin polymerization. Fibrin gels (40µL) contained HUVEC and ASC concentrations of 1.25, 2.5, or 5 million/mL. The fibrin gels were pipetted into 6mm diameter wells and incubated at 37°C for 30 minutes to complete polymerization. The constructs were cultured *in* vitro for 7 days and fed every other day with EGM-2 (Lonza).

AA1.2 hASC/hDF-HUVEC Co-Culture Ratio Study:

ECs (passage 5-6) and hASCs (passage 4) were suspended in 10mg/mL

fibrinogen solution (dissolved in DPBS). The cell solution was then mixed with

2U/mL thrombin to begin polymerization. Fibrin gels (40µL) contained HUVEC

concentration constant at 1.25 or 2.5 million/mL, while hASCs were varied at

ratios of 1:0,1:1,2:1,5:1,10:1, and 0:1 for each concentration of HUVECs. The

fibrin gels were pipetted into 6mm diameter wells and incubated at 37°C for 30

minutes to complete polymerization. The constructs were cultured *in* vitro for 7

days and fed every other day with EGM-2 (Lonza).

AA1.3 hDF/hASC-NRVCM Co-Culture System:

Coverslips were coated with Fibronectin (Sigma Aldrich) and NRVCMs were

plated at a concentration of 1 million/mL in NRVCM Medium containing 10%

FBS. Subsequently on the next day, hDFs/hASCs were plated in ratios of

1:0,1:5,1:10, and 0:1 on top of the NRVCMs. Medium was switched to 2% FBS

containing medium on the followed day and refreshed other day until day 5 of co-

culture. Cells underwent optical mapping and were fixed for subsequent

immunocytochemistry.

AA1.4 NRVCM Gel Formation:

NRVCMs were suspended in 5mg/mL fibrinogen (Sigma Aldrich) diluted in a (1:1

ratio of DPBS-NRVCM Media) at concentrations of 5, 10, 20, 40, and 60 million

cells/mL. Cells were then mixed with 2U/mL thrombin for polymerization at 37°C

for 30 minutes. Cells were fed daily with NRVCM culture medium containing 10%

HI-FBS (Sigma Aldrich/Atlanta Biologicals) and 33μg/mL of Aprotinin(USB Affymetrix).

AA1.5 Whole Mount Immunostaining:

Samples were fixed with 4% paraformaldehyde for 3 hours at 4°C and then washed three times with DPBS for 30 minutes. After fixation, gels were removed from wells and placed into microcentrifuge tubes for the remaining steps. Gels were then permeabilized and blocked for 4 hours with 5% normal goat serum (Sigma Aldrich) in DPBS with 0.1% Tween 20 (0.1% PTween). Gels were stained with primary antibodies which included mouse anti-CD31 (Sigma Aldrich), mouse anti-Sarcomeric α-Actinin(Sigma Aldrich), rabbit anti-Connexin 43 (Sigma Aldrich) at 4°C diluted in 5% normal goat serum and 0.1% PTween overnight. Samples were then washed three times with 0.1% PTween for one hour per wash. Samples were then incubated overnight with with DyLight 488-conjugated goat anti-mouse and DyLight 649-conjugated goat anti-rabbit (Jackson ImmunoResearch) secondary antibody in 5% normal goat serum with 0.1% PTween. Samples were then washed three times with 0.1% PTween for one hour per wash. Samples were then blocked for four hours with 5% normal mouse serum. After blocking, samples were incubated with Cy3-conjugated mouse anti-αSMA (Sigma Aldrich). The samples were washed with 0.1% PTween for one hour per wash. Gels were mounted in 70% glycerol in chamber slides and imaged using a Zeiss LSM 510 confocal microscope with a 5x and 20x objective.

2. Appendix Figures:
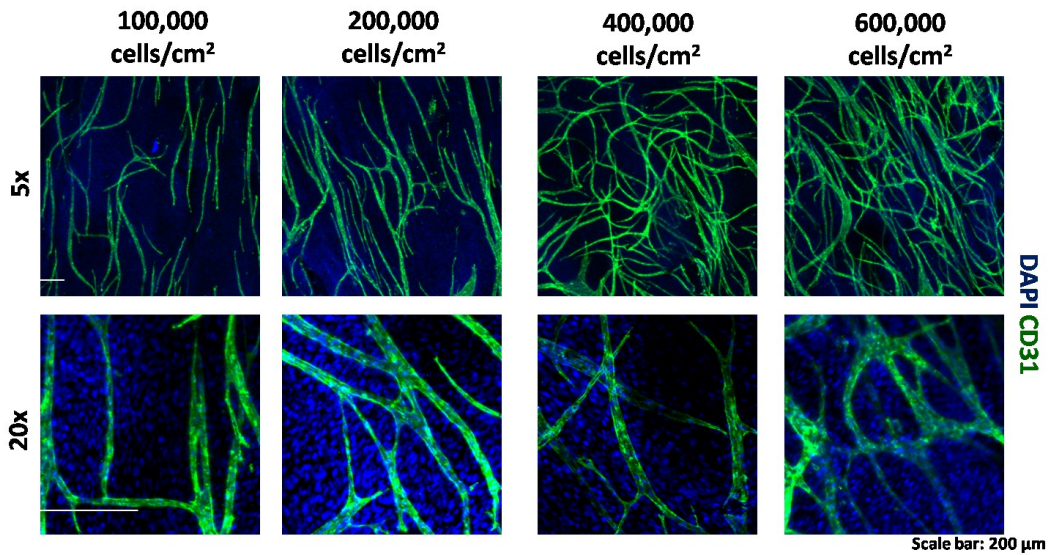
Appendix Figure 1: Heterogeneous Low Passage hASC vessel development. Immunofluorescent staining of CD31/PECAM-1 positive vascular structures (green) and cell nuclei (DAPI; blue) on 2.0% fibrin microfibers. Increasing the concentration of P2 hASCs resulted in the development of dense vessel structures on 2.0% fibrin microfibers. Scale Bar is 200 μm.
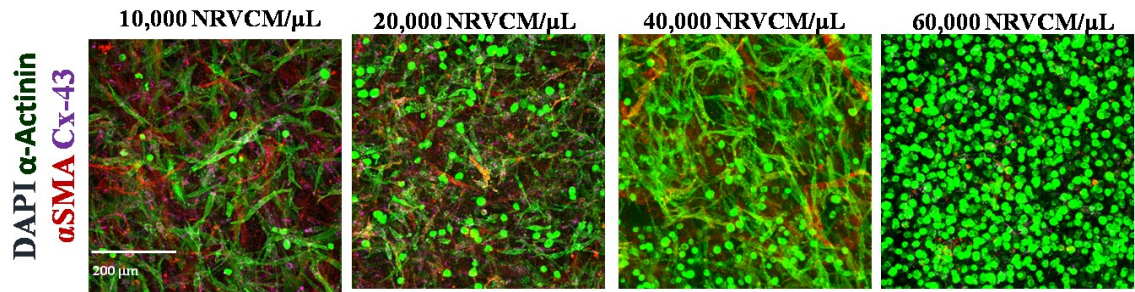
Appendix Figure 2: Cardiomyocyte development in fibrin hydrogels.

Immunofluorescent staining of cardiomyoyctes encapsulated in fibrin hydrogels

Increasing concentration of cardiomyocytes in fibrin hydrogels results in reduced

elongation of cardiomyocytes. Immunostaining of cardiomyocytes (green),

connexin-43 (purple). Scale Bar is 200 μm.
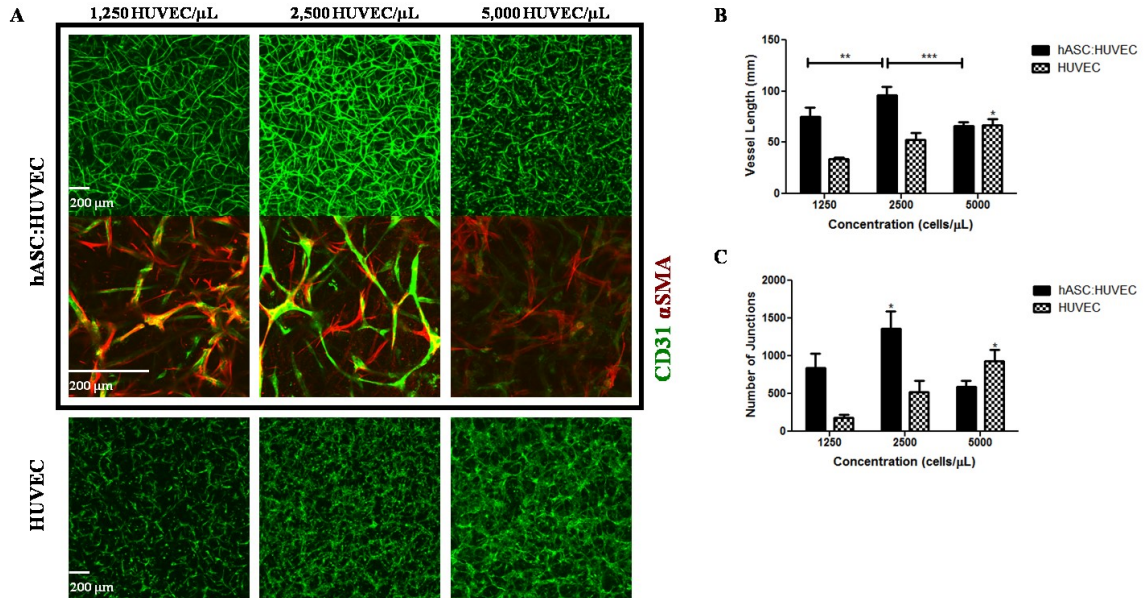
Appendix Figure 3: Vessel development in fibrin hydrogels with hASC-HUVEC co-cultures. A) Immunofluorescent staining of CD31 positive vascular structures (green) and pericyte-like cells stained with αSMA (red). Vessel assembly of co-cultured hASCs and endothelial cells encapsulated in fibrin hydrogels at a 1:1 ratio. Vessel assembly increases up until a HUVEC concentration of 2,500 HUVECs/μL and reduces at 5,000 HUVECs/μL. **B**, **C**) Quantification of vessel structure based on length (*n=3*) (**B**) and interconnectivity (*n=3*) (**C**). Scale Bar is 200 µm p < 0.05; **p < 0.01; ***p < 0.001
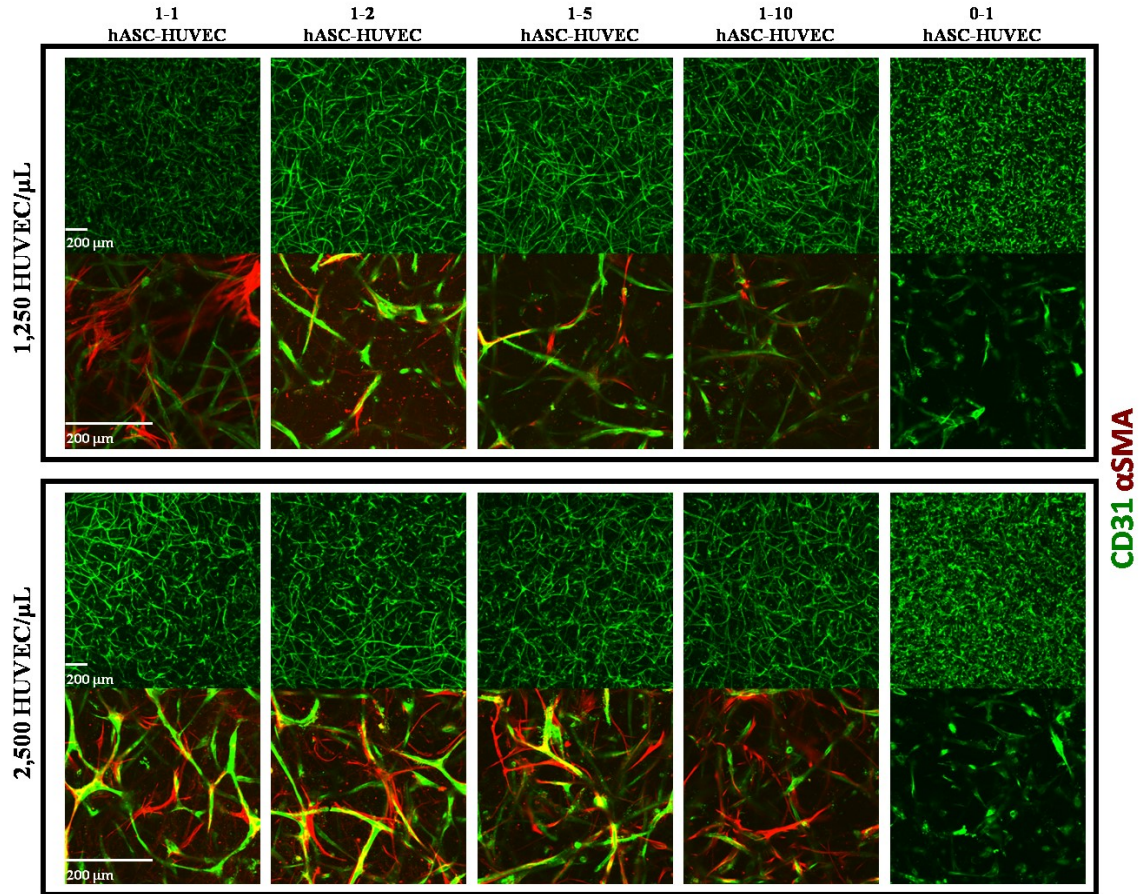
Appendix Figure 4: Effect of hASC:HUVEC ratios on vessel formation:

Immunofluorescent staining of CD31 positive vascular structures (green) and

pericyte-like cells stained with αSMA (red) with varying ratios of hASCs and

HUVECs. Scale Bar is 200 μm.
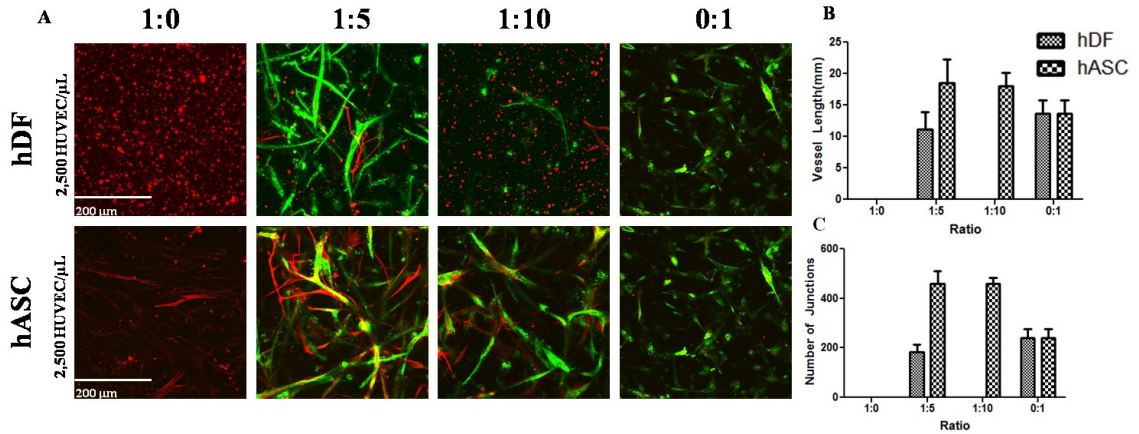
Appendix Figure 5: Effect of hDF:HUVEC compared to hASC:HUVEC ratios on vessel formation. Immunofluorescent staining of CD31 positive vascular structures (green) and pericyte-like cells stained with αSMA (red). **A)** Vessel formation of HUVECs when co-cultured with either hDFs or hASCs at the ratio of 1-5 and 1-10 (Stromal Cell-HUVEC). Increased vessel length and junctions were obtained with the presence of hASCs compared to hDFs. **B**, **C**) Quantification of vessel structure based on length (*n=3*) (**B**) and interconnectivity (*n=3*) (**C**). Scale Bar is 200 µm.
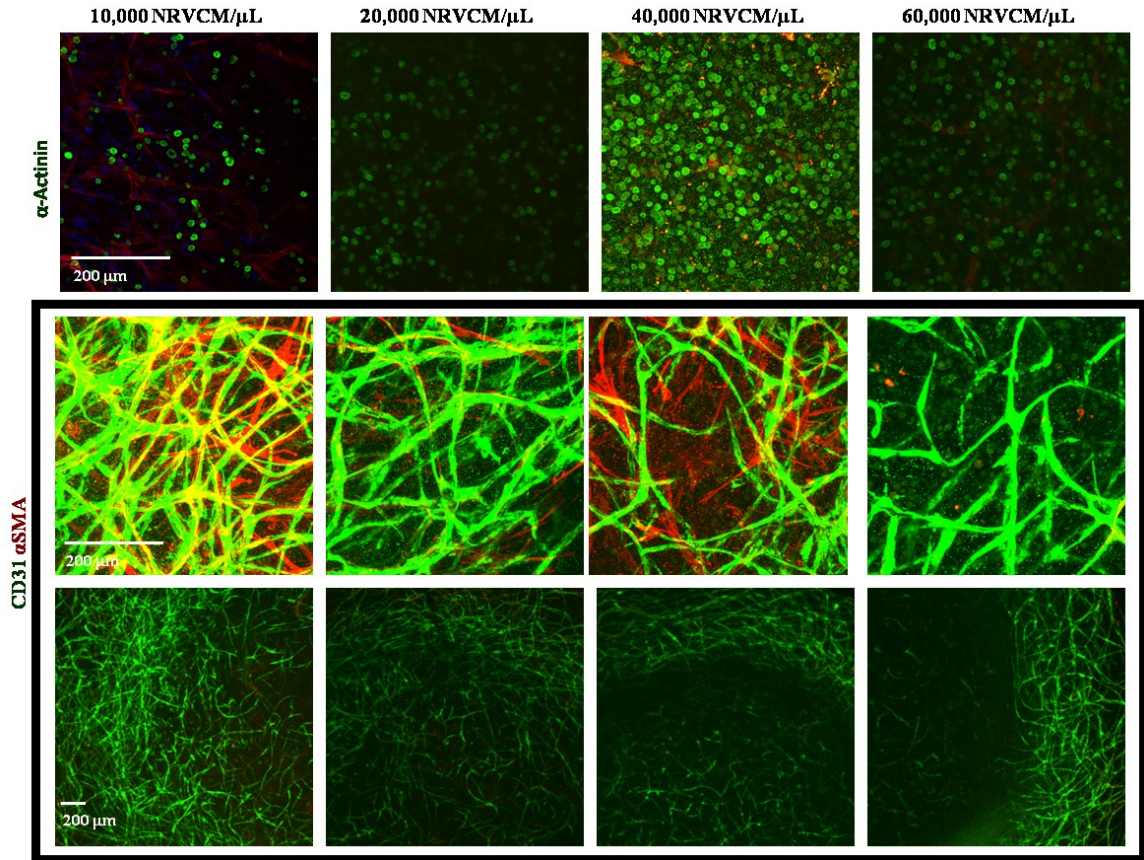
Appendix Figure 6: Simultaneous Tri-Culture (NRVCM:hASC:HUVEC) Encapsulation in Fibrin Hydrogels. Immunofluorescent staining of cardiomyocytes (green) and vasculature development CD31 positive vascular structures (green) and pericyte-like cells stained with αSMA (red) with increasing concentration of cardiomyocytes with hASC:HUVECs being held constant. Scale Bar is 200 µm.

Bibliography

1. Benjamin EJ, Blaha MJ, Chiuve SE, et al. *Heart Disease and Stroke Statistics'2017 Update: A Report from the American Heart Association*. Vol 135.; 2017. doi:10.1161/CIR.0000000000000485.

2. Weinberger F, Mannhardt I, Eschenhagen T. Engineering Cardiac Muscle Tissue: A Maturating Field of Research. *Circ Res*. 2017;120(9):1487-1500. doi:10.1161/CIRCRESAHA.117.310738.

3. Frantz S, Bauersachs J, Ertl G. Post-infarct remodelling: Contribution of wound healing and inflammation. *Cardiovasc Res*. 2009;81(3):474-481. doi:10.1093/cvr/cvn292.

4. Frangogiannis NG. The inflammatory response in myocardial injury, repair and remodeling. 2015;11(5):255-265. doi:10.1038/nrcardio.2014.28.The.

5. Hirt MN, Hansen A, Eschenhagen T. Cardiac tissue engineering : State of the art. *Circ Res*. 2014;114(2):354-367. doi:10.1161/CIRCRESAHA.114.300522.

6. Lesman A, Gepstein L, Levenberg S. Vascularization shaping the heart. *Ann N Y Acad Sci*. 2010;1188:46-51. doi:10.1111/j.1749-6632.2009.05082.x.

7. Shadrin IY, Allen BW, Qian Y, et al. Cardiopatch platform enables maturation and scale-up of human pluripotent stem cell-derived engineered heart tissues. *Nat Commun*. 2017;8(1):1825. doi:10.1038/s41467-017-01946-x.

8. Korhonen T, Hänninen SL, Tavi P. Model of excitation-contraction coupling of rat neonatal ventricular myocytes. *Biophys J*. 2009;96(3):1189-1209. doi:10.1016/j.bpj.2008.10.026.

9. Radisic M, Fast VG, Sharifov OF, Iyer RK, Park H, Vunjak-Novakovic G. Optical Mapping of Impulse Propagation in Engineered Cardiac Tissue. *Tissue Eng Part A*. 2009;15(4):851-860. doi:10.1089/ten.tea.2008.0223.

10. Ehler E, Moore-Morris T, Lange S. Isolation and Culture of Neonatal Mouse Cardiomyocytes. *J Vis Exp*. 2013;(79):1-10. doi:10.3791/50154.

11. Robertson C, Tran D, George S. Concise Review: Maturation Phases of Human Pluripotent Stem Cell-Derived Cardiomyocytes. *Stem Cells*. 2013;31(5):1-17. doi:10.1002/stem.1331.Concise.

12. Lundy SD, Zhu W, Regnier M, Laflamme MA. Structural and Functional Maturation of Cardiomyocytes Derived from Human Pluripotent Stem Cells. 2013;22(14). doi:10.1089/scd.2012.0490.

13. Yang X, Pabon L, Murry CE. Engineering adolescence: Maturation of human pluripotent stem cell-derived cardiomyocytes. *Circ Res*. 2014;114(3):511-523. doi:10.1161/CIRCRESAHA.114.300558.

14. Veerman CC, Kosmidis G, Mummery CL, Casini S, Verkerk AO, Bellin M. Immaturity of Human Stem-Cell-Derived Cardiomyocytes in Culture: Fatal Flaw or Soluble Problem? *Stem Cells Dev*. 2015;24(9):1035-1052. doi:10.1089/scd.2014.0533.

15. Kusuma S, Shen Y, Hanjaya-putra D, et al. matrix Self-organized vascular networks from human pluripotent stem cells in a synthetic matrix. 2017.

16. Kurokawa YK, Yin RT, Shang MR, Shirure VS, Moya ML, George SC. Human Induced Pluripotent Stem Cell-Derived Endothelial Cells for Three-Dimensional Microphysiological Systems. *Tissue Eng Part C Methods*. 2017;23(8):474-484. doi:10.1089/ten.tec.2017.0133.

17. Yoder MC. Differentiation of pluripotent stem cells into endothelial cells. *Curr Opin Hematol*. 2015;22(3):252-257. doi:10.1097/MOH.0000000000000140.Differentiation.

18. Zhang J, Chu L-F, Hou Z, et al. Functional characterization of human pluripotent stem cell-derived arterial endothelial cells. *Proc Natl Acad Sci*. 2017:201702295. doi:10.1073/pnas.1702295114.

19. Alt E, Yan Y, Gehmert S, et al. Fibroblasts share mesenchymal phenotypes with stem cells, but lack their differentiation and colony-forming potential. *Biol Cell*. 2011;103(4):197-208. doi:10.1042/BC20100117.

20. Chen X, Aledia AS, Popson S a, Him L, Hughes CCW, George SC. Rapid anastomosis of endothelial progenitor cell-derived vessels with host vasculature is promoted by a high density of cotransplanted fibroblasts. *Tissue Eng Part A*. 2010;16(2):585-594. doi:10.1089/ten.tea.2009.0491.

21. Costa-Almeida R, Gomez-Lazaro M, Ramalho C, Granja PL, Soares R, Guerreiro SG. Fibroblast-Endothelial Partners for Vascularization Strategies in Tissue Engineering. *Tissue Eng Part A*. 2015;21(5-6):1055-1065. doi:10.1089/ten.tea.2014.0443.

22. Pedrotty DM, Klinger RY, Kirkton RD, Bursac N. Cardiac fibroblast paracrine factors alter impulse conduction and ion channel expression of neonatal rat cardiomyocytes. *Cardiovasc Res*. 2009;83(4):688-697. doi:10.1093/cvr/cvp164.

23. Porter KE, Turner NA. Cardiac fibroblasts: At the heart of myocardial remodeling. *Pharmacol Ther*. 2009;123(2):255-278. doi:10.1016/j.pharmthera.2009.05.002.

24. Twardowski RL, Black LD. Cardiac Fibroblasts Support Endothelial Cell Proliferation and Sprout Formation but not the Development of Multicellular Sprouts in a Fibrin Gel Co-Culture Model. *Ann Biomed Eng*. 2014;42(5):1074-1084. doi:10.1007/s10439-014-0971-2.

25. Verseijden F, Posthumus-van Sluijs SJ, Pavljasevic P, Hofer SOP, van Osch GJVM, Farrell E. Adult human bone marrow- and adipose tissue-derived stromal cells support the formation of prevascular-like structures from endothelial cells in vitro. *Tissue Eng Part A*. 2010;16(1):101-114. doi:10.1089/ten.TEA.2009.0106.

26. Ikegame Y, Yamashita K, Hayashi S-I, et al. Comparison of mesenchymal stem cells from adipose tissue and bone marrow for ischemic stroke

therapy. *Cytotherapy*. 2011;13(6):675-685.
doi:10.3109/14653249.2010.549122.

27. Pill K, Hofmann S, Redl H, Holnthoner W. Vascularization mediated by mesenchymal stem cells from bone marrow and adipose tissue: A comparison. *Cell Regen*. 2015;4(1):1-10. doi:10.1186/s13619-015-0025-8.

28. Choi YS, Dusting GJ, Stubbs S, et al. Differentiation of human adipose-derived stem cells into beating cardiomyocytes. *J Cell Mol Med*. 2010;14(4):878-889. doi:10.1111/j.1582-4934.2010.01009.x.

29. Merfeld-Clauss S, Gollahalli N, March KL, Traktuev DO. Adipose tissue progenitor cells directly interact with endothelial cells to induce vascular network formation. *Tissue Eng Part A*. 2010;16(9):2953-2966. doi:10.1089/ten.tea.2009.0635.

30. Merfeld-Clauss S, Lupov IP, Lu H, et al. Adipose stromal cells differentiate along a smooth muscle lineage pathway upon endothelial cell contact via induction of activin A. *Circ Res*. 2014;115(9):800-809. doi:10.1161/CIRCRESAHA.115.304026.

31. Hutton DL, Logsdon EA, Moore EM, Mac Gabhann F, Gimble JM, Grayson WL. Vascular morphogenesis of adipose-derived stem cells is mediated by heterotypic cell-cell interactions. *Tissue Eng Part A*. 2012;18(15-16):1729-1740. doi:10.1089/ten.TEA.2011.0599.

32. Hutton DL, Moore EM, Gimble JM, Grayson WL. Platelet-derived growth factor and spatiotemporal cues induce development of vascularized bone tissue by adipose-derived stem cells. *Tissue Eng Part A*. 2013;19(17-18):2076-2086. doi:10.1089/ten.TEA.2012.0752.

33. Freiman A, Shandalov Y, Rozenfeld D, et al. Adipose-derived endothelial and mesenchymal stem cells enhance vascular network formation on three-dimensional constructs in vitro. *Stem Cell Res Ther*. 2016;7(1):5. doi:10.1186/s13287-015-0251-6.

34. Caspi O, Lesman A, Basevitch Y, et al. Tissue Engineering of Vascularized Cardiac Muscle From Human Embryonic Stem Cells. *Circ Res*. 2007;100:263-272. doi:10.1161/01.RES.0000257776.05673.ff.

35. Lesman A, Gepstein L, Levenberg S. Cell tri-culture for cardiac vascularization. *Methods Mol Biol*. 2014;1181:131-137. doi:10.1007/978-1-4939-1047-2_12.

36. Thomson KS, Korte FS, Giachelli CM, Ratner BD, Regnier M, Scatena M. Prevascularized Microtemplated Fibrin Scaffolds for Cardiac Tissue Engineering Applications. *Tissue Eng Part A*. 2013;19(7-8):967-977. doi:10.1089/ten.tea.2012.0286.

37. Ye L, Chang Y-H, Xiong Q, et al. Cardiac repair in a porcine model of acute myocardial infarction with human induced pluripotent stem cell-derived cardiovascular cell populations. *Cell Stem Cell*. 2014;15(6):750-761. doi:10.1016/j.stem.2014.11.009.Cardiac.

38. Schaefer JA, Guzman PA, Riemenschneider SB, Kamp TJ, Tranquillo RT. A Cardiac Patch from Aligned Microvessel and Cardiomyocyte Patches. *J Tissue Eng Regen Med*. 2017;(September):1-11. doi:10.1002/term.2568.

39. Iyer RK, Chiu LLY, Radisic M. Microfabricated poly(ethylene glycol) templates enable rapid screening of triculture conditions for cardiac tissue engineering. *J Biomed Mater Res A*. 2009;89(3):616-631. doi:10.1002/jbm.a.32014.

40. Schenke-Layland, Yland K, Strem BM, et al. Adipose Tissue-Derived Cells Improve Cardiac Function Following Myocardial Infarction. *J Surg Res*. 2010;153(2):217-223. doi:10.1016/j.jss.2008.03.019.Adipose.

41. Morrissette-Mcalmon J, Blazeski A, Somers S, Kostecki G, Tung L, Grayson WL. Adipose-derived perivascular mesenchymal stromal/stem cells promote functional vascular tissue engineering for cardiac regenerative purposes. *J Tissue Eng Regen Med*. 2017. doi:10.1002/term.2418.

42. Zhang B, Montgomery M, Chamberlain MD, et al. Biodegradable scaffold with built-in vasculature for organ-on-a-chip engineering and direct surgical anastomosis. *Nat Mater*. 2016;15(6):669-678. doi:10.1038/nmat4570.

43. Gershlak JR, Hernandez S, Fontana G, et al. Crossing kingdoms: Using decellularized plants as perfusable tissue engineering scaffolds. *Biomaterials*. 2017;125:13-22. doi:10.1016/j.biomaterials.2017.02.011.

44. Stevens KR, Kreutziger KL, Dupras SK, et al. Physiological function and transplantation of scaffold-free and vascularized human. 2009;106(39).

45. Ong CS, Fukunishi T, Zhang H, et al. Biomaterial-Free Three-Dimensional Bioprinting of Cardiac Tissue using Human Induced Pluripotent Stem Cell Derived Cardiomyocytes. *Sci Rep*. 2017;7(1):2-12. doi:10.1038/s41598-017-05018-4.

46. Vunjak-novakovic G, Tandon N, Godier A, et al. Challenges in Cardiac Tissue Engineering 1. 2010;16(2).

47. Levenberg S, Rouwkema J, Macdonald M, et al. Engineering vascularized skeletal muscle tissue. *Nat Biotechnol*. 2005;23(7):879-884. doi:10.1038/nbt1109.

48. Montgomery M, Ahadian S, Davenport Huyer L, et al. Flexible shape-memory scaffold for minimally invasive delivery of functional tissues. *Nat Mater*. 2017;16(August). doi:10.1038/nmat4956.

49. Iyer RK, Chui J, Radisic M. Spatiotemporal tracking of cells in tissue-engineered cardiac organoids. *J Tissue Eng Regen Med*. 2009;3(3):196-207. doi:10.1002/term.153.

50. Hasan A, Khattab A, Islam MA, et al. Injectable Hydrogels for Cardiac Tissue Repair after Myocardial Infarction. *Adv Sci*. 2015;2(11):1-18. doi:10.1002/advs.201500122.

51. Xiong Q, Hill KL, Li Q, et al. A fibrin patch-based enhanced delivery of human embryonic stem cell-derived vascular cell transplantation in a porcine model of postinfarction left ventricular remodeling. *Stem Cells*. 2011;29(2):367-375. doi:10.1002/stem.580.

52. Liau B, Christoforou N, Leong KW, Bursac N. Pluripotent stem cell-derived cardiac tissue patch with advanced structure and function. *Biomaterials*. 2011;32(35):9180-9187. doi:10.1016/j.biomaterials.2011.08.050.

53. Black LD, Meyers JD, Weinbaum JS, Shvelidze YA, Tranquillo RT. Cell-induced alignment augments twitch force in fibrin gel-based engineered myocardium via gap junction modification. *Tissue Eng Part A*. 2009;15(10):3099-3108. doi:10.1089/ten.TEA.2008.0502.

54. Schaaf S, Eder A, Vollert I, Stöhr A, Hansen A, Eschenhagen T. Generation of strip-format fibrin-based engineered heart tissue (EHT). *Methods Mol Biol*. 2014;1181:121-129. doi:10.1007/978-1-4939-1047-2_11.

55. Thompson SA, Copeland CR, Reich DH, Tung L. Mechanical coupling between myofibroblasts and cardiomyocytes slows electric conduction in fibrotic cell monolayers. *Circulation*. 2011;123(19):2083-2093. doi:10.1161/CIRCULATIONAHA.110.015057.

56. Riemenschneider SB, Mattia DJ, Wendel JS, et al. Inosculation and Perfusion of Pre-Vascularized Tissue Patches Containing Aligned Human Microvessels after Myocardial Infarction. *Biomaterials*. 2016;36(5):1011-1014. doi:10.1002/jmri.23741.Proton.

57. Wendel JS, Ye L, Tao R, et al. Functional Effects of a Tissue-Engineered Cardiac Patch From Human Induced Pluripotent Stem Cell-Derived Cardiomyocytes in a Rat Infarct Model. *Stem Cells Transl Med*. 2015;4(11):1324-1332. doi:10.5966/sctm.2015-0044.

58. Zhang S, Liu X, Barreto-Ortiz SF, et al. Creating polymer hydrogel microfibres with internal alignment via electrical and mechanical stretching. *Biomaterials*. 2014;35(10):3243-3251. doi:10.1016/j.biomaterials.2013.12.081.

59. Ott HC, Matthiesen TS, Goh S-K, et al. Perfusion-decellularized matrix: using nature's platform to engineer a bioartificial heart. *Nat Med*. 2008;14(2):213-221. doi:10.1038/nm1684.

60. Brennan J, Lu CC, Norris DP, Rodriguez TA, Beddington RS, Robertson EJ. Nodal signaling in the epiblast patterns the early mouse embryo. *Nature*. 2001;411(6840):965-969.

61. Naito AT, Shiojima I, Akazawa H, et al. Developmental stage-specific biphasic roles of Wnt/beta-catenin signaling in cardiomyogenesis and hematopoiesis. *Proc Natl Acad Sci*. 2006;103(52):19812-19817. doi:10.1073/pnas.0605768103.

62. Yuasa S, Itabashi Y, Koshimizu U, et al. Transient inhibition of BMP signaling by Noggin induces cardiomyocyte differentiation of mouse embryonic stem cells. *Nat Biotechnol*. 2005;23(5):607-611. doi:10.1038/nbt1093.

63. Kwon C, Arnold J, Hsiao EC, Taketo MM, Conklin BR, Srivastava D. Canonical Wnt signaling is a positive regulator of mammalian cardiac progenitors. *Proc Natl Acad Sci U S A*. 2007;104(26):10894-10899. doi:10.1073/pnas.0704044104.

64. Kwon C, Qian L, Cheng P, Nigam V, Arnold J, Srivastava D. A Regulatory Pathway Involving Notch1/β-Catenin/Isl1 Determines Cardiac Progenitor Cell Fate. *Nat Cell Biol*. 2009;11(8):951-957. doi:10.1038/ncb1906.A.

65. Lewandowski J, Kolanowski TJ, Kurpisz M. Techniques for the induction of human pluripotent stem cell differentiation towards cardiomyocytes. *J Tissue Eng Regen Med*. 2017;11(5):1658-1674. doi:10.1002/term.2117.

66. Burridge PW, Matsa E, Shukla P, et al. Chemically Defined and Small Molecule-Based Generation of Human Cardiomyocytes. *Nat Methods*. 2014;11(8):855-860. doi:10.1007/s10549-015-3663-1.Progestin.

67. Hao X, Silva EA, Månsson-Broberg A, et al. Angiogenic effects of sequential release of VEGF-A165 and PDGF-BB with alginate hydrogels after myocardial infarction. *Cardiovasc Res*. 2007;75(1):178-185. doi:10.1016/j.cardiores.2007.03.028.

68. Dvir T, Kedem A, Ruvinov E, et al. Prevascularization of cardiac patch on the omentum improves its therapeutic outcome. *Proc Natl Acad Sci*. 2009;106(35):14990-14995. doi:10.1073/pnas.0812242106.

69. Alberti K, Davey RE, Onishi K, et al. Functional immobilization of signaling proteins enables control of stem cell fate. *Nat Methods*. 2008;5(7):645-650. doi:10.1038/nmeth.1222.

70. Steffens GCM, Yao C, Prével P, et al. Modulation of angiogenic potential of collagen matrices by covalent incorporation of heparin and loading with vascular endothelial growth factor. *Tissue Eng*. 2004;10(9-10):1502-1509. doi:10.1089/ten.2004.10.1502.

71. Shen YH, Shoichet MS, Radisic M. Vascular endothelial growth factor immobilized in collagen scaffold promotes penetration and proliferation of endothelial cells. *Acta Biomater*. 2008;4(3):477-489. doi:10.1016/j.actbio.2007.12.011.

72. Chiu LLY, Radisic M. Biomaterials Scaffolds with covalently immobilized VEGF and Angiopoietin-1 for vascularization of engineered tissues. *Biomaterials*. 2010;31(2):226-241. doi:10.1016/j.biomaterials.2009.09.039.

73. Freeman I, Kedem A, Cohen S. The effect of sulfation of alginate hydrogels on the specific binding and controlled release of heparin-binding proteins. *Biomaterials*. 2008;29(22):3260-3268. doi:10.1016/j.biomaterials.2008.04.025.

74. Ruvinov E, Leor J, Cohen Smadar S. The effects of controlled HGF delivery from an affinity-binding alginate biomaterial on angiogenesis and blood perfusion in a hindlimb ischemia model. *Biomaterials*. 2010;31(16):4573-4582. doi:10.1016/j.biomaterials.2010.02.026.

75. Jacot JG, McCulloch AD, Omens JH. Substrate Stiffness Affects the Functional Maturation of Neonatal Rat Ventricular Myocytes. *Biophys J*. 2008;95(7):3479-3487. doi:10.1529/biophysj.107.124545.

76. Engler AJ, Carag-Krieger C, Johnson CP, et al. Embryonic cardiomyocytes beat best on a matrix with heart-like elasticity: scar-like rigidity inhibits beating. *J Cell Sci*. 2008;121(22):3794-3802. doi:10.1242/jcs.029678.

77. Bhana B, Iyer RK, Chen WLK, et al. Influence of substrate stiffness on the phenotype of heart cells. *Biotechnol Bioeng*. 2010;105(6):1148-1160. doi:10.1002/bit.22647.

78. Young JL, Engler AJ. Hydrogels with time-dependent material properties

enhance cardiomyocyte differentiation in vitro. *Biomaterials*. 2011;32(4):1002-1009. doi:10.1016/j.biomaterials.2010.10.020.

79. Hirata M, Yamaoka T. Effect of stem cell niche elasticity/ECM protein on the self-beating cardiomyocyte differentiation of induced pluripotent stem (iPS) cells at different stages. *Acta Biomater*. 2017;65:44-52. doi:10.1016/j.actbio.2017.10.032.

80. Sieminski AL, Hebbel RP, Gooch KJ. The relative magnitudes of endothelial force generation and matrix stiffness modulate capillary morphogenesis in vitro. *Exp Cell Res*. 2004;297(2):574-584. doi:10.1016/j.yexcr.2004.03.035.

81. Rao RR, Peterson AW, Ceccarelli J, Putnam AJ, Stegemann JP. Matrix composition regulates three-dimensional network formation by endothelial cells and mesenchymal stem cells in collagen/fibrin materials. *Angiogenesis*. 2012;15(2):253-264. doi:10.1007/s10456-012-9257-1.

82. Allen P, Melero-Martin J, Bischoff J. Type I collagen, fibrin and PuraMatrix matrices provide permissive environments for human endothelial and mesenchymal progenitor cells to form neovascular networks. *J Tissue Eng Regen Med*. 2011;5(4):1-18. doi:10.1002/term.389.

83. Lin Y-L, Chen C-P, Lo C-M, Wang H-S. Stiffness-controlled three-dimensional collagen scaffolds for differentiation of human Wharton's jelly mesenchymal stem cells into cardiac progenitor cells. *J Biomed Mater Res Part A*. 2016;104(9):2234-2242. doi:10.1002/jbm.a.35762.

84. Chung CY, Bien H, Entcheva E. The role of cardiac tissue alignment in modulating electrical function. *J Cardiovasc Electrophysiol*. 2007;18(12):1323-1329. doi:10.1111/j.1540-8167.2007.00959.x.

85. Rakusan K, Flanagan MF, Geva T, Southern J, Van Praagh R. Morphometry of human coronary capillaries during normal growth and the effect of age in left ventricular pressure-overload hypertrophy. *Circulation*. 1992;86(1):38-46. doi:10.1161/01.CIR.86.1.38.

86. Kajiya F, Goto M. Integrative physiology of coronary microcirculation. *Jpn J Physiol*. 1999;49(3):229-241. doi:10.2170/jjphysiol.49.229.

87. Hirota A, Fujii S, Kamino K. Optical monitoring of spontaneous electrical activity of 8-somite embryonic chick heart. *Jpn J Physiol*. 1979;29(5):635-639. doi:10.2170/jjphysiol.29.635.

88. Radisic M, Park H, Shing H, et al. Functional assembly of engineered myocardium by electrical stimulation of cardiac myocytes cultured on scaffolds. *Proc Natl Acad Sci*. 2004;101(52):18129-18134. doi:10.1073/pnas.0407817101.

89. Pietronave S, Zamperone A, Oltolina F, et al. Monophasic and biphasic electrical stimulation induces a precardiac differentiation in progenitor cells isolated from human heart. *Stem Cells Dev*. 2014;23(8):888-898. doi:10.1089/scd.2013.0375.

90. Eng G, Lee BW, Protas L, et al. Autonomous beating rate adaptation in human stem cell-derived cardiomyocytes. *Nat Commun*. 2016;7(May 2015):1-10. doi:10.1038/ncomms10312.

91. Mandel Y, Manivanh R, Dalal R, et al. Vasoconstriction by electrical stimulation: New approach to control of non-compressible hemorrhage. *Sci Rep*. 2013;3:1-7. doi:10.1038/srep02111.

92. Baker LL, Chambers R, DeMuth SK, Villar F. Effects of electrical stimulation on wound healing in patients with diabetic ulcers. *Diab Care*. 1997;20:405-412.

93. George PM, Bliss TM, Hua T, et al. Electrical preconditioning of stem cells with a conductive polymer scaffold enhances stroke recovery. *Biomaterials*. 2017;142:31-40. doi:10.1016/j.biomaterials.2017.07.020.

94. Hang J, Kong L, Gu JW, Adair T. VEGF gene expression is upregulated in electrically stimulated rat skeletal muscle. *Am J Physiol*. 1995;269(5):1827-1831. doi:10.1152/ajpheart.1995.269.5.H1827.

95. Zhao M, Bai H, Wang E, Forrester J V., McCaig CD. Electrical stimulation directly induces pre-angiogenic responses in vascular endothelial cells by signaling through VEGF receptors. *J Cell Sci*. 2004;117(3):397-405. doi:10.1242/jcs.00868.

96. Bai H, Forrester J V, Zhao M. DC electric stimulation upregulates angiogenic factors in endothelial cells through activation of VEGF receptors. *Cytokine*. 2015;55(1):110-115. doi:10.1016/j.cyto.2011.03.003.DC.

97. Tandon N, Cannizzaro C, Chao P-HG, et al. Electrical stimulation systems for cardiac tissue engineering. *Nat Protoc*. 2009;4(2):155-173. doi:10.1038/nprot.2008.183.

98. Nunes SS, Miklas JW, Liu J, et al. Biowire: A platform for maturation of human pluripotent stem cell-derived cardiomyocytes. *Nat Methods*. 2013;10(8):781-787. doi:10.1038/nmeth.2524.

99. Sun X, Nunes SS. Maturation of Human Stem Cell-derived Cardiomyocytes in Biowires Using Electrical Stimulation. *J Vis Exp*. 2017;(123):1-8. doi:10.3791/55373.

100. Radisic M, Fast VG, Sharifov OF, Iyer RK, Park H, Vunjak-Novakovic G. Optical Mapping of Impulse Propagation in Engineered Cardiac Tissue. *Tissue Eng Part A*. 2009;15(4):851-860. doi:10.1089/ten.tea.2008.0223.

101. Montgomery M, Jiao Y, Phillips S, et al. Alterations in sheep fetal right ventricular tissue with induced hemodynamic pressure overload. *Basic Res Cardiol*. 1998;93(3):192-200.

102. Taber LA. Mechanical aspects of cardiac development. *Prog Biophys Mol Biol*. 1998;69:237-255.

103. Kira Y, Nakaoka T, Hashimoto E, Okabe F, Asano S, Sekine I. Effect of long-term cyclic mechanical load on protein synthesis and morphological changes in cultured myocardial cells from neonatal rat. *Cardiovasc Drugs Ther*. 1994;8:251-262.

104. Yamazaki T, Komuro I, Yazaki Y. Molecular mechanisms of cardiac cellular hpertrophy by mechanical stress. *JMolCell Cardiol*. 1995;27:133-140.

105. Tulloch NL, Muskheli V, Razumova M V, et al. Growth of Engineered

Human Myocardium With Mechanical Loading and Vascular Coculture. *Circ Res*. 2011;109:47-59. doi:10.1161/CIRCRESAHA.110.237206.

106. Gwak SJ, Bhang SH, Kim IK, et al. The effect of cyclic strain on embryonic stem cell-derived cardiomyocytes. *Biomaterials*. 2008;29(7):844-856. doi:10.1016/j.biomaterials.2007.10.050.

107. Shimko VF, Claycomb WC. Effect of Mechanical Loading on Three-Dimensional Cultures of Embryonic Stem Cell-Derived Cardiomyocytes. *Tissue Eng Part A*. 2008;14(1):49-58. doi:10.1089/ten.a.2007.0092.

108. Topper JN, Gimbrone Jr MA. Blood flow and vascular gene expression: fluid shear stress as a modulator of endothelial phenotype. *Mol Med Today*. 1999;5(1):40-46. doi:10.1016/S1357-4310(98)01372-0.

109. van der Schaft DWJ, van Spreeuwel ACC, van Assen HC, Baaijens FPT. Mechanoregulation of Vascularization in Aligned Tissue-Engineered Muscle: A Role for Vascular Endothelial Growth Factor. *Tissue Eng Part A*. 2011;17(21-22):2857-2865. doi:10.1089/ten.tea.2011.0214.

110. Krishnan L, Underwood CJ, Maas S, et al. Effect of mechanical boundary conditions on orientation of angiogenic microvessels. *Cardiovasc Res*. 2008;78(2):324-332. doi:10.1093/cvr/cvn055.

111. Wilson CJ, Kasper G, Schütz MA, Duda GN. Cyclic strain disrupts endothelial network formation on Matrigel. *Microvasc Res*. 2009;78(3):358-363. doi:10.1016/j.mvr.2009.08.002.

112. Ceccarelli J, Cheng A, Putnam AJ. Mechanical strain controls endothelial patterning during angiogenic sprouting. *Cell Mol Bioeng*. 2012;5(4):463-473. doi:10.1109/TMI.2012.2196707.Separate.

113. Greiner AM, Biela SA, Chen H, Spatz JP, Kemkemer R. Featured Article: Temporal responses of human endothelial and smooth muscle cells exposed to uniaxial cyclic tensile strain. *Exp Biol Med*. 2015;240(10):1298-1309. doi:10.1177/1535370215570191.

114. Sinha R, Le Gac S, Verdonschot N, Van Den Berg A, Koopman B, Rouwkema J. Endothelial cell alignment as a result of anisotropic strain and flow induced shear stress combinations. *Sci Rep*. 2016;6(July):1-12. doi:10.1038/srep29510.

115. Underwood CJ, Edgar LT, Hoying JB, Weiss JA. Cell-generated traction forces and the resulting matrix deformation modulate microvascular alignment and growth during angiogenesis. *AJP Hear Circ Physiol*. 2014;307(2):H152-H164. doi:10.1152/ajpheart.00995.2013.

116. Lu L, Mende M, Yang X, et al. Design and validation of a bioreactor for simulating the cardiac niche: a system incorporating cyclic stretch, electrical stimulation and constant perfusion. *Tissue Eng Part A*. 2012;19:120919081657001. doi:10.1089/ten.TEA.2012.0135.

117. Miklas JW, Nunes SS, Sofla A, et al. Bioreactor for modulation of cardiac microtissue phenotype by combined static stretch and electrical stimulation. *Biofabrication*. 2014;6(2):1-27. doi:10.1088/1758-5082/6/2/024113.Bioreactor.

118. Wang B, Wang G, To F, et al. Myocardial scaffold-based cardiac tissue

engineering: Application of coordinated mechanical and electrical stimulations. *Langmuir*. 2013;29(35):11109-11117. doi:10.1021/la401702w.

119. Morgan KY, Black LD. Mimicking Isovolumic Contraction with Combined Electromechanical Stimulation Improves the Development of Engineered Cardiac Constructs. *Tissue Eng Part A*. 2014;20(11-12):1654-1667. doi:10.1089/ten.tea.2013.0355.

120. Cook CA, Huri PY, Ginn BP, et al. Characterization of a novel bioreactor system for 3D cellular mechanobiology studies. *Biotechnol Bioeng*. 2016;113(8):1825-1837. doi:10.1002/bit.25946.

121. Feng Z, Matsumoto T, Nomura Y, Nakamura T. An electro-tensile bioreactor for 3-D culturing of cardiomyocytes. *IEEE Eng Med Biol Mag*. 2005;24(4):73-79. doi:10.1109/MEMB.2005.1463399.

122. Sun X, Nunes SS. Bioengineering Approaches to Mature Human Pluripotent Stem Cell-Derived Cardiomyocytes. *Front Cell Dev Biol*. 2017;5(March):1-8. doi:10.3389/fcell.2017.00019.

123. Jackman CP, Shadrin IY, Carlson AL, Bursac N. Human cardiac tissue engineering: From pluripotent stem cells to heart repair. *Curr Opin Chem Eng*. 2015;7:57-64. doi:10.1016/j.coche.2014.11.004.

124. Eckermann CW, Lehle K, Schmid SA, Wheatley DN, Kunz-Schughart LA. Characterization and modulation of fibroblast/endothelial cell co-cultures for the *in vitro* preformation of three-dimensional tubular networks. *Cell Biol Int*. 2011;35(11):1097-1110. doi:10.1042/CBI20100718.

125. Lu Y, Yu T, Liang H, et al. Nitric oxide inhibits hetero-adhesion of cancer cells to endothelial cells: Restraining circulating tumor cells from initiating metastatic cascade. *Sci Rep*. 2014;4:1-9. doi:10.1038/srep04344.

126. Park H-J, Zhang Y, Georgescu SP, Johnson KL, Kong D, Galper JB. Human umbilical vein endothelial cells and human dermal microvascular endothelial cells offer new insights into the relationship between lipid metabolism and angiogenesis. *Stem Cell Rev*. 2006;2(2):93-101. doi:10.1007/s12015-006-0015-x.

127. Wu PK, Ringeisen BR. Development of human umbilical vein endothelial cell (HUVEC) and human umbilical vein smooth muscle cell (HUVSMC) branch/stem structures on hydrogel layers via biological laser printing (BioLP). *Biofabrication*. 2010;2(1). doi:10.1088/1758-5082/2/1/014111.

128. Critser PJ, Yoder MC. Endothelial colony-forming cell role in neoangiogenesis and tissue repair. 2010. doi:10.1097/MOT.0b013e32833454b5.

129. Forrester JS, White AJ, Matsushita S, Chakravarty T, Makkar RR. New Paradigms of Myocardial Regeneration Post-Infarction. Tissue Preservation, Cell Environment, and Pluripotent Cell Sources. *JACC Cardiovasc Interv*. 2009;2(1):1-8. doi:10.1016/j.jcin.2008.10.010.

130. Cho S-W, Yang F, Son SM, et al. Therapeutic Angiogenesis Using Genetically Engineered Human Endothelial Cells. 2012;160(3):515-524. doi:10.1016/j.jconrel.2012.03.006.Therapeutic.

131. Huang NF, Niiyama H, Peter C, et al. Embryonic stem cell-derived

endothelial cells engraft into the ischemic hindlimb and restore perfusion. *Arterioscler Thromb Vasc Biol*. 2010;30(5):984-991. doi:10.1161/ATVBAHA.110.202796.

132. Levenberg S, Golub JS, Amit M, Itskovitz-Eldor J, Langer R. Endothelial cells derived from human embryonic stem cells. *Proc Natl Acad Sci U S A*. 2002;99(7):4391-4396. doi:10.1073/pnas.032074999.

133. Kusuma S, Shen Y-I, Hanjaya-Putra D, Mali P, Cheng L, Gerecht S. Self-organized vascular networks from human pluripotent stem cells in a synthetic matrix. *Proc Natl Acad Sci*. 2013;110(31):12601-12606. doi:10.1073/pnas.1306562110.

134. Lian X, Bao X, Al-Ahmad A, et al. Efficient differentiation of human pluripotent stem cells to endothelial progenitors via small-molecule activation of WNT signaling. *Stem Cell Reports*. 2014;3(5):804-816. doi:10.1016/j.stemcr.2014.09.005.

135. Shen YI, Cho H, Papa AE, et al. Engineered human vascularized constructs accelerate diabetic wound healing. *Biomaterials*. 2016;102:107-119. doi:10.1016/j.biomaterials.2016.06.009.

136. Blasi A, Martino C, Balducci L, et al. Dermal fibroblasts display similar phenotypic and differentiation capacity to fat-derived mesenchymal stem cells, but differ in anti-inflammatory and angiogenic potential. *Vasc Cell*. 2011;3(1):5. doi:10.1186/2045-824X-3-5.

137. Lesman A, Koffler J, Atlas R, Blinder YJ, Kam Z, Levenberg S. Engineering vessel-like networks within multicellular fibrin-based constructs. *Biomaterials*. 2011;32(31):7856-7869. doi:10.1016/j.biomaterials.2011.07.003.

138. Baum J, Duffy HS. Fibroblasts and myofibroblasts: what are we talking about? *J Cardiovasc Pharmacol*. 2011;57(4):376-379. doi:10.1097/FJC.0b013e3182116e39.

139. Gaudesius G, Miragoli M, Thomas SP, Rohr S. Coupling of cardiac electrical activity over extended distances by fibroblasts of cardiac origin. *Circ Res*. 2003;93(5):421-428. doi:10.1161/01.RES.0000089258.40661.0C.

140. Souders C a., Bowers SLK, Baudino T a. Cardiac fibroblast: The renaissance cell. *Circ Res*. 2009;105(12):1164-1176. doi:10.1161/CIRCRESAHA.109.209809.

141. Riemenschneider SB, Mattia DJ, Wendel JS, et al. Inosculation and perfusion of pre-vascularized tissue patches containing aligned human microvessels after myocardial infarction. *Biomaterials*. 2016;97:51-61. doi:10.1016/j.biomaterials.2016.04.031.

142. Caspi O, Lesman A, Basevitch Y, et al. Tissue engineering of vascularized cardiac muscle from human embryonic stem cells. *Circ Res*. 2007;100(2):263-272. doi:10.1161/01.RES.0000257776.05673.ff.

143. Lesman A, Habib M, Caspi O, et al. Transplantation of a tissue-engineered human vascularized cardiac muscle. *Tissue Eng Part A*. 2010;16(1):115-125. doi:10.1089/ten.TEA.2009.0130.

144. Valarmathi MT, Fuseler JW, Davis JM, Price RL. A Novel Human Tissue-Engineered 3-D Functional Vascularized Cardiac Muscle Construct. *Front Cell Dev Biol*. 2017;5(January):1-24. doi:10.3389/fcell.2017.00002.

145. Schaefer JA, Guzman PA, Riemenschneider SB, Kamp TJ, Tranquillo RT. A Cardiac Patch from Aligned Microvessel and Cardiomyocyte Patches. *J Tissue Eng Regen Med*. 2017. doi:10.1002/term.2568.

146. Banerjee I, Fuseler JJW, Price RL, et al. Determination of cell types and numbers during cardiac development in the neonatal and adult rat and mouse. *… Physiol …*. 2007;29209:1883-1891. doi:10.1152/ajpheart.00514.2007.

147. Tandon V, Zhang B, Radisic M, Murthy SK. Generation of tissue constructs for cardiovascular regenerative medicine: From cell procurement to scaffold design. *Biotechnol Adv*. 2013;31(5):722-735. doi:10.1016/j.biotechadv.2012.08.006.

148. Kohl P, Camelliti P, Burton FL, Smith GL. Electrical coupling of fibroblasts and myocytes: Relevance for cardiac propagation. *J Electrocardiol*. 2005;38(4 SUPPL.):45-50. doi:10.1016/j.jelectrocard.2005.06.096.

149. Brutsaert DL. Cardiac endothelial-myocardial signaling: its role in cardiac growth, contractile performance, and rhythmicity. *Physiol Rev*. 2003;83(1):59-115. doi:10.1152/physrev.00017.2002.

150. Takeda N, Manabe I, Uchino Y. Cardiac fibroblasts are essential for the adaptve response of the murine heart to pressure overload. *J Clin*. 2010;120(1). doi:10.1172/JCI40295DS1.

151. Kawamura M, Miyagawa S, Fukushima S, et al. Enhanced survival of transplanted human induced pluripotent stem cell-derived cardiomyocytes by the combination of cell sheets with the pedicled omental flap technique in a porcine heart. *Circulation*. 2013;128(11 Suppl 1):S87-94. doi:10.1161/CIRCULATIONAHA.112.000366.

152. Hsieh PCH, Davis ME, Lisowski LK, Lee RT. Endothelial-Cardiomyocyte Interactions in Cardiac Development and Repair. *Annu Rev Physiol*. 2006;68(1):51-66. doi:10.1146/annurev.physiol.68.040104.124629.

153. Kamei M, Saunders WB, Bayless KJ, Dye L, Davis GE, Weinstein BM. Endothelial tubes assemble from intracellular vacuoles in vivo. *Nature*. 2006;442(7101):453-456. doi:10.1038/nature04923.

154. Thompson S a., Blazeski A, Copeland CR, et al. Acute slowing of cardiac conduction in response to myofibroblast coupling to cardiomyocytes through N-cadherin. *J Mol Cell Cardiol*. 2014;68:29-37. doi:10.1016/j.yjmcc.2013.12.025.

155. Liau B, Christoforou N, Leong KW, Bursac N. Pluripotent stem cell-derived cardiac tissue patch with advanced structure and function. *Biomaterials*. 2011;32(35):9180-9187. doi:10.1016/j.biomaterials.2011.08.050.

156. Poll D, Parekkadan B, Borel Rinkes IHM, Tilles a. W, Yarmush ML. Mesenchymal Stem Cell Therapy for Protection and Repair of Injured Vital Organs. *Cell Mol Bioeng*. 2008;1(1):42-50. doi:10.1007/s12195-008-0001-2.

157. Shadrin IY, Yoon W, Li L, Shepherd N, Bursac N. Rapid fusion between mesenchymal stem cells and cardiomyocytes yields electrically active, non-contractile hybrid cells. *Sci Rep*. 2015;5(July):12043. doi:10.1038/srep12043.

158. Koh YJ, Koh BI, Kim H, et al. Stromal vascular fraction from adipose tissue forms profound vascular network through the dynamic reassembly of blood endothelial cells. *Arterioscler Thromb Vasc Biol*. 2011;31(5):1141-1150. doi:10.1161/ATVBAHA.110.218206.

159. Strassburg S, Nienhueser H, Stark GB, Finkenzeller G, Torio-Padron N. Human adipose-derived stem cells enhance the angiogenic potential of endothelial progenitor cells, but not of human umbilical vein endothelial cells. *Tissue Eng Part A*. 2013;19(1-2):166-174. doi:10.1089/ten.TEA.2011.0699.

160. Crisan M, Yap S, Casteilla L, et al. A Perivascular Origin for Mesenchymal Stem Cells in Multiple Human Organs. *Cell Stem Cell*. 2008;3(3):301-313. doi:10.1016/j.stem.2008.07.003.

161. Crisan M, Corselli M, Chen WCW, Péault B. Perivascular cells for regenerative medicine. *J Cell Mol Med*. 2012;16(12):2851-2860. doi:10.1111/j.1582-4934.2012.01617.x.

162. Corselli M, Chin CJ, Parekh C, et al. Perivascular support of human hematopoietic stem / progenitor cells. 2013;121(15):2891-2901. doi:10.1182/blood-2012-08-451864.The.

163. Yoshimura K, Suga H, Eto H. Adipose-derived stem/progenitor cells: roles in adipose tissue remodeling and potential use for soft tissue augmentation. *Regen Med*. 2009;4(2):265-273. doi:10.2217/17460751.4.2.265.

164. Dubois SG, Floyd EZ, Zvonic S, et al. Isolation of human adipose-derived stem cells from biopsies and liposuction specimens. *Methods Mol Biol*. 2008;449:69-79. doi:10.1007/978-1-60327-169-1_5.

165. Toraason M, Luken ME, Breitenstein M, Krueger JA, Biagini RE. Comparative Toxicity of Allylamine and Acrolein in Cultured Myocytes and Fibroblasts from Neonatal Rat Heart. *Toxicology*. 1989;56:107-117.

166. Blazeski A, Kostecki GM, Tung L. Engineered heart slices for electrophysiological and contractile studies. *Biomaterials*. 2015;55:119-128. doi:10.1016/j.biomaterials.2015.03.026.

167. Girouard SD, Laurita KR, Rosenbaum DS. Unique properties of cardiac action potentials recorded with voltage-sensitive dyes. *J Cardiovasc Electrophysiol*. 1996;7(11):1024-1038.

168. Tritthart HA. Optical Techniques for the Recording of Action Potentials. *In-Vitro Tech*. 2005:215-232. doi:10.1007/b137833.

169. Entcheva E, Bien H. Macroscopic optical mapping of excitation in cardiac cell networks with ultra-high spatiotemporal resolution. *Prog Biophys Mol Biol*. 2006;92(2):232-257. doi:10.1016/j.pbiomolbio.2005.10.003.

170. Salama G, Hwang SM. *Simultaneous Optical Mapping of Intracellular Free Calcium and Action Potentials from Langendorff Perfused Hearts*.; 2009.

doi:10.1002/0471142956.cy1217s49.

171. Iyer RK, Odedra D, Chiu LLY, Vunjak-Novakovic G, Radisic M. Vascular Endothelial Growth Factor Secretion by Nonmyocytes Modulates Connexin-43 Levels in Cardiac Organoids. *Tissue Eng Part A*. 2012;18(17-18):1771-1783. doi:10.1089/ten.tea.2011.0468.

172. Sorrell JM, Baber MA, Caplan AI. A self-assembled fibroblast-endothelial cell co-culture system that supports in vitro vasculogenesis by both human umbilical vein endothelial cells and human dermal microvascular endothelial cells. *Cells Tissues Organs*. 2007;186(3):157-168. doi:10.1159/000106670.

173. Liu H, Kennard S, Lilly B. NOTCH3 expression is induced in mural cells through an autoregulatory loop that requires Endothelial-expressed JAGGED1. *Circ Res*. 2009;104(4):466-475. doi:10.1161/CIRCRESAHA.108.184846.

174. McSpadden LC, Kirkton RD, Bursac N. Electrotonic loading of anisotropic cardiac monolayers by unexcitable cells depends on connexin type and expression level. *Am J Physiol Cell Physiol*. 2009;297(2):C339-C351. doi:10.1152/ajpcell.00024.2009.

175. Traktuev DO, Merfeld-Clauss S, Li J, et al. A population of multipotent CD34-positive adipose stromal cells share pericyte and mesenchymal surface markers, reside in a periendothelial location, and stabilize endothelial networks. *Circ Res*. 2008;102(1):77-85. doi:10.1161/CIRCRESAHA.107.159475.

176. Simpson P, Savion S. Differentiation of rat myocytes in single cell cultures with and without proliferating nonmyocardial cells. Cross-striations, ultrastructure, and chronotropic response to isoproterenol. *Circ Res*. 1982;50(1):101-116. doi:10.1161/01.RES.50.1.101.

177. Milasinovic D. Contemporary perspective on endogenous myocardial regeneration. *World J Stem Cells*. 2015;7(5):793. doi:10.4252/wjsc.v7.i5.793.

178. Tang XL, Rokosh G, Sanganalmath SK, et al. Intracoronary administration of cardiac progenitor cells alleviates left ventricular dysfunction in rats with a 30-day-old infarction. *Circulation*. 2010;121(2):293-305. doi:10.1161/CIRCULATIONAHA.109.871905.

179. Li Y, Meng H, Liu Y, Lee BP. Fibrin gel as an injectable biodegradable scaffold and cell carrier for tissue engineering. *Sci World J*. 2015;2015. doi:10.1155/2015/685690.

180. Zhang B, Montgomery M, Chamberlain MD, et al. HHS Public Access. 2016;15(6):669-678. doi:10.1038/nmat4570.Biodegradable.

181. Fleischer S, Shapira A, Feiner R, Dvir T. Modular assembly of thick multifunctional cardiac patches. 2017. doi:10.1073/pnas.1615728114.

182. Boothe SD, Myers JD, Pok S, et al. The Effect of Substrate Stiffness on Cardiomyocyte Action Potentials. *Cell Biochem Biophys*. 2016;74(4):527-535. doi:10.1007/s12013-016-0758-1.

183. Young JL, Kretchmer K, Ondeck MG, Zambon AC, Engler AJ.

Mechanosensitive Kinases Regulate Stiffness-Induced Cardiomyocyte Maturation. *Sci Rep*. 2015;4(1):6425. doi:10.1038/srep06425.

184. Forte G, Pagliari S, Ebara M, et al. Substrate stiffness modulates gene expression and phenotype in neonatal cardiomyocytes in vitro. *Tissue Eng Part A*. 2012;18(17-18):1837-1848. doi:10.1089/ten.TEA.2011.0707.

185. Rodriguez AG, Han SJ, Regnier M, Sniadecki NJ. Substrate stiffness increases twitch power of neonatal cardiomyocytes in correlation with changes in myofibril structure and intracellular calcium. *Biophys J*. 2011;101(10):2455-2464. doi:10.1016/j.bpj.2011.09.057.

186. Pinto AR, Ilinykh A, Ivey MJ, et al. Revisiting cardiac cellular composition. *Circ Res*. 2016;118(3):400-409. doi:10.1161/CIRCRESAHA.115.307778.

187. Eng G, Lee BW, Protas L, et al. Autonomous beating rate adaptation in human stem cell-derived cardiomyocytes. *Nat Commun*. 2016;7(May 2015):10312. doi:10.1038/ncomms10312.

188. Cook CA, Huri PY, Ginn BP, et al. Characterization of a Novel Bioreactor System for 3D Cellular Mechanobiology Studies. 2016;113(8):1825-1837. doi:10.1002/bit.25946.

189. Black LD, Meyers JD, Weinbaum JS, Shvelidze YA, Tranquillo RT. Cell-induced alignment augments twitch force in fibrin gel-based engineered myocardium via gap junction modification. *Tissue Eng Part A*. 2009;15(10):3099-3108. doi:10.1089/ten.TEA.2008.0502.

190. Bian W, Liau B, Badie N, Bursac N. Mesoscopic hydrogel molding to control the 3d geometry of bioartifical muscle tissues. *Nat Protoc*. 2010;4(10):1522-1534. doi:10.1038/nprot.2009.155.Mesoscopic.

191. Jacot JG, Martin JC, Hunt DL. NIH Public Access. 2011;43(1):1-13. doi:10.1016/j.jbiomech.2009.09.014.Mechanobiology.

192. Bian W, Liau B, Badie N, Bursac N. Mesoscopic hydrogel molding to control the 3D geometry of bioartificial muscle tissues. *Nat Protoc*. 2009;4(10):1522-1534. doi:10.1038/nprot.2009.155.

193. Valderrábano M. Influence of anisotropic conduction properties in the propagation of the cardiac action potential. *Prog Biophys Mol Biol*. 2007;94(1-2):144-168. doi:10.1016/j.pbiomolbio.2007.03.014.

194. Reeder SB, Hu HH, Sirlin CB, Group LI, Diego S. HHS Public Access. 2016;36(5):1011-1014. doi:10.1002/jmri.23741.Proton.

195. Mannhardt I, Breckwoldt K, Letuffe-Brenière D, et al. Human Engineered Heart Tissue: Analysis of Contractile Force. *Stem Cell Reports*. 2016;7(1):29-42. doi:10.1016/j.stemcr.2016.04.011.

196. Jackman CP, Carlson AL, Bursac N. Dynamic culture yields engineered myocardium with near-adult functional output. *Biomaterials*. 2016;111:66-79. doi:10.1016/j.biomaterials.2016.09.024.

197. Yeh YT, Hur SS, Chang J, et al. Matrix Stiffness Regulates Endothelial Cell Proliferation through Septin 9. *PLoS One*. 2012;7(10):1-13. doi:10.1371/journal.pone.0046889.

198. Saunders RL, Hammer D a. Assembly of Human Umbilical Vein

Endothelial Cells on Compliant Hydrogels. *Cell Mol Bioeng*. 2010;3(1):60-67. doi:10.1007/s12195-010-0112-4.Assembly.

199. Wong JY. Vascular Smooth Muscle Cells : Implications for Atherosclerosis. 2011;225(1):115-122. doi:10.1002/jcp.22202.Effect.

200. Lopatina T, Bruno S, Tetta C, Kalinina N, Porta M, Camussi G. Platelet-derived growth factor regulates the secretion of extracellular vesicles by adipose mesenchymal stem cells and enhances their angiogenic potential. *Cell Commun Signal*. 2014;12(1):26. doi:10.1186/1478-811X-12-26.

201. Bala K, Ambwani K, Gohil NK. Effect of different mitogens and serum concentration on HUVEC morphology and characteristics: Implication on use of higher passage cells. *Tissue Cell*. 2011;43(4):216-222. doi:10.1016/j.tice.2011.03.004.

202. Kofron CM, Mende U. In vitro models of the cardiac microenvironment to study myocyte and non-myocyte crosstalk : bioinspired approaches beyond the polystyrene dish. 2017;12:3891-3905. doi:10.1113/JP273100.

203. Zhang P, Su J, Mende U. Cross talk between cardiac myocytes and fibroblasts : from multiscale investigative approaches to mechanisms and functional consequences. 2012;(76). doi:10.1152/ajpheart.01167.2011.

204. Rajamani K, Li Y, Hsieh D. Review Genetic and Epigenetic Instability of Stem Cells. 2014;23(1):417-433.

205. Robinton DA, Daley GQ. cells in research and therapy. 2012. doi:10.1038/nature10761.

206. Nishikawa S, Goldstein RA, Nierras CR. and therapy. 2008;9(September):725-729.

207. Matsa E, Burridge PW, Wu JC. Human Stem Cells for Modeling Heart Disease and for Drug Discovery. 2014;6(239):1-8.

208. Parham KA, Pitson SM, Bonder CS, Cfu-ecs EE. Regulation of EPCs : The Gateway to Blood Vessel Formation. 2014;2014.

209. Tan KS, Tamura K, Lai MI. Molecular Pathways Governing Development of Vascular Endothelial Cells from ES / iPS Cells. 2013:586-598. doi:10.1007/s12015-013-9450-7.

210. Zhu R, Millrod MA, Zambidis ET, Tung L. Variability of Action Potentials Within and among Cardiac Cell Clusters Derived from Human Embryonic Stem Cells. *Sci Rep*. 2016;6(January):1-12. doi:10.1038/srep18544.

211. Kim C, Majdi M, Xia P, et al. Non-Cardiomyocytes Infl uence the Electrophysiological Maturation of Human Embryonic Stem Cell-Derived Cardiomyocytes During Differentiation. 2010;19(6). doi:10.1089/scd.2009.0349.

212. Ravenscroft SM, Pointon A, Williams AW, Cross MJ, Sidaway JE. Cardiac Non-myocyte Cells Show Enhanced Pharmacological Function Suggestive of Contractile Maturity in Stem Cell Derived Cardiomyocyte Microtissues. 2017;152(December):99-112. doi:10.1093/toxsci/kfw069.

213. Zhang D, Shadrin IY, Lam J, Xian H, Snodgrass HR, Bursac N. Biomaterials Tissue-engineered cardiac patch for advanced functional

maturation of human ESC-derived cardiomyocytes. *Biomaterials*. 2013;34(23):5813-5820. doi:10.1016/j.biomaterials.2013.04.026.

214. Nunes SS, Miklas JW, Liu J, et al. Biowire : a platform for maturation of human pluripotent stem cell – derived cardiomyocytes. 2013;10(8). doi:10.1038/nmeth.2524.

215. Tulloch NL, Muskheli V, Razumova M V, et al. Growth of Engineered Human Myocardium With Mechanical Loading and Vascular Coculture. 2011. doi:10.1161/CIRCRESAHA.110.237206.

216. Cardiomyocytes C. E MBRYONIC S TEM C ELLS / I NDUCED P LURIPOTENT S TEM C ELLS Concise Review : Maturation Phases of Human Pluripotent Stem. doi:10.1002/stem.1331.

217. Sharma A, Wu JC, Wu SM. Induced pluripotent stem cell-derived cardiomyocytes for cardiovascular disease modeling and drug screening. 2013.

218. Lin H, Lai Y, Tai C, Tsai J, Hsu H. Effects of cultured human adipose-derived stem cells transplantation on rabbit cornea regeneration after alkaline chemical burn. *Kaohsiung J Med Sci*. 2013;29(1):14-18. doi:10.1016/j.kjms.2012.08.002.

219. Li Y, Asfour H, Bursac N. Acta Biomaterialia Age-dependent functional crosstalk between cardiac fibroblasts and cardiomyocytes in a 3D engineered cardiac tissue. *Acta Biomater*. 2017;55:120-130. doi:10.1016/j.actbio.2017.04.027.

220. Liau B, Jackman CP, Li Y, Bursac N. Developmental stage-dependent effects of cardiac fibroblasts on function of stem cell-derived engineered cardiac tissues. *Nat Publ Gr*. 2017;(February):1-11. doi:10.1038/srep42290.

221. Trieschmann J, Bettin D, Haustein M, et al. The Interaction between Adult Cardiac Fibroblasts and Embryonic Stem Cell-Derived Cardiomyocytes Leads to Proarrhythmic Changes in In Vitro Cocultures. 2016;2016.

222. Orlova V V, Drabsch Y, Freund C, et al. Functionality of Endothelial Cells and Pericytes From Human Pluripotent Stem Cells Demonstrated in Cultured Vascular Plexus and Zebrafish Xenografts. 2013. doi:10.1161/ATVBAHA.113.302598.

Curriculum Vitae

Justin received his Bachelor of Science in Chemical Engineering from Hampton University in Hampton, Virginia in 2009 graduating with departmental honors and *Magna Cum Laude*. While in undergrad, he had the opportunity to perform undergraduate research at the Massachusetts Institute of Technology in the lab of Douglas Lauffenburger, Ph.D. and Linda Griffith, Ph.D. He also had the opportunity to conduct research and coursework at sea with the Sea Education Program sailing from Hawaii to California. While at Hampton, he completed HIV modeling work with Dr. Morris Morgan.

Justin subsequently enrolled at Johns Hopkins University in 2009 to pursue a Ph.D. in Biomedical Engineering. Justin worked in the lab of Dr. Warren Grayson. His project brought together a cardiac electrophysiologist and a materials scientist to develop a cardiac graft. His doctoral research led to 1 peer reviewed publication and submitted another first-authored publication and first-authored book chapter. He has also co-authored 2 publications and 1 book chapter. Justin has submitted conference abstracts and presented 4 posters. Justin also attended the Gordon Research Conference Series and was awarded the Carl Storm Underrepresented Minority Fellowship. Outside of research, Justin was awarded the Baltimore Albert Schweitzer Fellowship to complete a health-related service project for the disadvantaged Baltimore community.